

Synthesis of Chromic Oxide and Molybdic Oxide
Supported on Mesoporous Silica using Direct Impregnation
Method and Their Catalytic Activities

Siyuan Xia

A thesis submitted to Auckland University of Technology
in partial fulfilment of the requirements for the degree
of

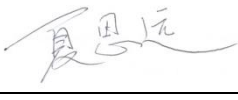
Master of Applied Science (MAppSc)

2013

School of Applied Sciences

ATTESTATION OF AUTHORSHIP

I hereby declare that this submission is my own work and that, to the best of my knowledge and belief, it contains no material previously published or written by another person except that which appears in the citations and acknowledgements. Nor does it contain material which to a substantial extent I have submitted for the qualification for any other degree of another university or other institution of higher learning.

Candidate Signature:  _____

Date: 21/10/2013

ACKNOWLEDGEMENT

I would like to express my great appreciation to my primary supervisor Dr. Roger Whiting of Auckland University of Technology. The thesis would not have been possible without Dr. Whiting's guidance, suggestions, and encouragement throughout the course.

Also thanks to my secondary and additional supervisor Dr. John Robertson of Auckland University of Technology and Dr. Yuhong Wang of Shanghai Institute of Technology for their valuable advices and help during the project.

In addition, I am indebted to Dr. Geoff Waterhouse and his student Henry of the University of Auckland for their assistance in the nitrogen adsorption isotherm and X-ray diffraction measurements.

ABSTRACT

This research describes further development of the direct impregnation method for synthesis of chromic oxide and molybdic oxide supported on the mesoporous silica molecular sieve (MCM-41) for use as a solid acid catalyst.

The catalysts were characterized by powder X-ray diffraction (XRD), thermo gravimetry (TG), Fourier transform infrared spectroscopy (FTIR) and surface area measurement using N₂ isotherm adsorption techniques.

Solid super acid catalysts are important industrial catalysts. By addition of the metals Cr and Mo to the mesoporous MCM-41 silica structure, solid super acid catalysts can be prepared. Both Brønsted and Lewis acid sites are formed which are responsible for the catalytic activities. Compared with the traditional solid acid catalysts and transition metals, the modified MCM-41 molecular sieve has a larger specific surface area and better hydrothermal stability.

A direct impregnation method has been developed to explore the positive characteristics of the materials discussed above. After calcination, all the samples exhibited the typical hexagonal arrangement of mesoporous structures with large surface area and the heteroatoms partly incorporated into the framework of MCM-41.

The results showed up to 50 percent metal oxide : silicate ratio of transition metal can be loaded into the framework of MCM-41. By the addition of Cr and Mo, two groups of new catalysts were prepared which had higher activity and selectivity than MCM-41 when evaluated using the condensation esterification of acetic acid and n-butanol. Further, the catalysts could be regenerated and reused by calcination.

LIST OF ABBREVIATIONS

B.E.T. theory	Brunauer, Emmett, and Teller theory
BJH pore size distribution	Barret-Joyner-Halenda pore size distribution
CTAB	Cetyl trimethylammonium bromide
DRIFTS	Diffuse reflectance infrared Fourier transform spectroscopy
FTIR	Fourier Transform Infrared Spectroscopy
GC	Gas chromatography
MCM-41	Mobile crystalline of materials
SBA-15	Santa Barbara amorphous
SEM	Scanning electron microscopy
TEOS	Tetraethyl orthosilicate
TGA	Thermal gravimetric analysis
XDR	X-ray diffraction

Table of Contents

Attestation Of Authorship	I
Acknowledgement.....	II
Abstract	III
List of Abbreviations	IV
List of Figures.....	VIII
List of Tables.....	XI
Chapter 1 Introduction.....	1
1.1 Mesoporous silica materials as catalysts.....	1
1.1.1 Production, History and development of mesoporous silica materials	1
1.1.2 Catalytic properties of mesoporous silica material.....	3
1.1.3 Limitation and development of mesoporous silica material	6
1.2 Acid Modified Transition Metal used in catalysts	10
1.2.1 Acid and super acid.....	10
1.2.2 Transition metals.....	13
1.2.3 Limitations and development of superacids.....	16
1.3 Transition Metal Oxides Supported on Mesoporous Silica.....	22
1.3.1 Advantages of transition metal oxides modified catalysts	22
1.3.2 Synthesis methods	22
1.3.3 Past work and current gap.....	24

1.4 Research Objective	24
1.5 Experimental Design	24
Chapter 2 Experimental Methods	27
2.1 Catalyst synthesis	27
2.1.1 Chemical Reagents	27
2.2 Catalyst Synthesis	28
2.3 Catalytic activity and selectivity	32
2.4 Characterization.....	36
2.4.1 Scanning electron microscope.....	36
2.4.2 Diffuse reflectance infrared fourier transform spectroscopy	37
2.4.3 Powder X-ray diffraction (XRD).....	39
2.4.4 Nitrogen adsorption-desorption isotherm method	39
2.4.5 Hammett indicators for acid strength measurement	40
2.4.6 Thermal gravimetric analysis (TGA).....	41
Chapter 3 Results and discussion.....	42
3.1 The synthesis process of catalysts	42
3.2 Thermal treatments.....	44
3.3 n-butyl acetate synthesis mechanism.....	48
3.4 Catalytic activity and selectivity analysis	51
3.4.1 Products qualitative analysis.....	51
3.4.2 Catalytic activity.....	54

3.5 Catalysts structure	58
3.5.1 Surface structure	58
3.5.2 Crystalline structure.....	63
3.5.3 Catalysts surface area and porosity determination	67
3.6 Type of active sites and acid strength.....	73
3.6.1 Active sites	73
3.6.2 The deactivation of active sites	80
3.6.3 Acid strength	81
Chapter 4 Conclusions and future work	84
4.1 Conclusions	84
4.2 Limitations and future work	85
References	86

LIST OF FIGURES

Figure 1 Electron micrographs of MCM-41 (Walcarius & Delacôte, 2003)	2
Figure 2 Ordered mesoporous silica (SBA-15 material) with high resolution field emission SEM image of the pore structure and the hexagonal pore arrangement representation (Kleitz, 2009)	3
Figure 3 Mechanistic pathways for the formation of MCM-41 ① liquid crystal phase initiated ② silicate anion initiated	4
Figure 4 Scheme for the formation of mesoporous phase by cooperative organization...	4
Figure 5 Schematic representation of the three types of SiOH group in siliceous MCM-41 and their characteristics (X. Zhao et al., 1997)	6
Figure 6 Lewis acid molecular orbital theory	11
Figure 7 Acid strength of liquid superacids and solid superacids (Schüth & Schmidt, 2002).	12
Figure 8 Surface electron transfer.....	15
Figure 9 Three kinds of coordination modes.....	19
Figure 10 Synthesis path direct impregnation method.....	25
Figure 11 Tetraethyl orthosilicate (TEOS)	27
Figure 12 Cetyltrimethylammonium bromide (CTAB)	27
Figure 13 The throstages drying process for porous material (Regalbuto, 2007).....	44
Figure 14 The mass change of the samples with temperature increase	46
Figure 15 n-butyl acetate.....	48

Figure 16 IR spectrum of the synthesized n-butyl acetate by using 50% Cr/MCM-41 and 50% Mo/MCM-41.	52
Figure 17 IR spectrum of butyl acetate (S.Kinugasa, K.Tanabe, & T.Tamura, 2013)....	52
Figure 18 Chromatogram of compounds after esterification catalyzed by 50% loading Mo/MCM-41	53
Figure 19 The relationship between metal content and catalytic activity	55
Figure 20 Catalytic activity change with number of use for 50% loading catalysts	56
Figure 21 Scanning electron micrograph of the MCM-41 molecular sieve on 10 μ m scale	59
Figure 22 Scanning electron micrographs of 50% Cr/MCM-41 on 2 μ m scale (left) and 50% Mo/MCM-41 on 10 μ m scale (right).	59
Figure 23 X-ray microanalysis of 1% Cr/MCM-41 based on scanning electron micrograph	60
Figure 24 X-ray microanalysis of 1% Mo/MCM-41 based on scanning electron micrograph	61
Figure 25 The Bragg's Law X-ray diffraction	63
Figure 26 XRD patterns of the MCM-41	64
Figure 27 XRD patterns of the Cr/MCM-41 composites with different chromium (1% to 50%, from left to right, up to down)	65
Figure 28 XRD patterns of the Cr/MCM-41 composites with different chromium (1% to 50%, from left to right, up to down)	66
Figure 29 Comparison of Langmuir and BET models for gas adsorption	68

Figure 30 The IUPAC Classification of Adsorption Isotherms for Gas–Solid Equilibria (Donohue & Aranovich, 1998).....	69
Figure 31 Adsorption isotherm for Cr/MCM-41 (1% to 50%, from left to right, up to down)	70
Figure 32 The pore size distribution curves of Cr/MCM-41 (1% to 50%, from left to right, up to down)	72
Figure 33 Adsorption isotherm for Mo/MCM-41 (10% to 50%, from left to right, up to down)	72
Figure 34 IR spectrum for MCM-41 without metal loading.....	74
Figure 35 IR spectra for 1%Cr/MCM-41(above) and 10%Cr/MCM-41(below).....	75
Figure 36 IR spectra for Mo/MCM-41 catalysts(from left to right, up to down:1% to 50%)	76
Figure 37 IR spectrum of MCM-41 with pyridine adsorption	77
Figure 38 IR spectra of Cr/MCM-41 catalysts with pyridine adsorption (from left to right, up to down:1% to 50%).....	78
Figure 39 IR spectra of Mo/MCM-41 catalysts with pyridine adsorption (from left to right, up to down:1% to 50%).....	79
Figure 40 IR spectra of 50 %Cr/MCM-41 catalysts with pyridine adsorption from 0°C to 400°C.....	80
Figure 41 IR spectra of 50 %Mo/MCM-41 catalysts with pyridine adsorption from 0°C to 400°C.....	81

LIST OF TABLES

Table 1 Transition metal.....	13
Table 2 Techniques used for catalyst characterization.....	26
Table 3 The ratio of compounds to synthesis Cr/MCM-41	29
Table 4 The ratio of compounds to synthesis MoMCM-41	30
Table 5 The classification of the new synthesized catalysts.....	31
Table 6 GC Parameters	35
Table 7 Hammett indicators used for acid strength measurement	41
Table 8 Picture for 50%Cr/MCM-41 and 50% Mo/MCM-41 after calcining at 300 °C and 600 °C.....	47
Table 9 Esterification rate using different ratio metal loading catalysts	54
Table 10 GC results for Cr/MCM-41	57
Table 11 GC results for Mo/MCM-41	57
Table 12 Atom presentage on the surface of 1%Cr/MCM-41	60
Table 13 Atom presentage on the surface of Cr/MCM-41 catalysts	61
Table 14 Atom presentage on the surface of 1%Cr/MCM-41	62
Table 15 Atom presentage on the surface of Mo/MCM-41 catalysts	62
Table 16 Surface area and porosity properties of Cr/MCM-41 catalysts.....	71
Table 17 Surface area and porosity properties of Mo/MCM-41 catalysts.....	73
Table 18 Acidity strength of Cr/MCM-41 catalysts measuring with Hammett indicators	82

Table 19 Acidity strength of Mo/MCM-41 catalysts measuring with Hammett indicators

.....83

CHAPTER 1 INTRODUCTION

1.1 MESOPOROUS SILICA MATERIALS AS CATALYSTS

According to IUPAC notation, microporous materials have pore diameters of less than 2 nm and macroporous materials have pore diameters of greater than 50 nm; the mesoporous category thus lies in the middle (Rouquerol et al., 1994). Therefore, mesoporous silica is a material on a ‘meso’ scale with a porous surface structure. Alternatively, mesoporous silica can be regarded as a molecular sieve with holes sized between 2 nm and 50 nm.

Mesoporous silica is synthesized by precipitation of silica in the presence of surfactants as templates for the polycondensation of silica species (Giraldo et al., 2007). Silica sources such as sodium silicate, tetraethylorthosilicate (TEOS) and tetramethylorthosilicate (TMOS) (Giraldo et al., 2007) are commonly used. This kind of surface structure has large surface area, and the large surface area gives great catalytic ability. Based on their unique surface structure and potentially active sites, this kind of molecular sieve provides the possibilities for a range of catalytic reactions to occur.

1.1.1 PRODUCTION, HISTORY AND DEVELOPMENT OF MESOPOROUS SILICA MATERIALS

Mesoporous silica material history: The method for producing mesoporous silica was invented around 1970 (Chiola, 1971), but the patent was almost unnoticed until the 1990's. In 1989, mesoporous silica was synthesized by Japanese researchers Yanagisawa et al. (T. Yanagisawa, T. Shimizu, K. Kuroda, & C. Kato, 1990). This can be regarded as the precursor of the mesoporous silica materials with three-dimensional silica structures, a pore size range from 2 nm to 4 nm in diameter and surface areas of around 900 m²g⁻¹ (T. Yanagisawa et al., 1990). Two years later, in 1992, Mobil's researchers (Beck et al., 1992)

synthesized a new family of silicate/aluminosilicate mesoporous molecular sieves named Mobil Crystalline Material (MCM).

Mobil Crystalline Material: MCM-41 (see **Figure 1** below) is one member of this family and exhibits a hexagonal arrangement of uniform mesopores whose dimensions may be engineered in the range of 15 Å to greater than 100 Å. The typical larger pore MCM-41 materials have surface areas above 700 m²/g and hydrocarbon sorption capacities of 0.7 cc/g and greater (Beck et al., 1992).

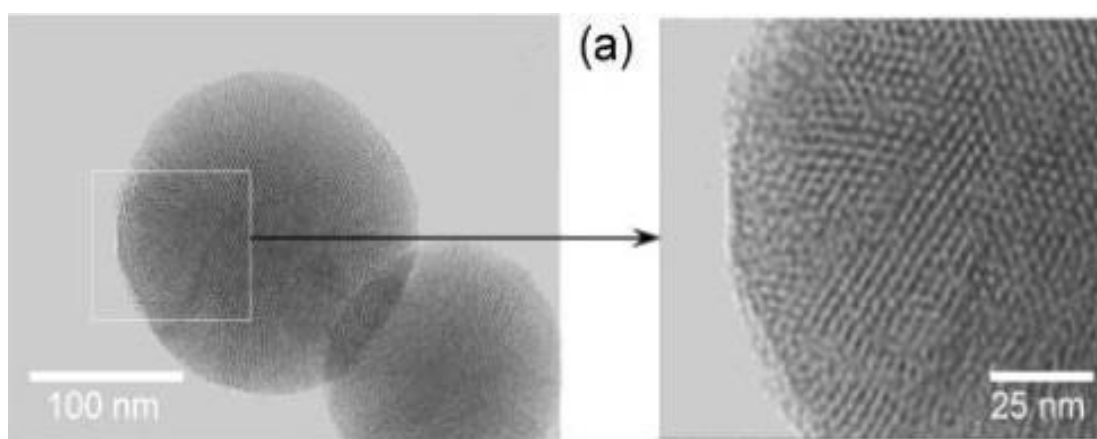


Figure 1 Electron micrographs of MCM-41 (Walcarius & Delacôte, 2003)

Development history According to the technology of liquid crystal templates, MCM-41 has the uniform mesopores between 3 and 10 nm (C. Kresge, M. Leonowicz, W. Roth, J. Vartuli, & J. Beck, 1992). Several years later in 1998, another member of the mesoporous silica family was developed. This milestone development was the synthesis of SBA-15 (Santa Barbara Amorphous type material) by the researchers in the University of California from Santa Barbara (D. Zhao et al., 1998). The SBA-15 (see **Figure 2** below) whose pore sizes are between 4.6 and 30 nm has the highly ordered two-dimensional hexagonal silica copolymer mesophases structure (D. Zhao et al., 1998).

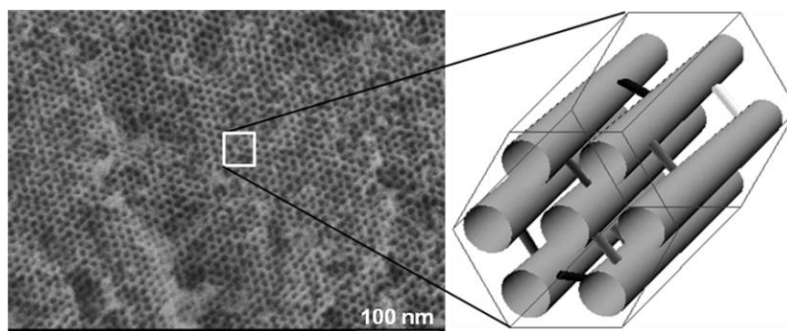


Figure 2 Ordered mesoporous silica (SBA-15 material) with high resolution field emission SEM image of the pore structure and the hexagonal pore arrangement representation (Kleitz, 2009)

Since then, different types of the mesoporous silica nanoparticles such as MCM-X type materials, SBA-X type materials, types MSU-, KSW-, FSM-, etc. have been developed with different porous and morphological characteristics with a wide range of applications (Wang, Gan, Whiting, & Lu, 2009).

1.1.2 CATALYTIC PROPERTIES OF MESOPOROUS SILICA MATERIAL

Synthesis of MCM-41: There are many methods for synthesis of MCM-41. It includes hydrothermal synthesis, room temperature synthesis, roasting synthesis, microwave synthesis and vapor phase synthesis. Of these methods, hydrothermal synthesis method is the most common.

The synthesis of MCM-41 materials take place at certain temperatures (below 393 K) with anionic, cationic, gemini or neutral surfactants, under either basic or acidic conditions (Giraldo et al., 2007). After that, calcination processes are necessary to remove anionic impurities and form hexagonal pore structure.

Anandan and Okazaki (Anandan & Okazaki, 2005) put forward the theory of a ‘Liquid Crystal Templating Mechanism’ to describe the formation of mesoporous structure (**Figure 3**). As a surfactant reaches a certain concentration, it can form rod micelles. A surfactant’s hydrophilic groups contact with water and silicon (including silicon hydrolyzate and gel particles) adsorbed on the nickel surface through electrostatic interaction forming orderly ‘liquid crystal’ structure. After silicon saturation, this kind of structure is firmly established and form a precipitate.

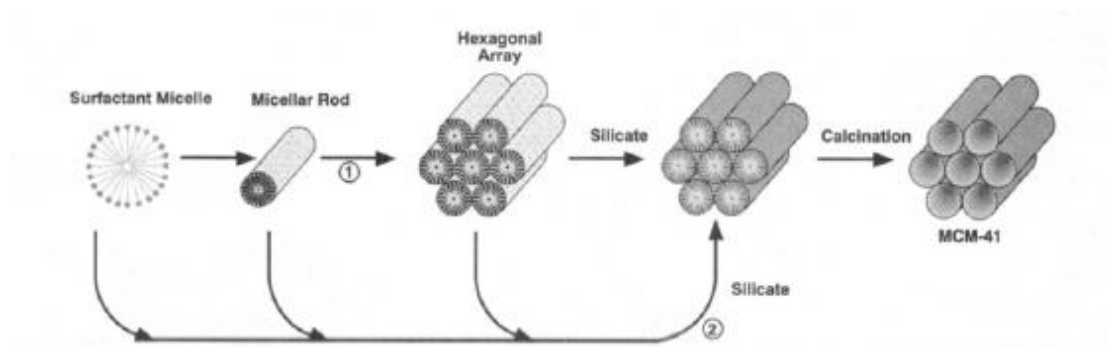


Figure 3 Mechanistic pathways for the formation of MCM-41 ① liquid crystal phase initiated ② silicate anion initiated

Because of the different preparation conditions, this mechanism cannot explain all the synthetic process. For instance, with a surfactant concentration of 10.3~10.2 mol/L, the surfactant forms a ball micelle instead of a rod micelle. The conditions could be adjusted in order to produce range of micelle structures, ‘Cooperative Organization Mechanism’ reported by G. D. Stucky is one of the most representative theories (Huo, Margolese, Feng, Gier, & Sieger, 1994). As shown in **Figure 4**, silicon combines with a surface active agent through electrostatic interaction, and condenses on the micelle surface. At the same time, due to the function of electrostatic force and van der Waals force, this complex interaction results in an optimized curvature. Then charge density can match, and finally certain ordered structure forms.

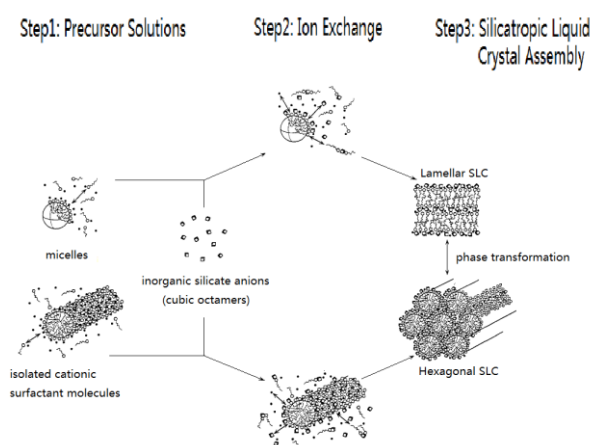


Figure 4 Scheme for the formation of mesoporous phase by cooperative organization

Catalyst carrier performance: MCM-41 mesoporous molecular sieves have an orderly hexagonal structure, so they can serve as good ‘micro reactors’. In addition, MCM-41 contains a wealth of silanol keys. This allows a lot of chemical reactions to be carried out in the pores. Several types of catalysts can be loaded into the mesoporous materials using various chemical or physical methods, in order to disperse and fix catalysts (Giraldo et al., 2007). Efficient catalysts have been synthesized using mesoporous material as a carrier in this way. Mesoporous materials as a special carrier supported catalyst, have high efficiency and good catalytic activity. They are also easier to recycle and reuse, especially in large volume chemical reactions.

Active sites: MCM-41 mesoporous material catalytic activities for heterogeneous reactions act out not only when they are independent catalysts, but also when they are loaded with metal or metal compounds (Giraldo et al., 2007).

The MCM-41 wall structure is thought to be amorphous (X. Zhao, Lu, Whittaker, Millar, & Zhu, 1997). So the surface chemical properties of MCM-41 are similar to that of silica. All SiOH groups, i.e., single, hydrogen-bonded, and germinal SiOH groups (**Figure 5**), which could be found on silica surfaces, are also found on MCM-41 surfaces (X. Zhao et al., 1997). The generation of an active acid site depends on single and germinal silanol group structures on the surface wall behaving as Brønsted acid sites (Giraldo et al., 2007). However, the acid strength of the Brønsted acid sites is weak due to the neutrality of silica molecules.

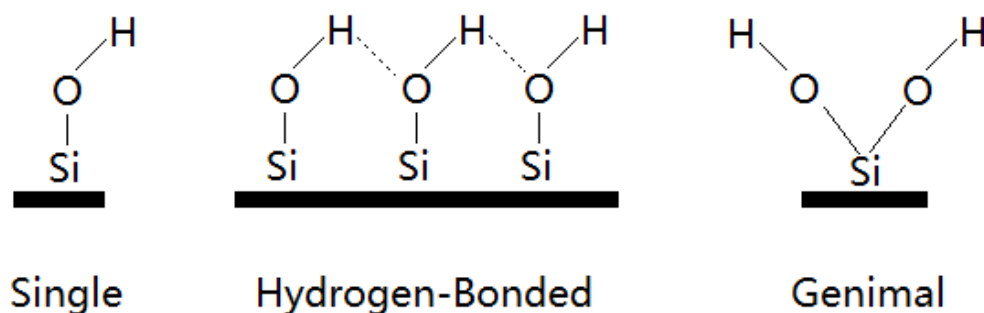


Figure 5 Schematic representation of the three types of SiOH group in siliceous MCM-41 and their characteristics (X. Zhao et al., 1997)

1.1.3 LIMITATION AND DEVELOPMENT OF MESOPOROUS SILICA MATERIAL

Limitation: After several years of development, MCM-41 mesoporous molecular sieves were found to have great potential in adsorption, heterogeneous catalysis and preparation of composite materials (Giraldo et al., 2007). The application of mesoporous materials is mainly based on its structure, but MCM-41 hole wall is thought to be amorphous, lower crystallinity, and poor hydrothermal stability (X. Zhao et al., 1997). Most petroleum processing reactions are under high temperature in the water vapor environment so the traditional MCM-41 leads to poor stability. Therefore, in order to be used in industry, improving the hydrothermal stability is very important.

Development: MCM-41 modification has been mainly developed in three aspects: expanding the pore, loading with heteroatoms and improving its hydrothermal stability.

Expanding the pore: At present, there are several ways to increase the molecular sieves: extension of activated carbon chain length, addition of a swelling agent, post-processing methods etc.

Huo, Q, et al. (Huo, Margolese, & Stucky, 1996) reported MCM - 41 pore sizes are related to the surfactant molecules' alkyl chain length; the pore diameter increases with the increasing carbon chain length of surfactant molecules. Adding some solubilized

hydrophobic substances into surfactant micelle can change the size and shape of the micelles. These methods can significantly increase the pore size of mesoporous molecular sieves.

In 1999, Sayari (Abdelhamid Sayari, Yang, Kruk, & Jaroniec, 1999) reported that a method using ammonium ions as swelling agent was used to synthesise MCM-41 molecular sieve with a larger pore size. In addition to single organic compounds, mixtures can also act as swelling agents. Blin, J. (Blin, Otjacques, Herrier, & Su, 2000) found a mixture of decane and trimethylbenzene can be used as a swelling agent.

Post-processing is dipping catalyst (unburned or calcined) at a certain temperature under its mother liquor or other solutions. It was investigated by Sayari (Abdelhamid Sayari et al., 1999) that dipping the synthesized mesoporous molecular sieve into an ammonium emulsion and holding it at 343 ~ 413K for 3 days can expand molecular sieve pore to as much as three times.

Loading with heteroatom: Because of their weak ion exchange capacity, low acid content and strength, traditional MCM-41 sieves do not have the ability to catalyse reactions. Therefore, researchers are interested in loading heteroatoms on the MCM - 41 sieve to improve their performance. At present, there are two main methods. One is directly mixing with heteroatom during the synthesis. In this way heteroatoms can be loaded into the molecular sieve framework. The other is loading active component on the molecular sieve surface.

In 2009, titanium sulfate was directly impregnated into a calcined MCM-41 material by Wang et al. (Wang et al., 2009). Ti/MCM-41 has many advantages, such as good structural stability, uniform pore distribution and high active center content on the surface of the catalyst (C. L. Chen, Cheng, Lin, Wong, & Mou, 2001; C. L. Chen, Li, et al., 2001; Wang et al., 2009; Xia, Hidajat, & Kawi, 2002).

Choudhary V R et al.(Choudhary, Jana, & Kiran, 2000) added Ga_2O_3 and In_2O_3 onto the surface of MCM-41 material to get $\text{Ga}_2\text{O}_3/\text{MCM-41}$ and $\text{In}_2\text{O}_3/\text{MCM-41}$ catalyst. These two kinds of catalysts showed good catalytic activity for benzyl reaction and acyl reaction. When the Ga_2O_3 and In_2O_3 loading reaches 20%, in a short period of time, benzyl chloride conversion rate reached 90% and the acyl products conversion rate reached 80% (Choudhary et al., 2000).

Improving hydrothermal stability: MCM-41 mesoporous molecular sieves have great potential in adsorption, heterogeneous catalysis and preparation of composite materials. But MCM - 41 in the amorphous state has low crystallinity, so it has poor hydrothermal stability.

At present, the methods to improve the hydrothermal stability of MCM-41 are:

1. Adding inorganic salt or organic amine during synthesis.
2. Some post-processing methods.
3. Using a new template agent to synthesize thick wall mesoporous molecular sieves.

Reyong Ryoo (Ryoo & Jun, 1997) found adding controlled concentrations of inorganic salts in the process of synthesis of MCM-41 mesoporous molecular sieve can improve hydrothermal stability. Experiments showed that this kind of modified molecular sieve in boiling water for 12 hours will not lose its characteristic structure (J. M. Kim, Jun, & Ryoo, 1999). In addition, loading cations (TAA^+ , TPA^+ , TMA^+ and TEA^+) can be used to improve the hydrothermal stability (Das, Tsai, & Cheng, 1999). Experiments confirmed that after loading cationic composite molecular sieves, although the pore size distribution and pore wall thickness have not changed much, it has obviously improved the hydrothermal stability.

That MCM-41's pore structure is in the amorphous state and has some hydroxyl groups on its surface. This is one of the reasons for its low thermal stability. Some of the silicon

hydroxyls are clearly associated with the destruction of the mesoporous molecular sieve framework. Further study found that, the more silicon hydroxyls on the surface of MCM-41 the worse its hydrothermal stability. So that, using silicon alkylation reagent (X. S. Zhao, Lu, & Hu, 1999) to react with silicon hydroxyl in MCM-41 molecular sieve is one of the methods used to synthesis MCM-41 molecular sieves. In this way, the hydrothermal stability of MCM-41 was improved (X. Zhao & Lu, 1998). But raising water thermal stability also increased the hydrophobic property of molecular sieve. This makes that the molecular sieve is only applicable to the no water environment, but not suitable for aqueous reaction.

Increasing the MCM - 41 molecular sieve pore wall thickness is also an effective method to improve the hydrothermal stability. Robert Mokaya (Mokaya, 2001) used per-synthetic molecular sieves as a silicon source, to make the molecular sieve recrystallization in order to increase the pore wall thickness. In this way, Robert successfully improves its hydrothermal stability (Mokaya, 2001).

To improve the hydrothermal stability of MCM-41 mesoporous molecular sieve, new templates can also be used to synthesis materials which have better hydrothermal stability than MCM - 41 mesoporous molecular sieve. For example Zhao (Dongyuan Zhao et al., 1998) synthesized SBA-15 and Kim (S. S. Kim, Zhang, & Pinnavaia, 1998) synthesized MSU-G. These materials not only can effectively broaden the mesoporous range, but also can dramatically improve the hydrothermal stability of mesoporous molecular sieves. After even hundreds of hour's water treatment, these kinds of catalysts can maintain their characteristic structure. This has great potential for development.

Microporous molecular sieves have very good thermal stability and acidity. The synthesis of microporous molecular sieves usually uses small molecule organic amines as template agents. An attempt to use composite template agents, which means using microporous molecular sieve template agents and organic amine molecules to synthesize mesoporous

molecular sieves. In this way a wide range of microporous/mesoporous molecular sieve composite materials can be synthesized.

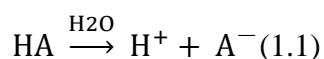
MCM - 41 mesoporous molecular sieve's pore wall is amorphous and there are some hydroxyl groups on its surface, so its hydrothermal stability is poor and difficult to apply in industry. In recent years researchers found many methods to modify MCM - 41 mesoporous molecular sieves, but fewer researchers have been interested in introducing heteroatoms into mesoporous molecular sieves. There have been some methods that are not only complicated, time-consuming, but also have poor results. Therefore, looking for a simple and effective method to improve the stability of heteroatom mesoporous molecular sieve is of vital significance for the practical application of MCM - 41 mesoporous molecular sieves.

1.2 ACID MODIFIED TRANSITION METAL USED IN CATALYSTS

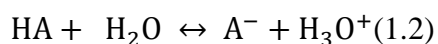
1.2.1 ACID AND SUPER ACID

Acid: There are three common definitions for acids: the Arrhenius definition, the Brønsted -Lowry definition, and the Lewis definition.

Arrhenius acid: The earliest definition of acidity can be traced back to 1880s. In 1884, the Swedish chemist Svante (Miessler & Tarr, 1991) attributed the properties of acidity to hydrogen ions (H^+) or protons. His electrolytic experiments explained that the acid is a substantial increase the concentration of H^+ in the water (Miessler & Tarr, 1991). It can be written as such an equilibrium (1.1):



Brønsted -Lowry acid: In 1923, J. N. Brønsted and T.M. Lowry published their theories separately. The essence of this theory is that an acid is defined to proton donate while a base is defined as a proton acceptor (Brønsted, 1923; Lewis, 1923). The Brønsted acid (HA) can be written as (1.2):



In this equation, this acid (HA) donates an H^+ ion to become A^- , its conjugate base. And water accepts the proton to become H_3O^+ , its conjugate acid. In the reverse reaction, H_3O^+ donates H^+ and A^- accepts it.

Lewis acids: The following theory was published by Gilbert N. Lewis in 1923 (George A. Olah, Prakash, & Sommer, 1985). A Lewis acid is a substance that can accept electrons without specifically having a proton transfer. All electrophilic reagents can be seen as Lewis acids but Lewis acids are not necessarily Brønsted–Lowry acids. As shown in **Figure 6**, in the Lewis approach, a Lewis acid is an electron pair acceptor (LUMO) and a Lewis base is an electron pair donor (HOMO).

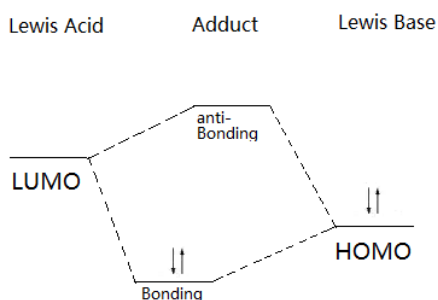


Figure 6 Lewis acid molecular orbital theory

Measurement of acidity: In chemistry, pH is a measure of the activity of the hydrogen ion (Bates, 1964). Pure water has a pH close to 7 at 25 °C. So an acid is a solution with a pH less than 7 and base is a solution with a pH greater than 7. Hydrogen ion concentration (pH) was first published by Danish chemist Søren Peder Lauritz Sørensen at the Carlsberg Laboratory in 1909 (Sørensen, 1909) and defined in 1924 as a modern pH. However, the pH scale has some limitations. Because the activity of the hydrogen ion deviates from simple linearity at pH extremes and in non-aqueous solvents, actual H^+ concentrations cannot be measured using the traditional pH scale (equation 1.3) (George A. Olah et al., 1985).

$$\text{pH} = -\log_{10}(a_{\text{H}^+}) = \log_{10}\left(\frac{1}{a_{\text{H}^+}}\right) \quad (1.3)$$

Superacid: The classical definition of super acid originally coined by James Bryant Conant it is an acid with the acidity greater than that of pure H_2SO_4 (Hall & Conant, 1927). And according to the modern definition, super acid is a medium in which the chemical potential of the proton is higher than in pure sulfuric acid (Himmel, Goll, Leito, & Krossing, 2010). In many cases, super acid is not a pure substance but a mixture such as aqua regia, fluoroantimonic acid and fluoroantimonic acid (“magic acid”), the strongest acid found so far in the system, is about 1000 times stronger than pure sulfuric acid (George A Olah, 2005). For example, fluoroantimonic acid is a mixture of HF and SbF_5 . In the solution fluorine ions and SbF_5 generate stable octahedral structure SbF_6^- . SbF_6^- is a very weak nucleophilic reagent and a very weak base so H^+ become free protons and create a system with extremely strong acidity (Figure 7).

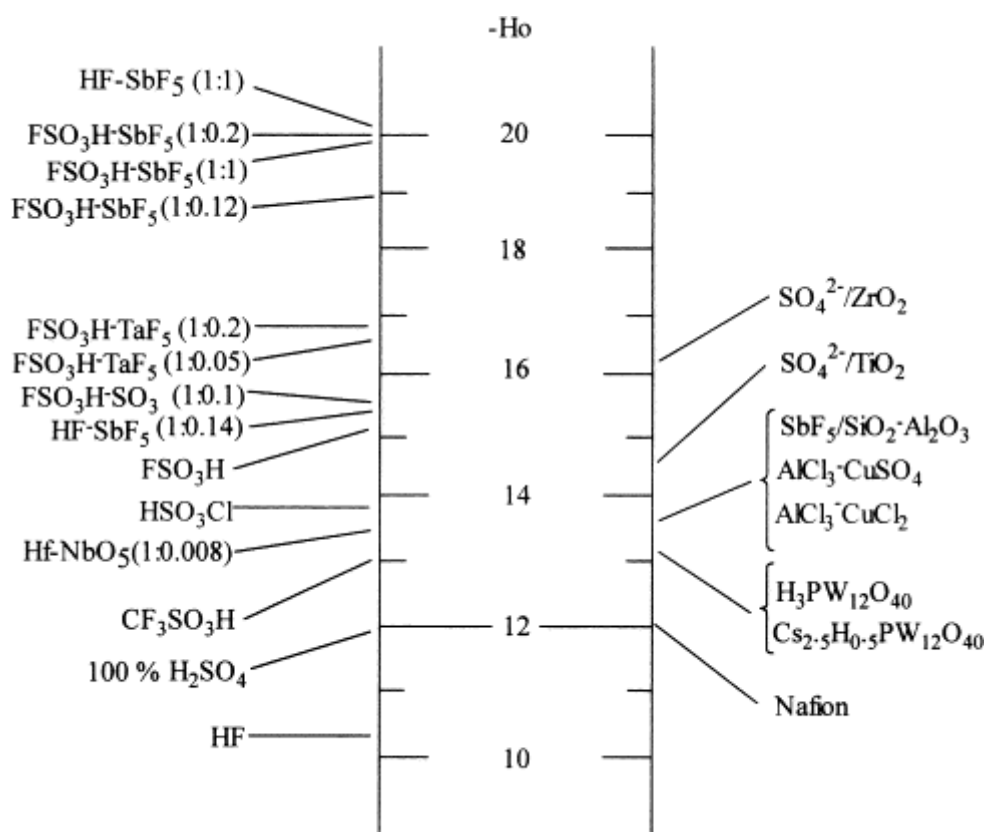


Figure 7 Acid strength of liquid superacids and solid superacids (Schüth & Schmidt, 2002).

Because of the strong acid and strong corrosiveness, some chemical reactions not achieved in the past, can run smoothly under the conditions of a super acid. For example n-butane in a super acid breaks the carbon-hydrogen bonds to generate hydrogen, and can also break carbon-carbon bonds end, generating methane. This does not happen with conventional acids.

In order to measure the acidity of super acid, Louis Plack Hammett proposed a function (equations 1.4 & 1.5) used for measuring very concentrated acid named Hammett acidity function (H_0). It is the best-known acidity function used to extend the measure of Brønsted-Lowry acidity beyond the dilute aqueous solutions for which the pH scale is useful.

$$H_0 = pK_{BH^+} + \log \frac{[B]}{[BH^+]} \quad (1.4)$$

$$H_0 = -\log \left(a_H + \frac{\gamma_B}{\gamma_{BH^+}} \right) \quad (1.5)$$

1.2.2 TRANSITION METALS

The IUPAC definition defines (Naught et al., 2006) a transition metal as “An element whose atom has an incomplete d sub-shell, or which can give rise to cations with an incomplete d sub-shell”. In general, the 38 elements in groups 3 through 12 of the periodic table are called “transition metals” (See **Table 1**).

Like all metals, transition metals are malleable, ductile and conduct electricity and heat. What is interesting is that their valence electrons can appear in more than one shell. This is why they often have more than one stable oxidation state (Bentor, 2012).

Table 1 Transition metal

Group	3	4	5	6	7	8	9	10	11	12
Period 4	Sc 21	Ti 22	V 23	Cr 24	Mn 25	Fe 26	Co 27	Ni 28	Cu 29	Zn 30
Period 5	Y 39	Zr 40	Nb 41	Mo 42	Tc 43	Ru 44	Rh 45	Pd 46	Ag 47	Cd 48
Period 6	57–71	Hf 72	Ta 73	W 74	Re 75	Os 76	Ir 77	Pt 78	Au 79	Hg 80
Period 7	89–103	Rf 104	Db 105	Sg 106	Bh 107	Hs 108	Mt 109	Ds 110	Rg 111	Cn 112

Characteristics of the transition metals: A transition metal is always described as a d-block metal is the portion of the periodic table from group 3 to group 12 (Housecroft & Sharpe, 2001). For example, Ti (titanium), $[\text{Ar}] 3d^1 4s^2$, Cr (chromium), $[\text{Ar}] 3d^5 4s^1$, Mo (molybdenum), Fe (iron), $[\text{Ar}] 3d^6 4s^2$, $[\text{Ar}] 4d^5 4s^1$ etc. The electrons with the highest energy in these elements fill in their d-orbital subshell of the second outermost shell (the outermost shell only has 1 or 2 electrons). As a result, in many transition metal oxidation states, there are some unpaired d-electrons (Matsumoto, 2005).

Why transition metal can be used in catalysts: Due to under-filled d-orbitals, transition metal oxides have an obvious difference from other metal oxides. Because many transition metal elements have many single electrons in their configuration, most of transition metals exhibit more than one oxidation state (e.g. iron has +2, +3, and chromium has +2, +3, +6).

In the case of copper (Cu), the single electron on 4s orbital is easy to lose to form a cuprous ion. Because cupric has higher hydration energy, cuprous loses an electrons in d-orbital to form a stable structure in solution (see electronic structures **Scheme 1** below).

Cu	$[\text{Ar}] 3d^{10} 4s^1$	
Cu ⁺	$[\text{Ar}] 3d^{10}$	losing $4s^1$
Cu ²⁺	$[\text{Ar}] 3d^9$	losing $4s^1$ then $3d^1$

Scheme 1

The rich electron states of transition metal ions can help electron movements of their d-orbitals. Transition metal ions may lose electrons or capture electrons, so they have strong oxidation/reduction performance. Thus transition metal oxides easily form intermediates in catalytic reactions, thereby reducing the reaction activation energy, in order to promote the reaction (Rao & Raveau, 1995).

Another feature of the transition metal oxides is the surface adsorption of the metal elements (Rao & Raveau, 1995). Electron transfer between adsorbent and transition metal oxides, a space charge layer created on the surface of metal oxide, at the same time, a boundary layer appeared on the catalyst surface (See **Figure 8**).

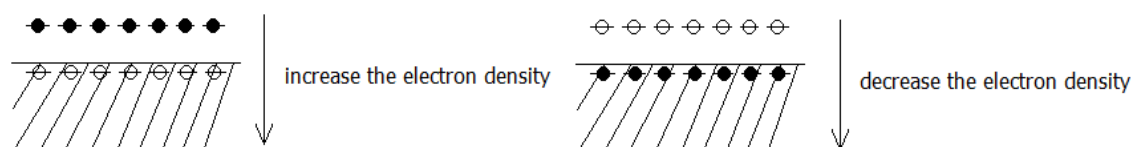


Figure 8 Surface electron transfer

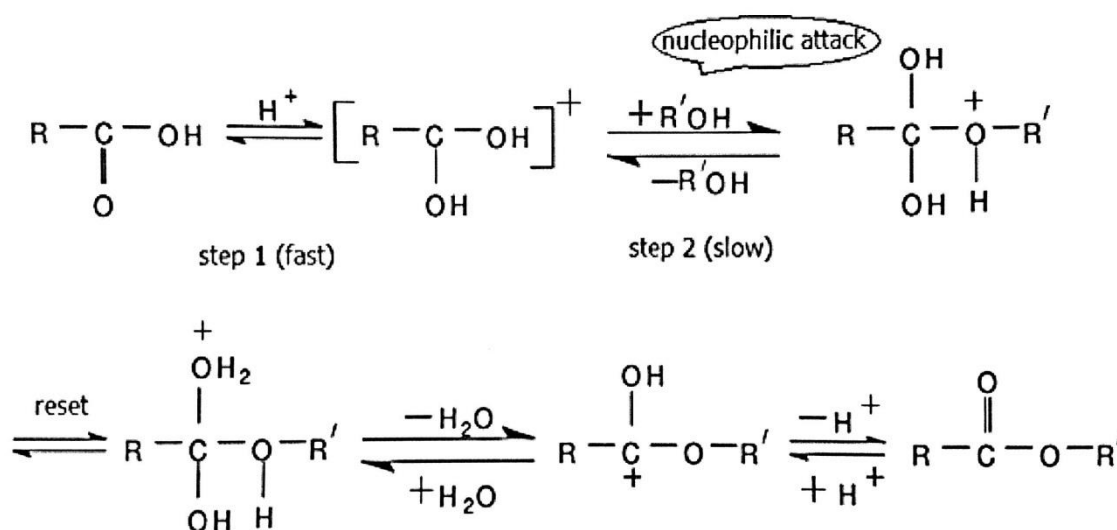
In addition transition metal oxide ions have heat resistance, strong toxicity resistance, and also have the characteristics of optical, thermal, impurity sensitivity. Because of these reasons, a lot of transition metal oxides are considered to be ideal catalysts.

Preparation of sulfate transition metal oxide catalysts. The nature of the sulphate metal oxide largely depends on the nature of precursor substances. As well, some synthetic conditions can also change the nature of these substances, such as the kinds of sulfating agents, different impregnation methods, and the calcinations temperatures (George A. Olah et al., 1985). There are a lot of different preparation methods that can be used, but all these methods have three common purposes (George A. Olah et al., 1985; Yadav & Nair, 1999): Increasing specific surface area, improving the acidity and improving the ability of acid remaining after calcinations (higher than 500°C). In addition, most of them are easy to regenerate and reuse (George A. Olah et al., 1985; Yadav & Nair, 1999).

Catalytic performance Sulfate transition metal oxides can be used in a lot of organic reactions as a super acid. Stable carbocations are easily changed by nucleophiles. In these reactions the super acid medium itself will accept the protonation effect, thus preventing any further electrophilic attack. In this way, many new selective reactions achieve high yields (George A Olah, Prakash, & Sommer, 1979). Olah's early

investigations of the structure of the cations formed in these reactions resulted in a very useful in organic synthesis (George A Olah et al., 1979). Selectivity of the reaction is based on the fact that usually only the thermodynamically more stable ionic reaction, leads to high selectivity (George A Olah et al., 1979). So this kind of catalyst is mainly used in organic conversion reactions such as carboxylation, formylation, esterification, polymerization, acylation of aromatic and alkylation of aromatic hydrocarbons (George A. Olah et al., 1985).

For example, in esterification super acid is used to promote nucleophilic attack (see scheme 2).



Scheme 2 (Kulkarni, Chaudhari, & Mishra, 2013)

In this type of acid catalytic reaction, H^+ always attack firstly which resulting in a carbon cations. Carbon cations are easily combined with anionic to form relatively stable ion pair. This process reduces the activation energy, thus it is advantageous to the reaction.

1.2.3 LIMITATIONS AND DEVELOPMENT OF SUPERACIDS

Advantages and Limitation: In the petrochemical industry, the acid catalytic reaction involves hydrocarbon cracking and restructuring, heterogeneous oil refining process,

and also involves olefins hydration, polymerization, aromatic alkylation, aromatic acetoxylation and alkyd esterification of petrochemical. Superacids are an important industrial foundation of a series of solid acid catalysts (George A. Olah et al., 1985). In today's production process liquid acid is mainly used as an acid catalyst. Although the process is very mature, developing environmental damage is inevitable, and also there exists unavoidable and insurmountable shortcomings with homogeneous catalysis. For example corrosion of equipment, continuous production problems, poor selectivity, and the catalyst is hard to separate from products. Overcoming the drawbacks of liquid acid, a solid acid is easily separated from the liquid phase reaction system, does not corrode equipment, has simple post-treatment, less environmental pollution, high selectivity, etc (Ecormier, Wilson, & Lee, 2003; Sohn & Seo, 2003). Also, solid acid can be used in a higher temperature range, expanding on the thermodynamic potential of the application scope of acid catalytic reaction and can be reused.

In a one-component solid super acid catalyst, it was found that the main active component in the reaction, the sulfuric acid is easily lost, especially under the conditions of high temperature. This kind of one-component solid catalyst has good initial catalytic activity, but the life is shorter.

The limitation of solid super acid catalyst is mainly manifested in the deactivation:

- ① Losing acidic centers: In esterification, water or water vapor will contact with SO_4^{2-} on the surface of catalyst. The reduction of the acidic center causes acid catalyst activity decrease.
- ② Carbon deposits: Because of the reactants and products adsorption, stripping and surface reaction. Carbon and impurities will adsorb, deposit on catalysts' active site and decreased the activity of the catalyst (Matsushashi, Sato, & Arata, 2004).
- ③ Reduction of sulfur ions: Due to the 'poison' in the system, promoter S will be reduced by some solvents and products. When S was reduced from +6 to +4, the

electronegativity of sulfur and metal dropped significantly. Sulfur and metal oxide coordination mode changes, causing the surface acid strength to decrease, and loss of catalytic activity.

The above three kinds of inactivation is temporary only. Through washing, drying, acidification and calcination, added active sites restore the activity of catalyst.

Development: Improvement of SO_4^{2-} super acid catalysts has the following requirements:

- ① Increasing the surface area, improving the catalytic activity of catalysts, improving stability.
- ② Prolong the service life
- ③ Adjusting the acid strength and density of the catalyst (Matsushashi et al., 2004).

Carrier can provide proper specific surface area, increasing acid density, acid type, poison resistance and improve the mechanical strength, etc., Modification research has focused on:

- a. The metal oxide (ZrO_2 , TiO_2 and Fe_2O_3) for maternal, adding other metal or oxide formed multiple sets of solid super acid;
- b. Loading with a rare earths;
- c. Modification with specific molecular sieves and nano-scale metal oxides.

Loading with other metals or metal oxides: The preparation of solid super acid catalysts requires the addition of metal oxide. Some oxides such as MgO , CaO , CuO , ZnO , CdO , La_2O_3 , MaO and ThO_2 , etc., after processing with suitable concentrations of SO_4^{2-} , its acid catalytic activity does not improve. It suggests that not all of the metal oxide have conditions for the synthesis of a solid super acid, because it is not only associated with the electronic structure of oxide, but also related with the

electronegativity of the metal ions and the size of the coordination number. S/ZrO₂, S/TiO₂ and S/Fe₂O₃ are common superacids.

Electronegativity and the coordination number of the metal oxides seriously influences the coordination structure. So some of them can not form superacids, or simply generate the corresponding sulfate which has a relatively weak acidity. Moreover the formation of super acid is associated with the crystalline state of oxide. Metal oxide and SO₄²⁻ ions mainly have three kinds of coordination modes: monodentate, chelating and bridging (see below). Infrared spectrum (IR) analysis shows that the three kinds of structure in the solid surface produces a strong Lewis acid or Brønsted–Lowry acid. These acid sites are used as active centers in catalytic reactions.

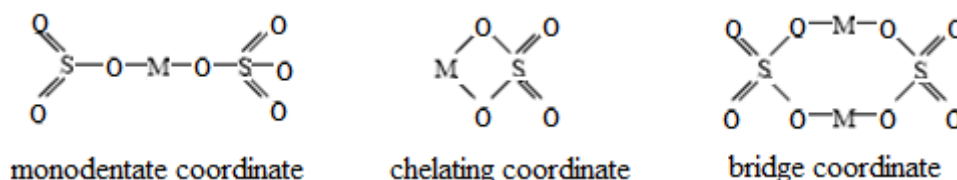


Figure 9 Three kinds of coordination modes

Lu Guanzhong (Dongsen, Guanzhong, Qinglin, & Wenkui, 2001) loaded Al into catalysts to prepare SO₄²⁻/Ti-2Al₂O solid super acid in 2002. When the titanium to aluminum atomic ratio is two. The new catalyst performance is better than that of SO₄²⁻/TiO₂, and has been used to synthesize dioctyl phthalate (DOP). The catalyst characterization results confirmed that in the titanium base solid super acid, adding a certain amount of aluminium can increase the specific surface area significantly. It is possible to produce weak acid, medium strong acid and super acid centers on the surface. It is argued that the active site is likely to be a moderate acid on the surface of the catalyst for the reactions in the synthesis of DOP (Dongsen et al., 2001).

Loading with rare earth elements: In recent years, adding some rare earth elements in the process of solid super acid preparation in order to improve the catalyst performance has attracted a lot of interest. A small amount of rare earth elements can change the

chemical state on the surface of the catalyst, increasing the catalyst surface element polarization degree in order to improve the activity and life of the catalysts.

Research (Lin, She, Pan, Chen, & Huang, 2000) shows that adding rare earth Dy_2O_3 can improve $\text{SO}_4^{2-}/\text{Fe}_3\text{O}_4$ iron-based solid catalyst activity, improve the stability of the synthetic reaction. Reddy, etc. produced a new type of catalyst $\text{SO}_4^{2-}/\text{Ce}_x\text{Zr}_{1-x}\text{O}_2$ which showed good structure stability even at 913 K (Reddy, Sreekanth, Lakshmanan, & Khan, 2006). Studies have shown that $\text{Ce}_{0.16}\text{Zr}_{0.84}\text{O}_2$ crystalline phases formed because of the strong interaction between SO_4^{2-} and ZrO_2 which leads to the formation of a surface acidity (Reddy et al., 2006). A mixture of Ce-Zr hydroxide colloid and sulfuric acid roasted under 923 k, lead to the formation of super acid catalyst. Without sulfuric acid modification, catalyst acidity was found to be weak (Reddy et al., 2006).

Introducing molecular sieves : In recent years, many researchers have attached importance to the modification of $\text{SO}_4^{2-}/\text{M}_x\text{O}_y$ type solid super acid catalyst to make it have a certain pore structure. Loading zirconium or titanium oxide onto the molecular sieve then treatment with sulfuric acid yields a catalyst with high specific surface area and a range of pore structures.

Studies of $\text{S}_2\text{O}_8^{2-}/\text{TiO}_2\text{-MCM-41}$ (J. Chen, Sun, Tang, Guo, & Wang, 2006) have shown that: this kind of solid super acid keeps MCM - 41 mesoporous structure. The specific surface area can reach as large as $211\text{m}^2/\text{g}$, and has strong acidity ($\text{H}_0 < -12.70$). If it used for catalysis of acetic acid with isoamyl alcohol, the esterification rate can reach more than 98% (J. Chen et al., 2006).

Introducing crosslinking agents: Guo Xikun etc. (Guo, Lin, Fu, & Deng, 2002) successfully synthesized mesoporous super acid $\text{SO}_4^{2-}/\text{SiZrR}$. Experiments show that, after 500°C calcinations, $\text{SO}_4^{2-}/\text{SiZrR}$ has strong acidity ($\text{H}_0 < -11.93$), the most probable pore distribution is 2.3nm and a mesoporous structure. Its super acid center is a Lewis acid and the major center of catalytic activity (Guo et al., 2002). Employment of these catalysts in the esterification of salicylic acid and n-butyl alcohol showed a significant

improvement in performance compare to traditional sulfuric acid catalyst. Salicylic acid conversion rate reached as high as 86.85%, the esterification selectivity reached up to 99.5% (Guo et al., 2002).

Introducing of magnetic materials: Magnetic materials produce the solid super acid in the form of micro-particle with nanometer ranges and has many advantages. Because the catalyst particle size is so small, it is not easily separated from the reaction system but magnetic catalyst particles can use magnetic separation to remove the catalyst.

Xiangyu Shi etc. (Shi & Wang, 2006) synthesis magnetic nanometer-sized solid superacids $\text{SO}_4^{2-}/\text{Fe}_3\text{O}_4\text{-ZrO}_2$ and used them for the synthesis of adipic acid octyl ester. Under certain conditions, the conversion rate of adipic acid was 99%.

Nanoparticles catalyst can be rapidly separated with magnetic systems giving recovery rates as high as 93.8% (Shi & Wang, 2006).

Using other groups instead of SO_4^{2-} : Sohn impregnated $\gamma\text{-Al}_2\text{O}_3$ with $\text{Zr}(\text{SO}_4)_2$ solution, and after high temperature calcination, a $\text{Zr}(\text{SO}_4)_2/\gamma\text{-Al}_2\text{O}_3$ catalyst was produced (Sohn & Seo, 2003). When the content of $\text{Zr}(\text{SO}_4)_2$ in the catalyst reached as high as 50%, there was no characteristic peak of $\text{Zr}(\text{SO}_4)_2$ in the XRD trace. It means $\text{Zr}(\text{SO}_4)_2$ has well dispersed on the surface of $\gamma\text{-Al}_2\text{O}_3$.

Recently there have been other ways to replace SO_4^{2-} as a catalyst. Furuta etc. introduce some chalcogen elements (Se, Te) into the super acid preparation (Furuta, Matsushashi, & Arata, 2004). The method was to dip amorphous zirconium hydroxide in H_2SeO_4 or H_6TeO_6 . This kind of super acid catalyst has a strong effect on oxidative dehydrogenation (Furuta et al., 2004). The selectivity for catalytic oxidation of acetone reached as high as 100%.

1.3 TRANSITION METAL OXIDES SUPPORTED ON MESOPOROUS SILICA

1.3.1 ADVANTAGES OF TRANSITION METAL OXIDES MODIFIED CATALYSTS

Transition metal oxides modified MCM-41 have the advantages of super acid and molecular sieves. After modification, the new catalyst not only has strong acidity, but also a large specific surface area and high porosity. MCM-41 catalyst modified with metal oxides also has a good thermal stability in presence of water and high mechanical strength. Although some of the modified catalyst acidity is weaker than that of the unmodified, but on the whole, metal oxide modified MCM-41 catalysts have a high content of active sites on the catalyst surface, uniform pore distribution, adequate pore volumes, stable performance, long service life and can be easily recycled (Wang et al., 2009).

1.3.2 SYNTHESIS METHODS

There are many synthesis methods for MCM – 41: hydrothermal synthesis methods, room temperature synthesis, roasting synthesis, microwave synthesis, synthesis in vapor phase, dry powder synthesis, direct impregnation method to name a few reactions. Here several common synthesis methods will be introduced.

Hydrothermal synthesis method : This refers to under temperature of 100 ~ 1000°C and pressures of 1 Mpa ~ 1 Gpa. Reported by Zhao et al.(Q. Zhao, Yin, Jiang, Yin, & Tang, 2007) Cu/MCM-41 was synthesized using the hydrothermal synthesis method. Sodium silicate and cupric chloride dissolve in distilled water respectively, and then CTAB was adding into sodium silicate solution drop by drop. This was stirred for 10 minutes and a cupric chloride solution was added slowly. The maxture was dried and calcined. This produced the Cu-MCM-41 mesoporous molecular sieve (Q. Zhao et al., 2007).

The process of the hydrothermal synthesis is relatively simple and easy to control.

However physical properties of the solvents (density, viscosity, etc.) are easy to affect the synthesis, and the products are not very stable. Further, the hydrothermal synthesis

method is slow and the whole process generally need 5 ~ 7 days. So it is not good for many practical applications.

Microwave synthesis method: Microwaves are very short wavelength electromagnetic waves (Tsuneo Yanagisawa, Toshio Shimizu, Kazuyuki Kuroda, & Chuzo Kato, 1990). Microwave heating is different from the ordinary of conduction and convection heating. It has many features, such as rapid heating, uniform heating and high penetration. Microwave heating can greatly shorten the crystallization time, and produce uniform crystalline grains. Therefore microwave heating has been widely applied in the preparation of molecular sieves.

Wu, etc. (Wu & Bein, 1996) reported that by adjusting the microwave time, reaction temperature, concentration of template agent, silica and alumina ratio etc. MCM – 41 molecular sieve with high crystallinity and thermal stability could be synthesized. Zhang etc. (Zhang & Chu, 1998) first used a microwave radiation method. Materials were crystallized under microwaves for 15 minutes. Then the microwave power was increased to roast the sample for 1 hour. This yields MCM–41 as a white crystalline powder. The results of synthesis MCM – 41 mesoporous material using microwave radiation show that microwave synthesis method has a lot of advantages (Yao, Zhang, & Yang, 2001). These advantages include convenient operation and saving time. In addition, the product has structure stability, uniform particle size distribution, specific surface area, high porosity and good thermal stability. Kresge et al. (C. Kresge et al., 1992) thought that using microwaves to synthesise molecular sieves, not only can reduce the amount of template agent and shorten the crystallization time, but also may affect the types of synthetic molecular sieves produced.

Direct impregnation: Impregnation method is based on the active components impregnated into the porous carrier. The active components are in a salt solution and penetrate into the inner surfaces. This give a highly efficient catalyst.

To introduce transition metal ions into molecular sieve, strongly acidic solution will break the skeleton structure of the molecular sieve. In order to solve this problem, the direct impregnation method was used by Wang et al. to form S-TiO₂/MCM-41 (Wang et al., 2009). In this study, titania sulfate was directly impregnated into the mixed solution instead of into the as-synthesized molecular sieves. In this way, the S-TiO₂/MCM-41 catalyst can be synthesized directly and titanium can be evenly distributed inside the molecular sieve pore (Wang et al., 2009). In addition, more than 50% of titania can be loaded then using as-synthesized MCM-41 molecular sieve.

1.3.3 PAST WORK AND CURRENT GAP

Past work: Wang et al. (Wang et al., 2009) reported that Ti-MCM-41 was synthesized in 2009 using the direct impregnation method. In their work, titania sulfate was loaded into the molecular sieve without blocking the pores and the new catalyst showed high activity and selectivity in esterification of acetic acid and *n*-butanol. Shengkai Li (Li, 2011) carried out a similar synthesis in 2011 using two different transition metal salt (Zr(SO₄)₂ and Fe₂(SO₄)₃).

Current gap: Although there are many studies of mesoporous catalyst, few studies about other transition metal modified mesoporous catalysts. The effect of this kind of catalyst synthesized with other transition metal is worth further investigate.

1.4 RESEARCH OBJECTIVE

Objective: Based on the study of Shengkai Li (Li, 2011) on zirconia sulfate and ferric oxides sulfate and study of Wang et al. (Wang et al., 2009) on titania sulfate, the aim of this research was to synthesise VI subgroup element (Cr and Mo) modified MCM-41 molecular sieve using the direct impregnation method and analyze some of the properties of the new-synthesized catalyst and their catalytic activity.

1.5 EXPERIMENTAL DESIGN

Chromium and molybdenum modified MCM - 41 mesoporous molecular sieves were

synthesized using the direct impregnation method. Their catalytic activities were tested with acetic acid and *n*-butyl alcohol esterification reaction, and the catalyst's structure, aperture, acidity, etc. was analyzed by techniques such as SEM and FTIR.

Catalysts synthesis: In this synthesis, tetraethyl orthosilicate (TEOS) was used as the silica source and cetyl trimethylammonium bromide (CTAB) was chosen as the template solution. In alkaline solution, TEOS, CTAB mixed with metal salt (chromium sulfate and molybdate) to form the modified mesoporous molecular sieve structure. In these mixtures, the metal content accounted for 1% ~ 50%. After stirring for 2 hours the corresponding sol-gel was formed. Through crystallization at 100°C and calcination at 550 °C, Cr-MCM-41 and Mo-MCM-41 were synthesized as the final catalysts. The synthesis process as shown in the figure below:

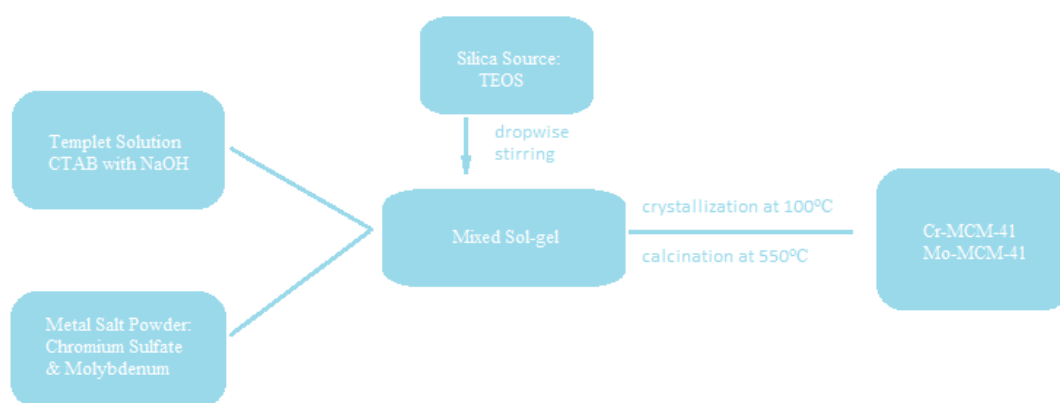


Figure 10 Synthesis path direct impregnation method

Catalytic activity test: The catalytic activity of these two catalysts was evaluated by esterification reaction. Acetic acid and *n*-butanol reactions were used and the acidity before and after reaction were determined to evaluate the catalytic activity of catalysts loading different types and different concentrations of metal. KOH titration was used to test the catalytic activity and gas chromatography (GC) was used to test the selectivity of the catalyst.

Characterization of catalysts: The catalysts synthesized were characterized by following

methods: scanning electron microscopy (SEM), X-ray diffraction (XRD), nitrogen adsorption, diffuse reflectance infrared fourier transform spectroscopy (DRIFT), hammett indicators and thermal gravimetric analysis (TGA). As listed in **Table 2**, catalyst's pore structure and physical nature were analyzed by scanning electron microscopy and powder X-ray diffraction. Then the nitrogen isotherm adsorption method was used to measure the surface area of synthetic samples. Diffuse reflectance infrared fourier transform spectroscopy can identify the type of acid and their active sites after adsorbing pyridine. Hammett indicators were used to identify molecular sieves' acidity. Finally, thermal gravimetric analysis (TGA) was used to record the decrease of weight with increasing the temperature in order to find out the applicable scope of the catalyst.

Table 2 Techniques used for catalyst characterization

Methods	Objects
<i>Physical properties</i>	
SEM	Pore structure
N ₂ adsorption isotherm	Surface area
<i>Acid tests</i>	
DRIFT	Types of acid and active sites
Hammett Indicator	Acid strength
<i>Temperature tests</i>	
TGA	Weight changes with temperature

Data analysis: The data for the catalytic activity of the different catalysts was collected and compared. The results are shown in the graphs in Chapter 3. In addition, some other characterization results of the catalysts are discussed from pictures, graphs and tables for further study.

CHAPTER 2 EXPERIMENTAL METHODS

2.1 CATALYST SYNTHESIS

2.1.1 CHEMICAL REAGENTS

Silica Source: The linear formula of tetraethyl orthosilicate (TEOS) is $\text{Si}(\text{OC}_2\text{H}_5)_4$. This molecule consists of four ethyl groups and a SiO_4^{4-} center (see **Figure 11**). TEOS (CAS No. 78-10-4, Acrös Organics, 98 %, 1L, ThermoFisher) is a colorless liquid with slight mint smell which has a molecular weight 208.33. In this study, TEOS was used as a silica source in order to synthesize MCM-41 molecular sieve.

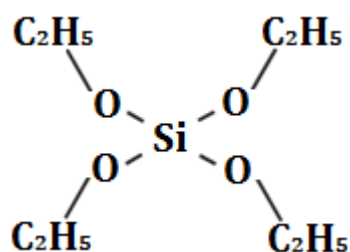


Figure 11 Tetraethyl orthosilicate (TEOS)

Template solution: The linear formula of Cetyltrimethylammonium bromide (CTAB) is $\text{CH}_3(\text{CH}_2)_{15}\text{N}^+(\text{Br})^-(\text{CH}_3)_3$. It is a white powder with a pungent smell whose molecular weight is 336.45. Because of CTAB's long chain structure (see **Figure 12**), it is easy formed tubular micelles used as the template for the catalyst formation. CTAB (CAS No. 57-09-0, AJAX Chemicals, 95%, 500g, Fisher Chemical) mixed with an NaOH solution are used as a template solution in the synthesis.

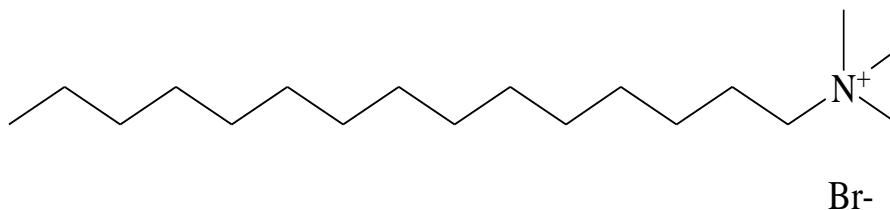


Figure 12 Cetyltrimethylammonium bromide (CTAB)

Metal Salt: Two metal salts were used in this synthesis: chromic sulfate and ammonium molybdate. Chromic (VI) sulfate with 15 waters of crystallization $[\text{Cr}_2(\text{SO}_4)_3 \cdot 15\text{H}_2\text{O}]$,

CAS Number 15244-38-9, Molecular Weight 662.41, B.D.H. Laboratory chemicals and ammonium molybdate $[(\text{NH}_4)_6\text{Mo}_7\text{O}_{24} \cdot 4\text{H}_2\text{O}]$ CAS Number 12054-85-2, Molecular Weight 1235.86, Riedel-De Haen AG Seelze-Hannoven.

2.2 CATALYST SYNTHESIS

The direct impregnation method was chosen in this synthesis. Different concentrations of chromium sulfate or ammonium molybdate were mixed with the template agent (CTAB) and the silicon source (TEOS). After crystallization, washing and calcinations, Cr/MCM-41 and Mo/MCM-41 were synthesized. The following direct impregnation method has been reported by Wang et al. (Wang et al., 2009) and Shengkai Li (Li, 2011).

Different weights of the transition metal salt were dissolved in distilled water. Then cetyltrimethylammonium bromide (CTAB) powder and 2 M NaOH was added to these solutions. While stirring, tetraethyl orthosilicate (TEOS) was added dropwise to the mixture.

The mole ratios of compounds in the mixture was shown below:

$$\text{CTAB:TEOS:NaOH:H}_2\text{O:Metal Salt} = 1.0 : 3.75 : 1.64 : 434 : \text{M\%}$$

The M% means how much metal (as the % element) was added into the mixture. Six different ratios were added in this synthesis: 1%, 10%, 20%, 30%, 40% and 50%. Both chromic sulfate and ammonium molybdate were added using these ratios.

First, MCM-41 molecular sieve without a metal loading was synthesized. The mole ratio of compounds were shown below:

$$\text{CTAB:TEOS:NaOH:H}_2\text{O} = 1.0 : 3.75 : 1.64 : 434$$

To synthesise Cr/MCM-41, by changing the mole ratio of chromium and silicon, different concentration of chromium was loaded into MCM-41 molecular sieve. From 1% to 50%, the mole ratio between chromium and silicon should be:

1% loading $\text{Cr}_2(\text{SO}_4)_3$, Cr:Si = 1 : 99

10% loading $\text{Cr}_2(\text{SO}_4)_3$, Cr:Si = 10 : 90

20% loading $\text{Cr}_2(\text{SO}_4)_3$, Cr:Si = 20 : 80

30% loading $\text{Cr}_2(\text{SO}_4)_3$, Cr:Si = 30 : 70

40% loading $\text{Cr}_2(\text{SO}_4)_3$, Cr:Si = 40 : 60

50% loading $\text{Cr}_2(\text{SO}_4)_3$, Cr:Si = 50 : 50

The same amount of CTAB were used in every preparation. The mole ratio and weight of compounds to synthesis Cr/MCM-41 are shown in the table 4:

Table 3 The ratio of compounds to synthesis Cr/MCM-41

	Cr Loading	CTAB	TEOS	NaOH	H ₂ O	$\text{Cr}_2(\text{SO}_4)_3 \cdot 15\text{H}_2\text{O}$
molecular weight	--	364.4500	208.3300	40.0100	18.0000	662.4100
molecular ratio	1%	0.0100	0.0375	0.0164	4.3400	0.00019
	10%	0.0100	0.0375	0.0164	4.3400	0.00209
	20%	0.0100	0.0375	0.0164	4.3400	0.00469
	30%	0.0100	0.0375	0.0164	4.3400	0.00804
	40%	0.0100	0.0375	0.0164	4.3400	0.0125
	50%	0.0100	0.0375	0.0164	4.3400	0.01875
weight ratio (g)	1%	3.6445	7.8124	0.6562	78.1200	0.1255
	10%	3.6445	7.8124	0.6562	78.1200	1.3850
	20%	3.6445	7.8124	0.6562	78.1200	3.1050
	30%	3.6445	7.8124	0.6562	78.1200	5.3229
	40%	3.6445	7.8124	0.6562	78.1200	8.2801
	50%	3.6445	7.8124	0.6562	78.1200	12.4202

To synthesis Mo/MCM-41, the similar ratios were used as chromium ones:

1% loading $(\text{NH}_4)_6\text{Mo}_7\text{O}_{24}$, Mo:Si = 1 : 99

10% loading $(\text{NH}_4)_6\text{Mo}_7\text{O}_{24}$, Mo:Si = 10 : 90

20% loading $(\text{NH}_4)_6\text{Mo}_7\text{O}_{24}$, Mo:Si = 20 : 80

30% loading $(\text{NH}_4)_6\text{Mo}_7\text{O}_{24}$, Mo:Si = 30 : 70

40% loading $(\text{NH}_4)_6\text{Mo}_7\text{O}_{24}$, Mo:Si = 40 : 60

50% loading $(\text{NH}_4)_6\text{Mo}_7\text{O}_{24}$, Mo:Si = 50 : 50

Because there are seven molybdenum atoms in each mole of ammonium molybdate, the mole ratio and weight ratio of compounds to synthesis Mo-MCM-41 were shown in table 4.

Table 4 The ratio of compounds to synthesis MoMCM-41

	Mo Loading	CTAB	TEOS	NaOH	H ₂ O	$(\text{NH}_4)_6\text{Mo}_7\text{O}_{24}$
molecular weight	--	364.4500	208.3300	40.0100	18.0000	1235.86
	1%	0.0100	0.0375	0.0164	4.3400	0.000054
	10%	0.0100	0.0375	0.0164	4.3400	0.000595
molecular ratio	20%	0.0100	0.0375	0.0164	4.3400	0.001339
	30%	0.0100	0.0375	0.0164	4.3400	0.002296
	40%	0.0100	0.0375	0.0164	4.3400	0.003571
	50%	0.0100	0.0375	0.0164	4.3400	0.005357
	1%	3.6445	7.8124	0.6562	78.1200	0.0669
	10%	3.6445	7.8124	0.6562	78.1200	0.7356
weight ratio(g)	20%	3.6445	7.8124	0.6562	78.1200	1.6552
	30%	3.6445	7.8124	0.6562	78.1200	2.8374
	40%	3.6445	7.8124	0.6562	78.1200	4.4138
	50%	3.6445	7.8124	0.6562	78.1200	6.6207

All sol-gels were treated with 35% ammonia solution (Fisher Chemical) to maintain the pH value around 10.2.

After heating for 48 hours at 100°C in a convection oven (MODEL: MOV-112F,

SANYO, Japan, see **Picture 1**), the samples were washed with water and filtered using a buchner filter. Then they were removed into the convection oven again for drying overnight at room temperature. Finally, the samples were heated for 5 hours at 550°C in a furnace in a fume hood (MODEL: McGregor, NL 200, Auckland, New Zealand, see **Picture 1**). In this manner MCM-41 molecular sieve catalysts with different transition metal loading were synthesized. Catalysts compositions are shown in **Table 5**.



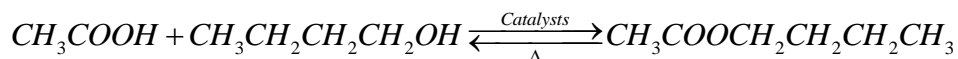
Picture 1 Convection oven (left) and furnace oven (right)

Table 5 The classification of the new synthesized catalysts

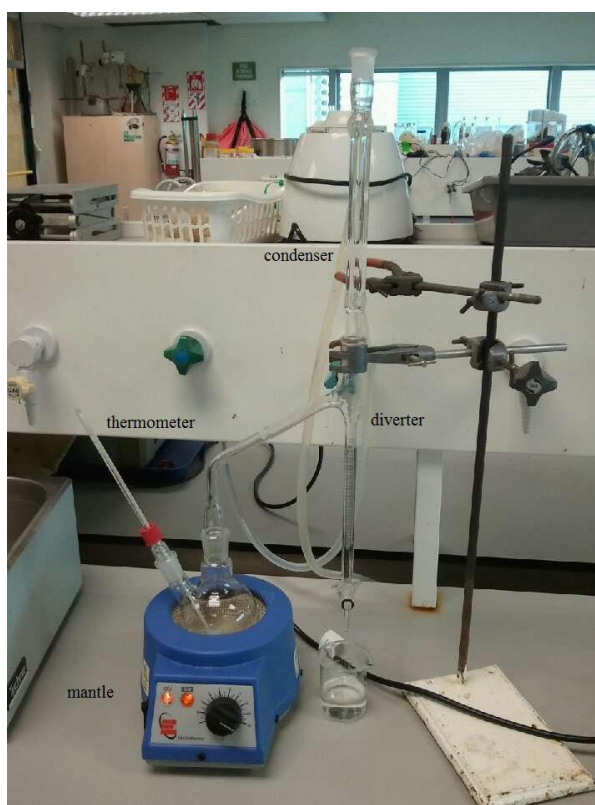
<i>Group 1</i>	Cr_1	Cr_{10}	Cr_{20}	Cr_{30}	Cr_{40}	Cr_{50}
Cr-MCM-41	1wt%	10wt%	20wt%	30wt%	40wt%	40wt%
<i>Group 2</i>	Mo_1	Mo_{10}	Mo_{20}	Mo_{30}	Mo_{40}	Mo_{50}
Mo-MCM-41	1wt%	10wt%	20wt%	30wt%	40wt%	50wt%
MCM-41 were recorded as 'Blank'						

2.3 CATALYTIC ACTIVITY AND SELECTIVITY

Esterification: Glacial acetic acid and *n*-butanol were used to test the activity of synthesized catalysts. The reaction equation is shown below:

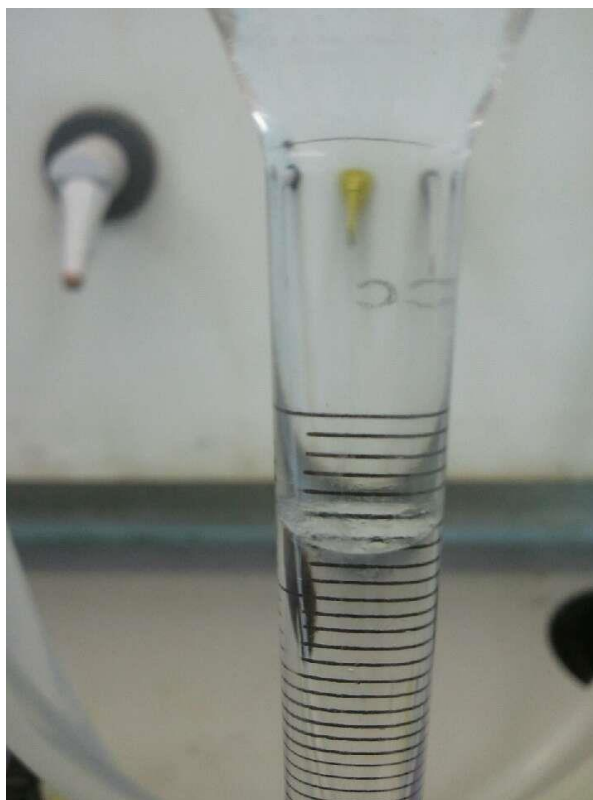


The Dean-Starke apparatus with a mantle, 100 mL round bottom flask and condenser (see **Picture 2**) were assembled to test the catalytic esterification reaction.



Picture 2 The distillation apparatus for esterification

20 mL of glacial acetic acid and 22 mL of *n*-butanol were mixed, then about 0.2 g of one of the catalysts were added into the mixture. The temperature was maintained at between 115°C and 120 °C for 3 hours. During the reaction, excess water was removed by the Dean & Stark apparatus (see **Picture 3**).



Picture 3 Dean & Stark apparatus (organic phase on the top and water phase on the bottom)

The activity of the catalysts was shown from their esterification rates. The esterification rates were measured by the titration of glacial acetic acid content in the mixture before and after the reaction. The titration method was shown below:

1. **Preparation of ethanolic KOH:** 35g solid KOH was weighed and dissolved in 100 mL of distilled water. Then the solution was moved into a 1 L volumetric flask and diluted to the mark with 95% ethanol. After mixing well, the solution was transferred into a plastic bottle and stood for 24 hours at room temperature. The supernatant liquid was collected for further use.
2. **Standardization:** Accurately weighed 0.2 ~ 0.3 g of potassium hydrogen phthalate and dissolved in 40 mL distilled water. After boiling to remove CO_2 , 2~3 drops of phenolphthalein were added and titrated with the KOH/ethanol solution. The calculation is shown below:

$$C(KOH) = \frac{m_{php}}{V_{KOH} \times 0.2042}$$

m_{php} ---The weight of potassium hydrogen phthalate

V_{KOH} ---The volume of KOH solution

3. **Titration:** 1 mL of glacial acetic acid and n-butanol mixture (1:1.1 v/v) was transferred into 50 mL conical flask and titrated with 0.05 M KOH ethanol standard solution. Phenolphthalein was used as the indicator. The titre of the KOH ethanol standard solution was recorded as V_0 when the solution turned pink. The same titration method was used for the reaction products (from the round bottom flask). The titre of KOH solution was recorded as V_t ('t' means reaction time). So the esterification rate can be written as:

$$\text{Esterification rate} = \frac{V_0 - V_t}{V_0} \times 100\%$$

SHIMADZU 2010 gas chromatograph (Shimadzu, Kyoto, Japan) with a flame ionization detector (see **Picture 4**) was used to measure the selectivity of the catalyst and check rate of reaction as determined by titration. The same volume of the samples before and after reaction were analyzed by the GC method, the peak numbers and peak areas were recorded for data analysis. Gas chromatography parameters were shown in **Table 6**.



Picture 4 SHIMADZU 2010 gas chromatography with autoinjector

Table 6 GC Parameters

Items	Parameters
Column	ZP-Wax
Column Temperature	Temperature Programming*
Detector	FID
Detector Temperature	250°C
Injection Temperature	250°C
Pressure	100.0 kPa
Total Flow	124.3 mL/min
Column Flow	1.19 mL/min

* Temperature Programming: Keep 80 °C for 2 minutes and increase to 160 °C as a ratio 20 °C /min.

2.4 CHARACTERIZATION

2.4.1 SCANNING ELECTRON MICROSCOPE

Pretreatment: Catalyst powder was compressed using compressor and a small piece of compressed sample was sputter coated using a MODEL:E1045 Ion Sputter Coater (Hitachi, Japan), see **Picture 5**.



Picture 5 E1045 Ion Sputter Coating Unit

SEM analysis: Samples after coating were removed into the sample chamber of scanning electron microscope (MODEL: SU-70 FESEM, Hitachi, Japan, see **Picture 6**).



Picture 6 SU-70 FESEM (Field Emission SEM)

2.4.2 DIFFUSE REFLECTANCE INFRARED FOURIER TRANSFORM SPECTROSCOPY

Diffuse reflectance infrared fourier transform (DRIFT) is an infrared spectroscopy spectrum technique used on powder samples without tableting. In this study the DRIFT tests include two parts: pretreatment with pyridine and FT-IR detection.

Pretreatment with pyridine: Pyridine or ammonia molecules bind to the acidic sites in the catalyst and are typically used as a probe molecule. Because pyridine has better thermal stability than ammonia, and because its infrared signature is easier to see, it was selected in this pretreatment. Before this pretreatment, catalysts were heated at 550 °C for 2 hours in order to remove the H₂O and CO₂ in the pores. After the samples were placed in an ‘in-situ’ cell, pyridine was moderately heated and introduced into the cell for half an hour. The equipment is shown in **Picture 7**. And samples were then placed in a dessicator with pyridine vapor atmosphere overnight.



Picture 7 ‘in-situ’ cell vacuum unit for pyridine pretreatment

Diffuse reflectance measurements by infrared Fourier transform spectrometry

reflectance (DRIFT) detection: Infrared spectrophotometer (MODEL: Prestige-21 Infrared spectrophotometer, SHIMADZU, Kyoto, Japan) equipped with a Pike Technologies “Easydif” DRIFT accessory was used (see **Picture 8**). The spectra of the treated samples were recorded on the computer. The wavelength range was used from 1700 cm⁻¹ to 1400 cm⁻¹. Samples were preconditioned at selected temperatures from

room temperature ($\sim 23^{\circ}\text{C}$) to 500°C in order to look for the pyridine desorption temperature.



Picture 8 Prestige-21 Infrared spectrophotometer SHIMADZU, Kyoto, Japan

FT-IR absorption: All catalyst samples were analyzed without dilution and compression. The spectrum was recorded between 4000 cm^{-1} and 525 cm^{-1} using another spectrophotometer (MODEL: Nicolet iS10 FT-IR Spectrometer, Thermo Scientific, USA, see **Picture 9**).



Picture 9 Nicolet iS10 FT-IR Spectrometer, Thermo Scientific, USA

2.4.3 POWDER X-RAY DIFFRACTION (XRD)

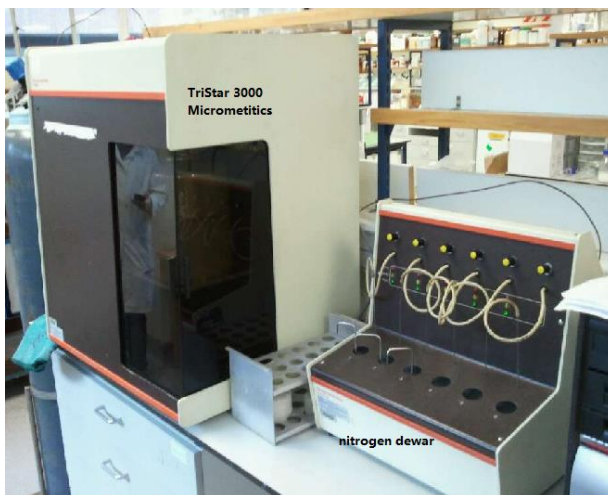
The powder X-ray diffraction (XRD) patterns of these two groups of samples and MCM-41 were analysed on the SIEMENS D5000 diffractometer (Madison, WI, U.S.A.) (see **Picture 10**). CuK α radiation (wavelength $\lambda = 0.15406$ nm) was chosen at 40 kV and 50 mA. The 2θ angle was recorded from 10° (min) and 90° (max) with a scanning rate of $2^\circ/\text{min}$. The diffraction intensity in different angles were recorded and plotted.



Picture 10 SIEMENS D5000 diffractometer

2.4.4 NITROGEN ADSORPTION-DESORPTION ISOTHERM METHOD

The catalysts surface area and porosity was analyzed using nitrogen adsorption-desorption isotherm method. The TriStar 3000 Micrometitics (Norcross, GA, U.S.A., see **Picture 11**) was chosen for this analysis.



Picture 11 TriSTAR 3000 micromeritics and nitrogen dewar

All samples were outgassed at 100 °C overnight before using. For each sample, after about 20 hours of adsorption, the equilibrated pressure (P) and the saturation pressure (P_0) of nitrogen were recorded. This measurement was always happen in a liquid nitrogen bath to keep a low temperature (-196 °C). At this temperature, because of its low cost and inert nature, nitrogen is an ideal adsorbent. Because nitrogen can be uniformly adsorbed on solid surface and filled the pore. Specific surface area and pore diameter can be measured accurately through some theory, i.e. B.E.T. and B.J.H. theory (Li, 2011; Osborne, 2004).

2.4.5 HAMMETT INDICATORS FOR ACID STRENGTH MEASUREMENT

Acid strength: The acid strength for two groups of transition metal loading MCM-41 catalysts using Hammett indicators was referred by J.L. Ropero-Vega et al. (Ropero-Vega, Aldana-Perez, Gomez, & Nino-Gomez, 2010).

A small amount of sample (about 10 mg) was soaked in 5 mL benzene for 24 hours. Then two drops of indicator were added. After standing for half an hour at room temperature, the colour change was recorded to identify the sample as ‘acid’ or ‘base’.

Indicators (See **Picture 10**) and their color ranges are shown in **Table 7**.

Table 7 Hammett indicators used for acid strength measurement

Indicator	pK_a	Acid color	Basic color
Bromothymol blue	+ 7.2	Yellow	Blue
Methyl red	+ 4.8	Red	Yellow
Cresol bromine green	+ 3.8	Yellow	Blue
Thymol blue	+ 1.2	Red	Yellow
2-Nitroaniline	- 0.2	Yellow	Red/Orange



Picture 12 Indicators for measuring acid strength (Bromothymol blue, Methyl red, Bromo cresol green, Thymol Blue and 2-Nitroaniline from left to right)

2.4.6 THERMAL GRAVIMETRIC ANALYSIS (TGA)

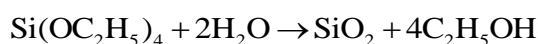
The calcining furnace (Model: McGregor, NL 200, Auckland, New Zealand) was used to calcine samples. From 100 °C to 800 °C, the weight of each sample was recorded every 50 °C. The MCM-41 molecular sieve and metal salt were analyzed using the same method. The percentage weight loss versus temperature was recorded in a table and curves were plotted. The material decomposition temperature range was found in

Figure 14.

CHAPTER 3 RESULTS AND DISCUSSION

3.1 THE SYNTHESIS PROCESS OF CATALYSTS

TEOS used as a silica source: TEOS is used as a crosslinking agent in silicon polymers because it hydrolyzes to silicain water (shown below) and polysilicic acid can be obtained via polycondensation.



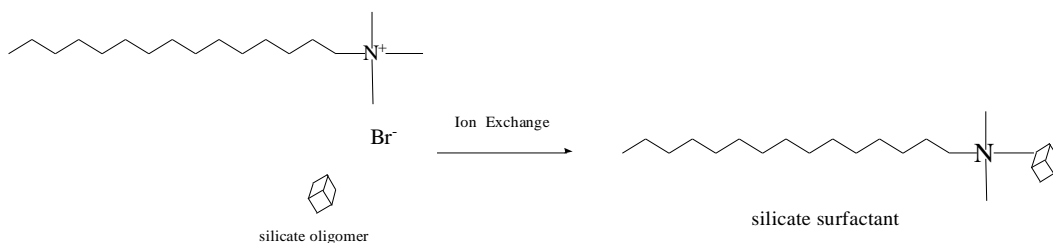
Zheng et al. (Zheng et al., 2009) synthezed Poly-ferric Silicate Sulfate (PFSS) in 2009. Because TEOS has the characteristics of slow hydrolyzation, the synthesis was easy to control and the products have good pore structure. In addition, after adding a surfactant, the silicate oligomers show ion exchange ability which gives it the ability to be loaded with hetero-ions such as transition metals (Gaydhankar, Samuel, Jha, Kumar, & Joshi, 2007).

CTAB as surfactant: The template agent is one of the key factors in the process of preparation of mesoporous materials, the template agent can control the happening of the reaction and crystallization (Stucky et al., 1997). In the reaction process, the charge density between the surfactant and silicate determines the formation of coordination. The dosage of template agent influences the crystallization of the molecular sieve directly (Stucky et al., 1997).

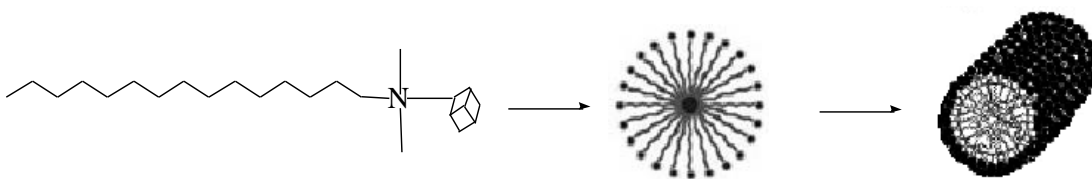
Zhu et al. (Zhu et al., 2007) reported that when the mole ratio of CTAB:TEOS is between 0.1 and 0.8, hexagonal pore structure molecular sieve can be formed. With the increase of CTAB, the shape of the molecular sieve transforms from rod to ball, and the grain size becomes smaller. This is because with the increase of template agent concentration, template agent micelles increase in solution, which is conducive to the formation of MCM-41 (Zhu et al., 2007).

The synthesis of MCM – 41: The synthesis of MCM-41 by CTAB and TEOS always follow these three steps:

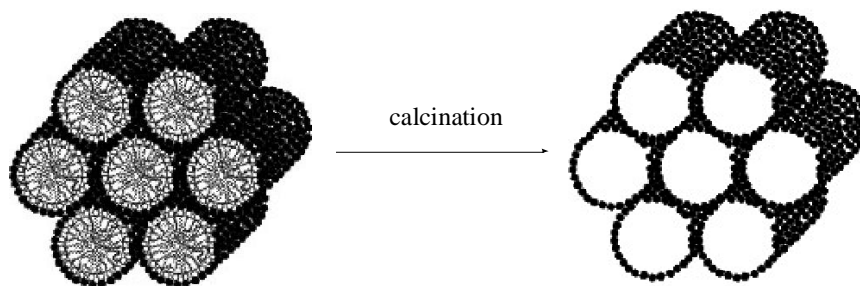
1. Ion exchange: The Br^- in CTAB template were exchanged by silicate oligomer which produced by the hydrolysis of TEOS.



2. Self-assembled: Silicate surfactant self-assembled in the solution and form a rod shape.



3. Arrangement and calcinations: After arrangement and calcinations, the MCM-41 molecular sieve were formed.



3.2 THERMAL TREATMENTS

Compared with liquid superacids, some solid superacids need to activate their catalyst activity by thermal treatments. High temperature treatment is one of the effective methods to activate active sites in catalyst. The thermal treatment includes two parts: drying and calcination. Each part has its own function.

Drying: The drying process generally has three stages. They are preheating period, constant temperature period and falling rate period.

During preheating period, the ratio of liquid on the surface of the sample increases with the increasing temperature. In this stage, only the water on the surface of evaporates, there is no pore formation. For the constant rate period, the temperature of the wet support remains constant so the temperature is called ‘wet bulb temperature’. Under the wet bulb temperature, all inside water is removed which makes the sample porous. Then the active metal compounds are transferred into the pore. The falling rate period was found when the moisture transport inside the sample is no longer sufficient to keep the surface saturated. From this stage, the drying rate decreased. After the temperature drop, the sample volume has shrunk, and formed some pores inside the sample. The process is shown in *Figure 13*.

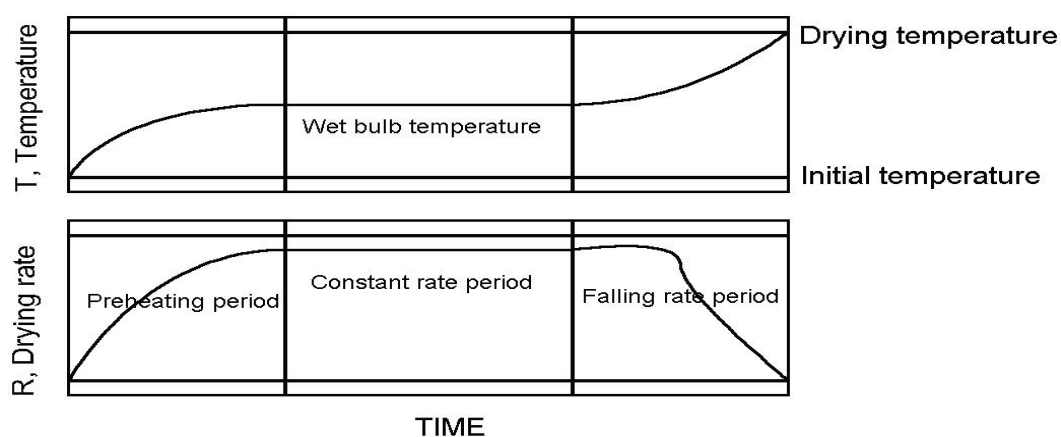


Figure 13 The throstages drying process for porous material (Regalbuto, 2007)

Metal redistribution In this three-stages drying process, the active compounds (i.e. Cr^{6+} , Mo^{6+} and SO_4^{2-}) are redistributed into the porous sample (Lekhal, Glasser, & Khinast, 2001, 2004; Lekhal, Khinast, & Glasser, 2001; Li, 2011).

Calcination: Calcination is the heat treatment in air or inert gas under a certain temperature. The dried sample was treated under high temperature in order to get a crystal phase catalyst and it is the final step in this catalyst preparation.

In the process of calcination, one of the important things is thermal decomposition. Some compounds block up the MCM-41 pores like the water of crystallization and CO_2 is removed in this process. As temperatures rise, micelle templates within the cylindrical pores are burnt down and form a tubular structure. In addition, at higher temperatures, solid phase reactions occur and form the active sites. The chemical changes in thermal decomposition can be detected using the thermal gravimetric analysis (TGA) method.

Another important part is recrystallization. With high temperature treatment, porous catalysts can be formed with certain crystal shape, crystal size, pore structure and specific surface area. Their crystal structure can be detected by powder X-ray diffraction (XRD) method.

The choice of the temperature is very important in the process of calcinations. The calcination temperature should be high enough to burn off all the template agent but can not reach the temperature that will sinter the tubular structure of MCM-41 support and transition metal active sites. The better calcination temperature were found out from the TGA analysis.

Thermal gravimetric analysis: According to the definition of International Confederation for Thermal Analysis (ICTA), thermal gravimetric analysis (TGA) is a method of thermal analysis in which changes in physical and chemical properties of materials are measured as a function of increasing temperature in air or inert gas (Coats & Redfern, 1963). thermal gravimetric analysis is often used to detect material

composition and thermal stability.

For transition metal loaded MCM-41 catalysts, mass changes are mainly related to the decomposition of the template agent (CTAB in this study) and some metal compounds (like SO_4^{2-} in chromium salt).

Thermal decomposition analysis: After drying at 100 °C for 24h, five samples (chromium sulfate, ammonium molybdate, MCM-41, 50% Cr/MCM-41 and 50% Mo/MCM-41) were heated from 100 °C. The mass change of the samples with temperature increase were recorded and shown in the following figure.

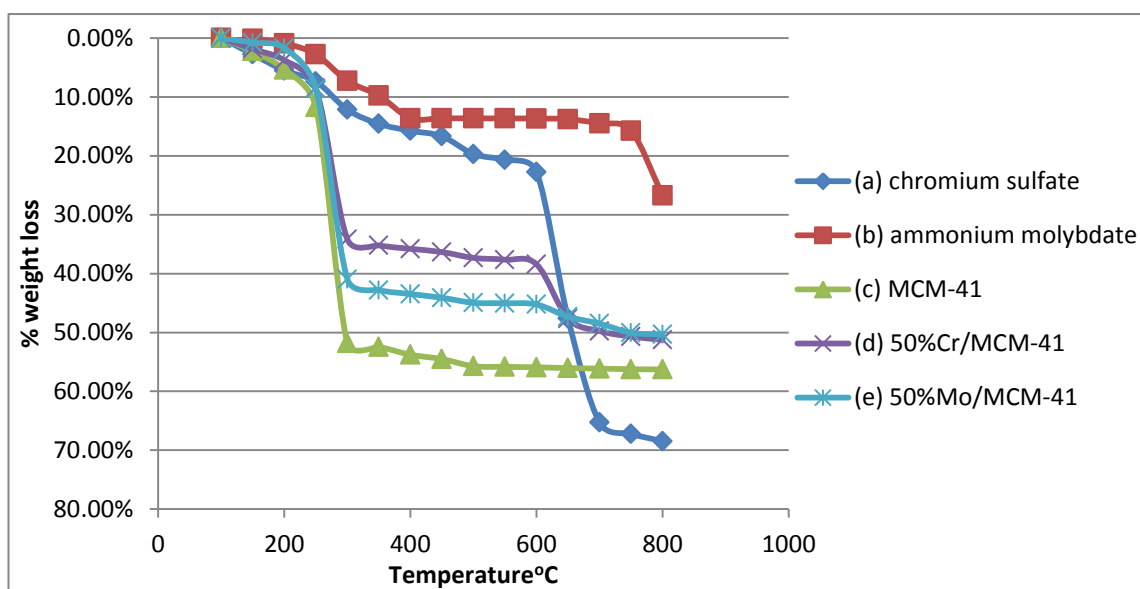


Figure 14 The mass change of the samples with temperature increase


As shown in curves (a) and (b), these two metal salt lose weight slowly from 100 °C to 600 °C. In this range, a part of the water of crystallization might be evaporated. Most of chromium sulfate was decomposed between 600 °C and 700 °C. For ammonium molybdate, from 400 °C to 600 °C, the mass changes little. At 600 °C ammonium molybdate changed from the white powder into a light yellow crystal (**Picture 13**). The crystal might be molybdenum oxide. And with a temperature higher than 600 °C, the molybdenum oxide loses weight because of sublimation.



Picture 13 molybdenum salt after calcining at 800 °C

For curve (c), (d) and (e), these three curves proved that template agent was burned between 250 °C to 300 °C. During this temperature range, black smoke appeared from furnace and the sample became a little black. The comperation of MCM-41 loaded with different metal salt at 300 °C and 600 °C are shown in **Table 8**.

Table 8 Picture for 50%Cr/MCM-41 and 50% Mo/MCM-41 after calcining at 300 °C and 600 °C

	50%Cr/MCM-41	50% Mo/MCM-41
300 °C		
600 °C		

Curve (c) shown, after 300 °C MCM-41 molecular sieve maintains a good thermal stability. For metal loading MCM-41, both 50%Cr/MCM-41 and 50% Mo/MCM-41 shown the similar character with their corresponding metal salt.

In conclusion, based on the decomposition temperature of metal salt and MCM-41 molecular sieve, the suitable calcination temperature for synthesise these catalysts are between 400 °C and 550 °C. The temperature range is similar to the result of Wang (Wang et al., 2009) and Li (Li, 2011).

3.3 N-BUTYL ACETATE SYNTHESIS MECHANISM

***n*-Butyl acetate:** *n*-Butyl acetate (See **Figure 15**) is a colorless and flammable liquid which always used as a solvent in industry. In addition to the industrial synthesis, *n*-butyl acetate can also found in some fruit, such as banana and apple. Besides used in synthesis lacquer, fiber and plastic, because its fruit flavor *n*-butyl acetate always been used in food additives. In industry, *n*-Butyl acetate always synthesized with acetic acid and *n*-butanol under the condition of sulfuric acid catalysis.

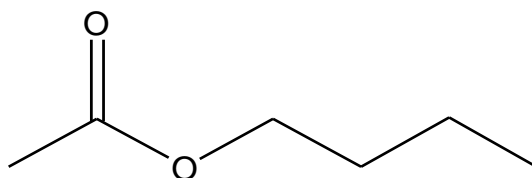
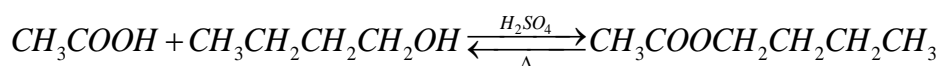


Figure 15 *n*-butyl acetate

Conditions and equations of n-Butyl acetate synthesis

The equation of synthesisi of *n*-Butyl acetate is shown below:



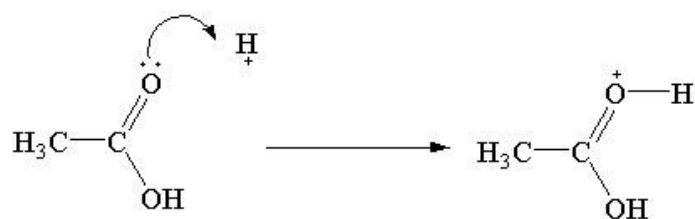
This acid catalyzed reaction always happens in the liquid-phase, at a temperature of around 120 °C at 1 atm (Song, Venimadhavan, Manning, Malone, & Doherty, 1998).

Acetic acid and *n*-butanol esterification reaction is often used to evaluate the catalytic performance the new kind of solid super acid catalysts (Li, 2011; Nagaraju, 1997; Song

et al., 1998; Timofeeva et al., 2001; Wang et al., 2009; Xia et al., 2002). The consumption of acetic acid was used to evaluate the catalytic ability.

Kinetics of butyl acetate synthesis: This esterification reaction is an example of a Fischer esterification or a nucleophilic acyl substitution mechanism. There are six steps for acetic acid and *n*-butanol esterification (Brown, 1995).

Step 1: The catalyst produces a proton, and then the proton attaches the lone pair electrons on the oxygen belongs to an acyl group (Step 1).



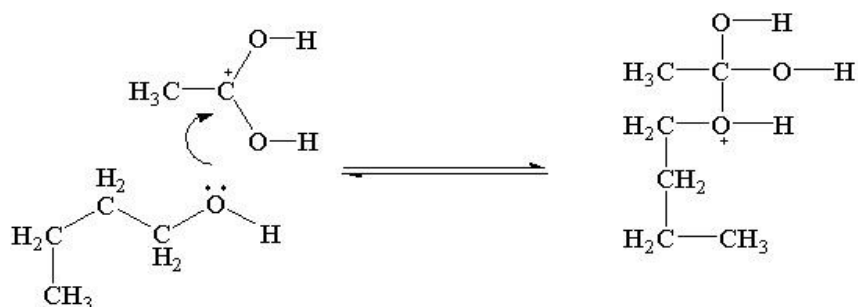
(Step 1)

Step 2: The positive charge transfer to the carbon atom and then forms a resonance structure (Step 2).



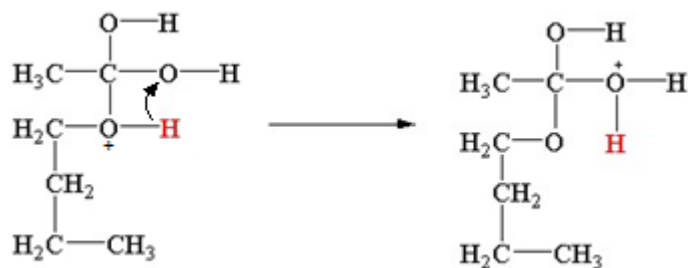
(Step 2)

Step 3: The positive charge on the carbon atom attached by the lone pair electrons on the oxygen which belongs to the hydroxyl on *n*-butanol (Step 3).



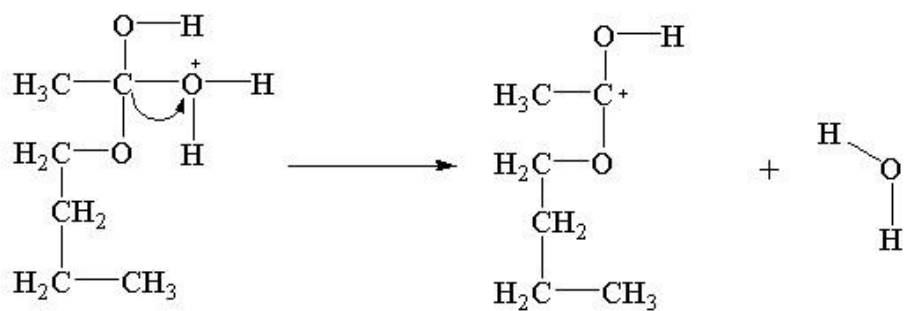
(Step 3)

Step 4: Because of the difference of electron density, the hydrogen (red one) transfers to one of the oxygen belongs to hydroxyl



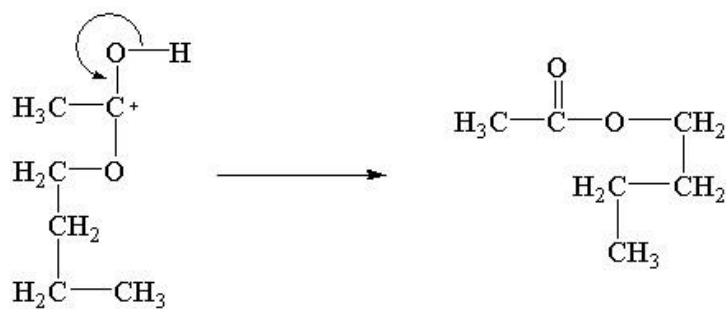
(Step 4)

Step 5: A mole of water was removed from one mole of products.



(Step 5)

Step 6: Hydrogen bond was broken and a proton is returned to the system. The protons are released back to participate in the reaction from **step 1**.



(Step 6)

Based on these six steps, butyl acetate has been synthesized. In theory, the concentration of H^+ has not changed in the system so the acid catalyst was reusable. During the synthesis, the water generated in **step 5** were moved in order to promote the reaction.

In this reaction, acidity of catalyst and the contact area of reactants are both important influential factors on esterification rate.

3.4 CATALYTIC ACTIVITY AND SELECTIVITY ANALYSIS

The activity of different pre-synthesized catalysts were shown in esterification rate and their selectivity which depends on the number of by-products.

3.4.1 PRODUCTS QUALITATIVE ANALYSIS

Infrared spectroscopy: Infrared spectroscopy is an effective method for detecting functional groups in organic compounds. Based on molecular vibrations, different functional groups appear in different positions (wavenumbers expressed as cm^{-1}) on the infrared spectrum. The mixed solution after reaction catalytic with different catalysts was analyzed by IR. **Figure 16** shown the IR spectra of the products for esterification catalyst with 50% Cr/MCM-41 and 50% Mo/MCM-41.

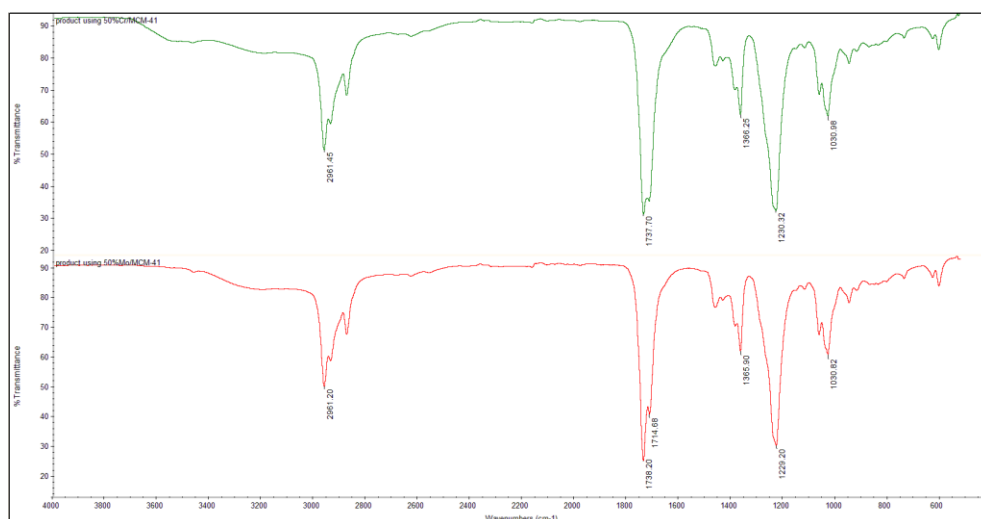


Figure 16 IR spectrum of the synthesized n-butyl acetate by using 50% Cr/MCM-41 and 50% Mo/MCM-41.

These two products have a similar spectrum. Around 1740cm^{-1} , both of these two products shown a large peak. It implies that there are saturated ester structure in the product compounds. And C-O-C bonds stretching vibration absorption appeared around 1230 cm^{-1} . Around 2960 cm^{-1} , the adsorption peak should be caused by C-H bonds. All of the characteristic peak location are similar with the spectrum (See **Figure 17**) supported by Spectral Database for Organic Compounds (SDBS). This suggests that the product is reasonably n-butyl acetate. A reference spectrum is shown in **Figure 17**.

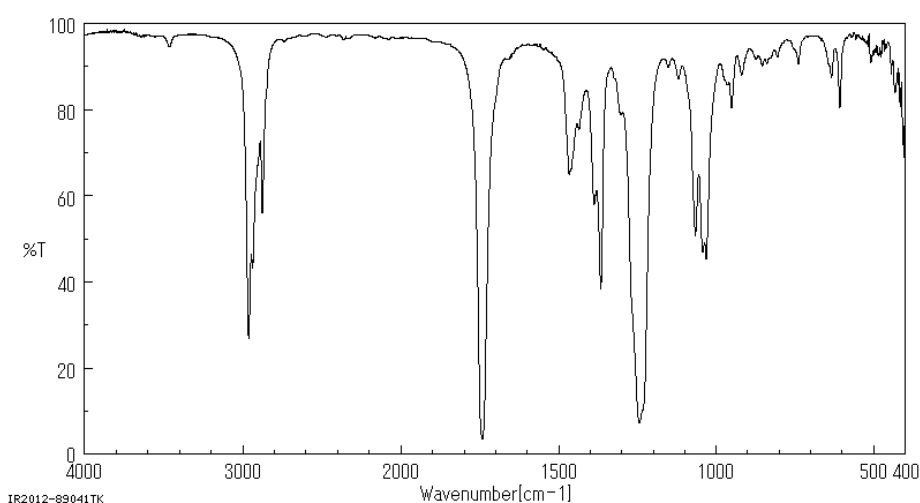


Figure 17 IR spectrum of butyl acetate (S.Kinugasa, K.Tanabe, & T.Tamura, 2013)

In addition, there are no characteristic peaks around $1070\text{--}1150\text{ cm}^{-1}$ and 1650 cm^{-1} . It means there are no ether or alkenyl in the synthesized products. Under conditions of general acid catalysis both dibutyl ether formation and elimination of the alcohol to give butenes would be expected. This proves that the two kinds of catalysts have high selectivity.

Gas chromatography analysis: The compounds in the solution before and after reaction were analyzed by gas chromatography (GC). Gas chromatography (GC), is a common type of chromatography used in separating and analyzing mixed organic compounds which can be vaporized but not easy decompose. Different settings and different columns are used to separate different compounds. The compounds can be matched by retention time. In these analyses, three peaks were found as shown below.

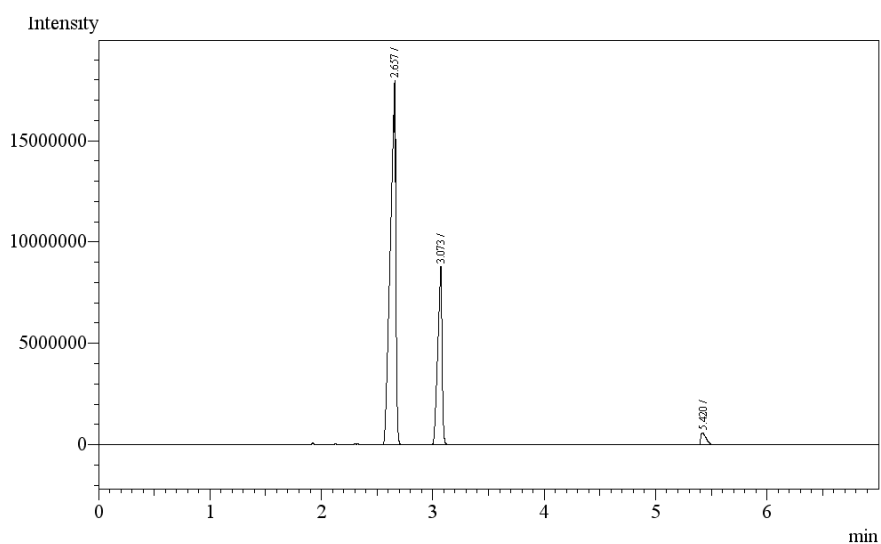


Figure 18 Chromatogram of compounds after esterification catalyzed by 50% loading Mo/MCM-41

In all GC chromatogram for the products catalyzed by different catalysts, the same three peaks were found. By comparison with known standards of retention time, these three compounds were identified *n*-butyl acetate, *n*-butanol and acetic acid. In these three compounds *n*-butanol and acetic acid are the reactants, *n*-butyl acetate is the only

product. This result can prove that the MCM-41 catalysts loaded with transition metal have high selectivity for esterification.

3.4.2 CATALYTIC ACTIVITY

Esterification rates: After three hours reaction, the liquid was removed from the round bottom flask. And then accurately weighing 1mL of liquid from the Dean-Stark was accurar and remove it into a conical flask. Diluted with distilled water and titrated with 0.05 mol/L KOH ethanol standard solution ahead, the consuming volume of KOH solution was recorded below:

Table 9 Esterification rate using different ratio metal loading catalysts

		Reaction time (hours)	Volume of KOH (mL)	Esterification rate*
Group 1		0	17.11	0.00%
	Cr ₅₀	3	3.24	81.06%
	Cr ₄₀	3	4.02	76.50%
	Cr ₃₀	3	4.25	75.16%
	Cr ₂₀	3	4.40	74.28%
	Cr ₁₀	3	6.05	64.64%
	Cr ₁	3	8.50	50.32%
Group 2		0	17.03	0.00%
	Mo ₅₀	3	1.85	89.14%
	Mo ₄₀	3	2.13	87.49%
	Mo ₃₀	3	4.76	72.05%
	Mo ₂₀	3	5.32	68.76%
	Mo ₁₀	3	6.60	61.24%
	Mo ₁	3	7.10	58.31%

* Esterification rate: the measured/theoretical amount of ester assuming 100% conversion after 3 hours reaction (see Chapter 2.3)

As shown in **Table 9**, loading with transition metals have obvious effect for MCM-41

molecular sieve catalysts. In these reactions, the results show that both these catalysts have strong acidity. Active sites (Brønsted or Lewis acid sites) might be concentrated on the catalyst surface or in the pores. The type of active sites were analyzed in following experiments. Comparison between these two groups, Mo/MCM-41 catalysts with high presentage of metal loading have a better catalytic activity (the rate was as high as 89.14%). The results demonstrate that the catalytic activity increased with increasing the metal ratio.

The relationship between metal content and catalytic activity intuitive expression in the histogram below.

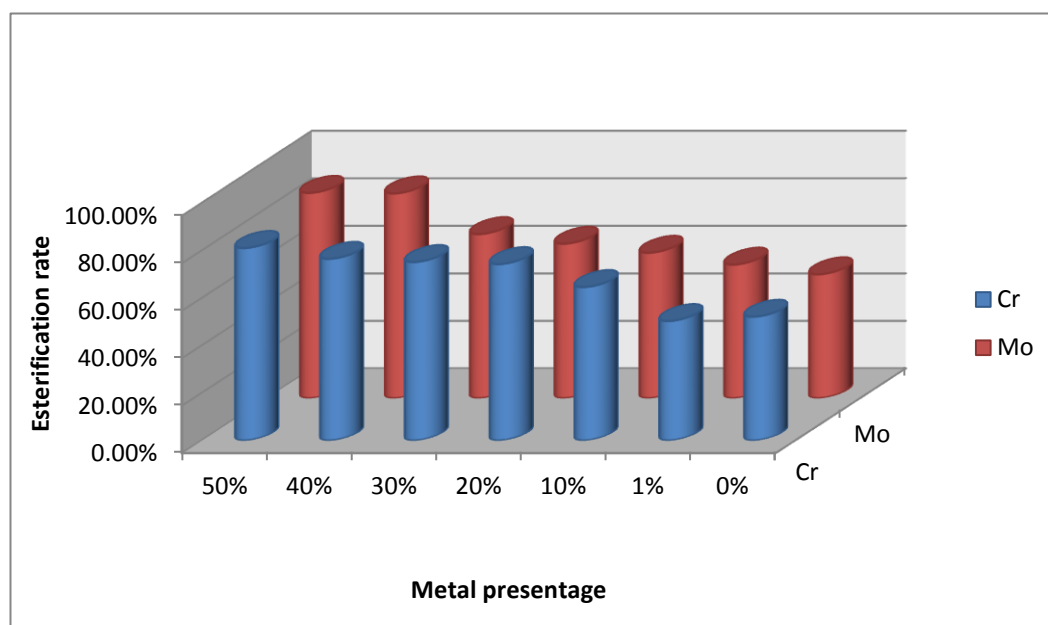


Figure 19 The relationship between metal content and catalytic activity

For group 1, from 20% to 40% loading, the promotion of catalytic activity are not obvious. It perhaps because the acetic acid was providing all the acid needed. And 1% Cr/MCM-41 catalyst's performance has no significantly difference from MCM-41 molecular sieve without modification. For group 2, from 1% to 30% loading, the catalysts have not show an excellent catalytic ability. But when molybdenum ratio reached as high as 40%, the catalytic activity increased a lot. The reason for catalytic activity sudden increase were discussed in further study.

After the catalytic reaction, the catalysts were separated from the solution. After drying and calcination, the catalysts were reused (around 0.2g catalysts were used each time, the shortage part were added with new synthesized catalysts). The change of 50% Cr/MCM-41 and 50% Mo/MCM-41 catalytic activity as shown in the figure below:

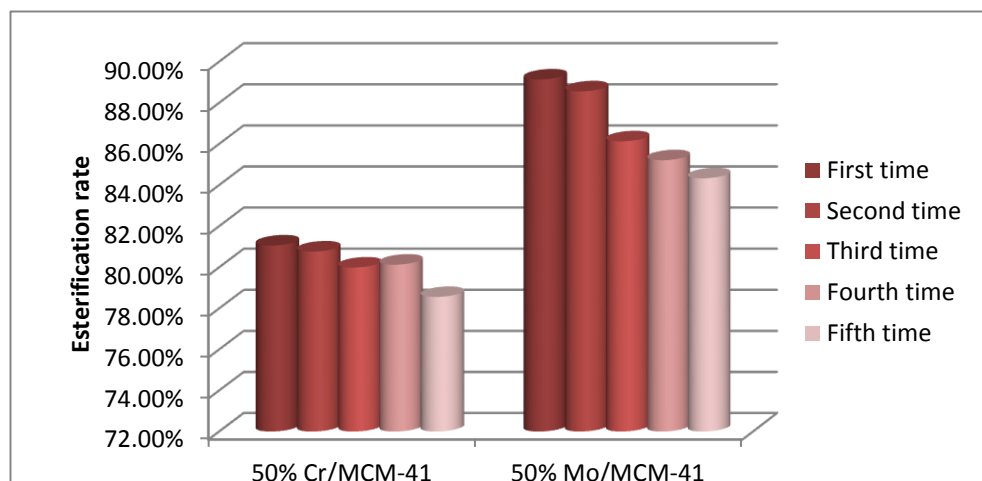


Figure 20 Catalytic activity change with number of use for 50% loading catalysts

The esterification rate for both of these two groups of catalysts shows a decrease after being used for five times. The cause of the catalytic ability decrease is likely to be some active sites was dissolved into the reactants in the process of reaction. After calcinations, the ratio of transition metal can not reach as high as new-synthesis catalysts. It reduced the concentration of active sites on the surface of the catalysts. Comparing between these two groups, the catalytic activity of Mo/MCM-41 decreased relatively obvious. However, the results shown both of these two groups of catalysts can be reused.

Verify esterification rate using GC: The same volume of samples before and after the reaction was injected by auto-injector. The retention time and peak area were recorded by GC. The esterification rate will be calculated and compared with the result from titration method. **Table 10** and **Table 11** recorded the results of GC analysis:

Table 10 GC results for Cr/MCM-41

	Reaction time (hours)	Peak Area	Esterification rate*
Sample before reaction	0	7807172.6	0.00%
50% Cr	3	1798142.4	76.97%
40% Cr	3	2092363.0	73.20%
30% Cr	3	2228312.2	71.46%
20% Cr	3	2496537.0	68.02%
10% Cr	3	3113822.3	60.12%
1% Cr	3	3937263.1	49.57%

* Esterification rate: the measured/theoretical amount of ester assuming 100% conversion after 3 hours reaction

Table 11 GC results for Mo/MCM-41

	Reaction time (hours)	Peak Area	Esterification rate*
Sample before reaction	0	14267909.0	0.00%
Mo ₅₀	3	1947782.4	86.35%
Mo ₄₀	3	1979330.5	86.13%
Mo ₃₀	3	4418138.3	69.03%
Mo ₂₀	3	4996183.0	64.98%
Mo ₁₀	3	5540842.2	61.17%
Mo ₁	3	6247245.0	56.21%

* Esterification rate: the measured/theoretical amount of ester assuming 100% conversion after 3 hours reaction

The esterification rates calculated from GC data are similar to the results using the titration method. All the esterification rates calculated from GC data are a little lower than that using a titration method. The results proved that both of the two groups of catalysts have good catalytic ability on esterification reaction.

3.5 CATALYSTS STRUCTURE

Characterization of catalyst structure contains the following sections: crystallography, morphology, porosity, and surface study (Li, 2011). Powder X-ray diffraction was used to determine the geometric structure of the catalyst. The pore size and specific surface area of catalyst loading with different transition metal were analyzed by the nitrogen adsorption method. Via scanning electron microscopy, the surface structure of different metal loading MCM-41 were compared. Other properties of the catalysts were analyzed using methods such as Hammett indicator, diffuse reflectance infrared fourier transform spectroscopy after the per-treatment with pyridine. The effects of different types and loading of transition metals on the catalyst structure were investigated.

3.5.1 SURFACE STRUCTURE

Scanning electron microscope: A scanning electron microscope (SEM) is a type of electron microscope that imaging using fine focused electron beam on the sample surface scan out of some kinds of physical signal. The signal obtained by scanning contains a lot of information, such as sample's surface topography and composition.

In this study, catalysts' surface structure can be seen from the photomicrograph directly. And atomic distribution on the surface of the catalyst were shown using X-ray microanalysis.

Structure: The follow figure shows the surface structure of MCM-41 molecular sieve. This figure gave an index to the prism structure of MCM-41.

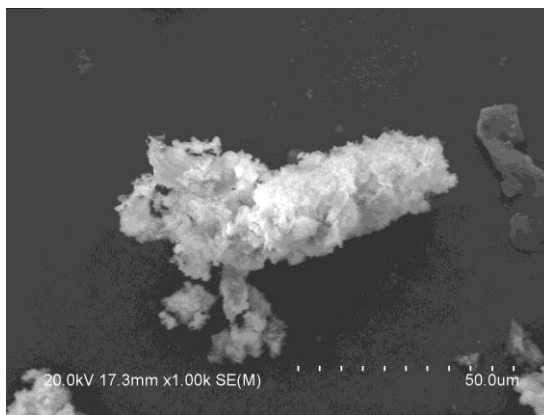


Figure 21 Scanning electron micrograph of the MCM-41 molecular sieve on 10μm scale

From the transition metal modified MCM-41 SEM micrographs in **Figure 22**. It was shown clearly both of these two kinds of samples have a porous structure. Even the metal loading reached as high as 50%, the structure can still be maintained.

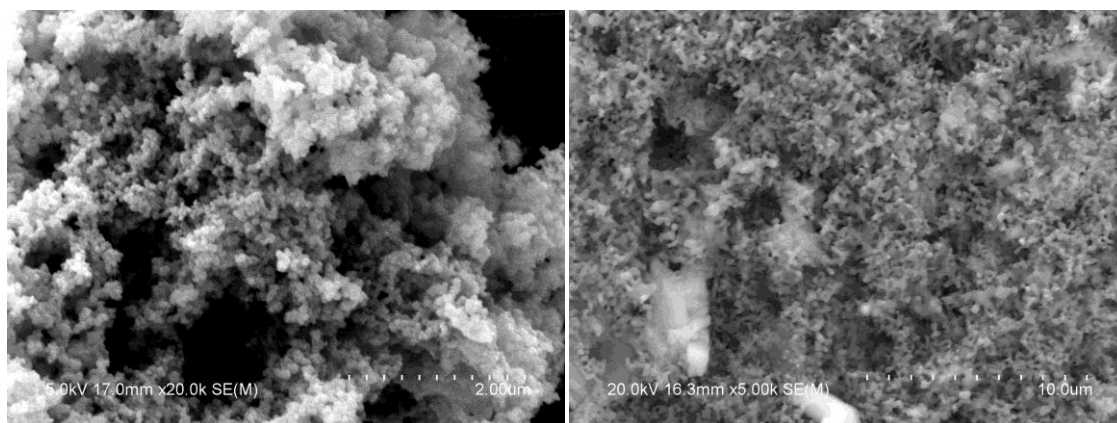


Figure 22 Scanning electron micrographs of 50% Cr/MCM-41 on 2μm scale (left) and 50% Mo/MCM-41 on 10μm scale (right).

Atomic distribution: The atomic distribution for Cr/MCM-41 and Mo/MCM-41 were determined using X-ray microanalysis. Different areas of the solid surface were analyzed, and the atom content were calculated by computer. By comparing the content of silicon and transition metal, metal loading position can be explored.

Figure 23 and Table 12 displays the atomic distribution of 1% Cr/MCM-41 sample.

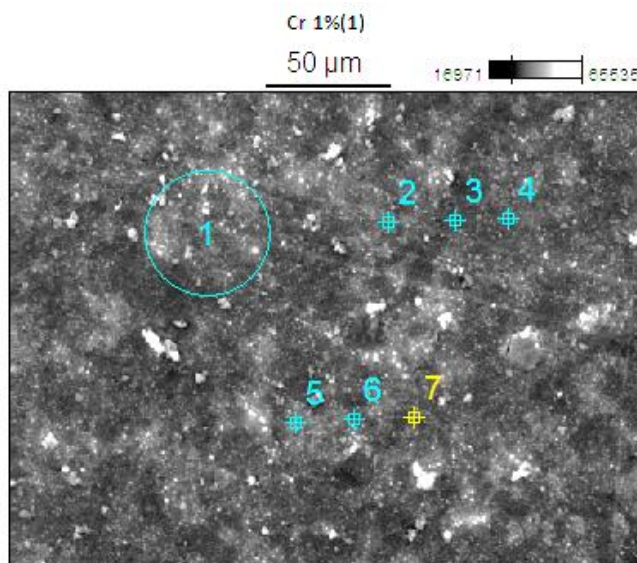


Figure 23 X-ray microanalysis of 1% Cr/MCM-41 based on scanning electron micrograph

Table 12 Atom presentage on the surface of 1%Cr/MCM-41

	<i>C-K</i>	<i>O-K</i>	<i>Na-K</i>	<i>Si-K</i>	<i>S-K</i>	<i>Cr-K</i>	<i>Zr-L</i>	<i>Mo-L</i>
<i>Cr 1%(1)_pt</i>	<i>no</i>	71.21	<i>no</i>	28.19	<i>no</i>	0.36	0.20	0.01
<i>Cr 1%(1)_pt</i>	6.04	64.20	0.55	28.17	0.37	0.30	0.37	0.00
<i>Cr 1%(1)_pt</i>	<i>no</i>	<i>no</i>	<i>no</i>	<i>no</i>	<i>no</i>	<i>no</i>	<i>no</i>	<i>no</i>
<i>Cr 1%(1)_pt</i>	5.63	65.36	0.50	27.69	0.25	0.30	0.24	0.03
<i>Cr 1%(1)_pt</i>	5.51	66.21	0.55	26.75	0.37	0.33	0.28	0.00
<i>Cr 1%(1)_pt</i>	6.92	65.24	0.41	26.44	0.34	0.37	0.28	0.00
<i>Cr 1%(1)_pt</i>	6.56	64.28	0.48	27.65	0.35	0.36	0.30	0.02

Seven areas were analyzed, in 1%Cr/MCM-41 atoms well-distributed. It is worth mentioning that most of the atoms were oxygen, which shows the catalyst is probably composed of silicon dioxide and transition metal oxide.

Table 13 Atom presentage on the surface of Cr/MCM-41 catalysts

	Si%	S%	Cr%	Cr/(Cr+Si)
1% Cr/MCM-41	27.48	0.28	0.34	1.21%
10% Cr/MCM-41	21.96	1.10	2.47	10.11%
20% Cr/MCM-41	20.71	1.39	5.87	22.09%
30% Cr/MCM-41	19.45	1.32	7.20	27.01%
40% Cr/MCM-41	16.37	1.20	11.14	40.49%
50% Cr/MCM-41	15.22	1.12	15.32	50.16%

From **Table 13**, the content of chromium and silicon measured by X-ray microanalysis are closed to the content in synthesis. It proves that chromium distributed evenly on the surface and in the pore of MCM-41 skeleton. In addition, sulfur content did not increase with chromium. It showed that the chromium in the catalyst is not in the form of chromium sulfate.

Figure 24 and table 14 displays the atomic distribution of 1% Mo/MCM-41 sample.

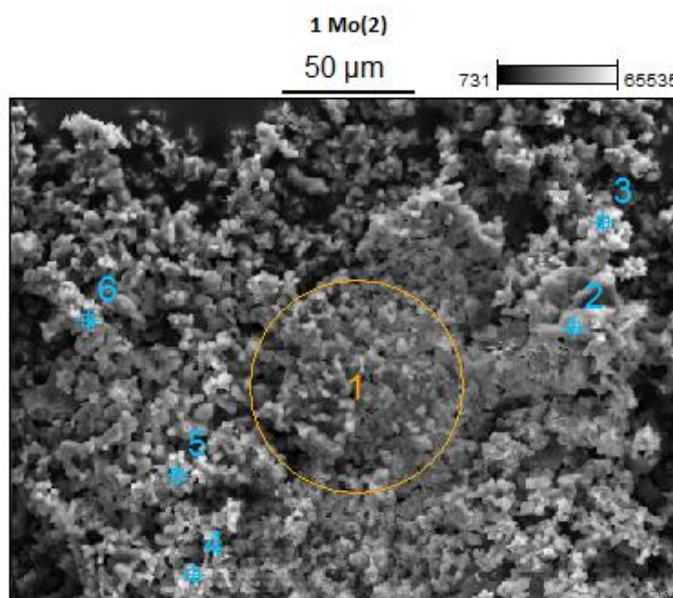


Figure 24 X-ray microanalysis of 1% Mo/MCM-41 based on scanning electron micrograph

Table 14 Atom presentage on the surface of 1%Cr/MCM-41

	<i>C-K</i>	<i>O-K</i>	<i>Na-K</i>	<i>Si-K</i>	<i>Cr-K</i>	<i>Br-L</i>	<i>Mo-L</i>
<i>Mo 1%(1)_pt1</i>	5.59	63.66	3.68	25.27	0.00	1.43	0.04
<i>Mo 1%(1)_pt2</i>	18.68	50.23	24.63	3.98	0.00	2.16	0.00
<i>Mo 1%(1)_pt3</i>	<i>no data</i>	<i>no data</i>	<i>no data</i>	<i>no data</i>	<i>no data</i>	<i>no data</i>	<i>no data</i>
<i>Mo 1%(1)_pt4</i>	8.08	67.54	3.89	19.72	0.00	0.53	0.00
<i>Mo 1%(1)_pt5</i>	10.43	60.11	2.53	25.31	0.00	1.08	0.19
<i>Mo 1%(1)_pt6</i>	10.75	62.38	1.96	23.81	0.00	0.60	0.16

Six areas were analyzed this time. In 1% Mo/MCM-41, the distribution of molybdenum was not uniform and the carbon content is higher. Similar to Cr/MCM-41, oxygen content is still the highest, which means Mo/MCM-41 catalyst is probably composed of silicon dioxide and transition metal oxide.

Table 15 Atom presentage on the surface of Mo/MCM-41 catalysts

	Si%	Mo%	Mo/(Mo+Si)
1% Mo/MCM-41	19.62	0.08	0.40%
10% Mo/MCM-41	23.77	0.41	1.69%
20% Mo/MCM-41	25.82	0.91	3.39%
30% Mo/MCM-41	22.97	3.48	13.15%
40% Mo/MCM-41	24.54	3.28	11.80%
50% Mo/MCM-41	18.43	4.51	19.65%

From **Table 15**, the content of molybdenum and silicon measured by X-ray microanalysis are much lower than the content used in the synthesis of the catalyst. It proves that most molybdenum filled in molecular sieve pores first, and only a little molybdenum was adsorbed on the surface of MCM-41 molecular sieve. The reason might be in the process of crystallization and calcine, ammonium molybdate

decomposed and released ammonia and water vapor which might change the pH value and affect the skeleton structure.

3.5.2 CRYSTALLINE STRUCTURE

Powder X-ray diffraction: Powder X-ray diffraction (XRD) is a technique used to study atomic and molecular arrangement in crystals. Crystalline structure diffract a beam of X-rays, because of diffraction wave superposition, the intensity of the beam increase in some directions and decrease in the other directions. By measuring diffraction angles and intensities, crystalline structure can be determined by the diffraction pattern.

Powder x-ray crystallography measures the distance between atomic layers in a crystal, based on the angle of incidence and wavelength of the incident X-ray beam). This relationship is called Bragg's law, and explains the phenomena of crystal diffraction at certain angles of incidence (Jenkins & Snyder, 1996).

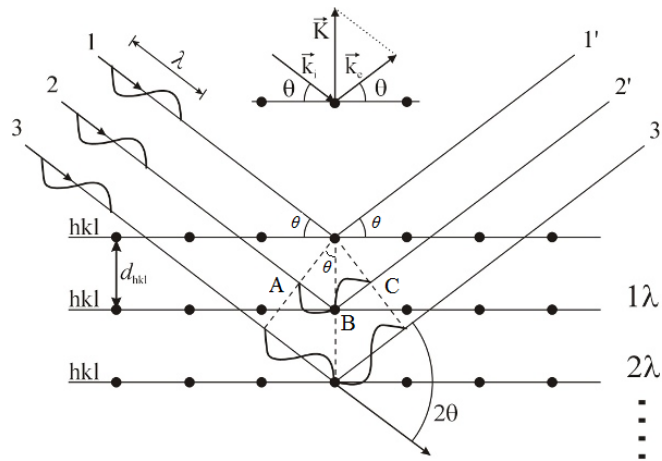


Figure 25 The Bragg's Law X-ray diffraction

As shown in **Figure 25**, constructive interference occurs only when $n\lambda = AB + AC$.

Because: $AB = AC$ so: $n\lambda = 2 \times AB$

And in this figure: $\sin \theta = AB / d_{hkl}$ so: $AB = d_{hkl} \times \sin \theta$

Bragg's law can be written as: $n\lambda = 2 \times d_{hkl} \times \sin \theta$

Figure 26 shows the X-ray diffraction pattern of MCM-41 sample.

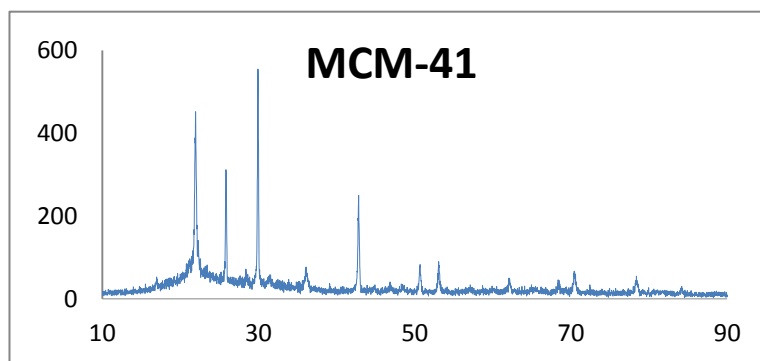
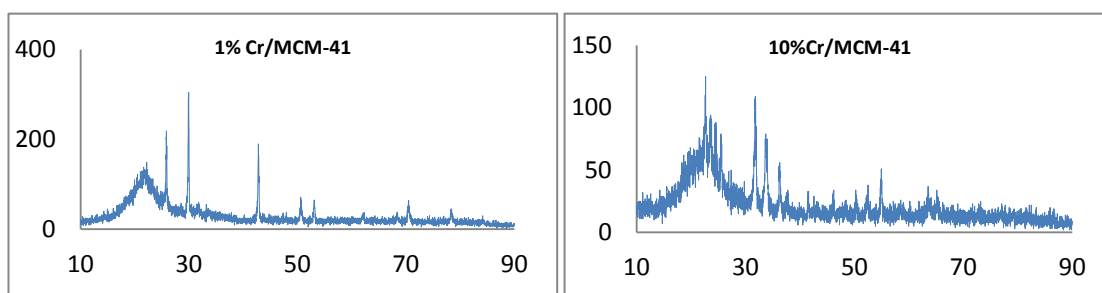


Figure 26 XRD patterns of the MCM-41

From **Figure 26**, three peaks between 20° and 30° come from the silica crystal structure. Because of the limitation of instruments, small angles can not be measured. The diffraction peak that would show a highly ordered hexagonal crystal mesostructure at Bragg angle of around 2.4° can not be found (Carvalho, Varaldo, Wallau, & Schuchardt, 1997; C. L. Chen, Li, et al., 2001; Giraldo et al., 2007; C. Kresge et al., 1992; C. T. Kresge, M. E. Leonowicz, W. J. Roth, J. C. Vartuli, & J. S. Beck, 1992; Li, 2011; A. Sayari, 1996; Wang et al., 2009).

Figure 27 is the XRD patterns of ranges of Cr/MCM-41 catalyst composites from 1% to 50% metal compounds loading.



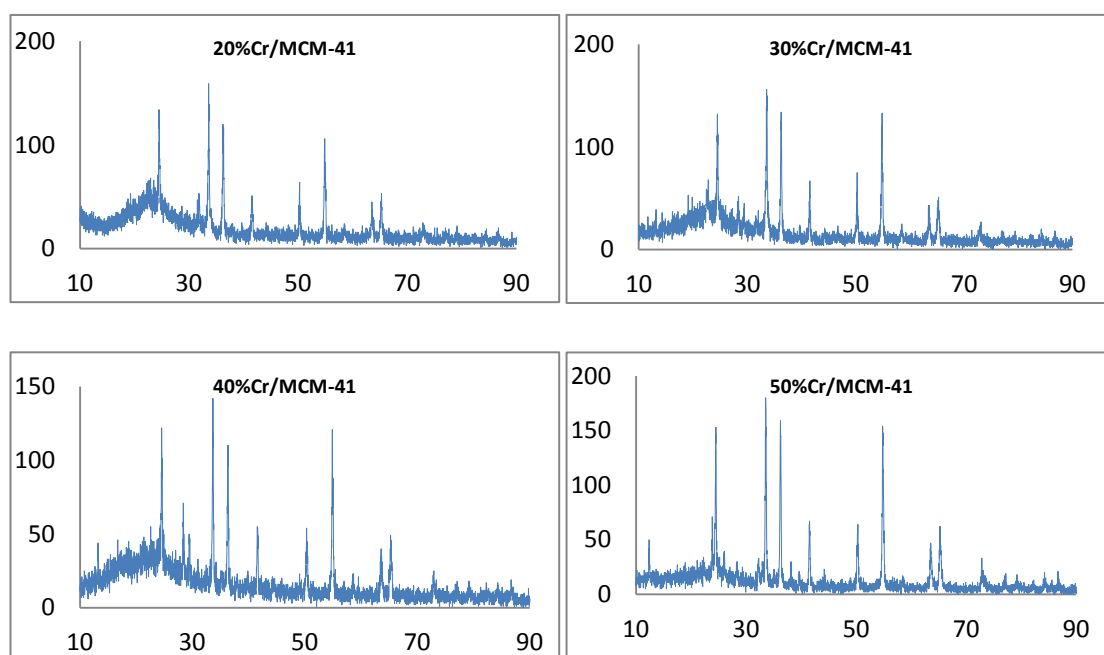


Figure 27 XRD patterns of the Cr/MCM-41 composites with different chromium (1% to 50%, from left to right, up to down)

Compared with the XRD patterns of MCM-41, some new diffraction peaks appeared in the XRD patterns of Cr/MCM-41. The diffractions peaks around 25° , 34° , 36° , 42° , 51° , 55° and 65° look like chromic oxide (Cr_2O_3) XRD diffraction peaks (Takehira et al., 2004). This result agrees with the SEM micrographs of Cr/MCM-41 in **chapter 3.5.1**. Both of the result show that chromic oxide evenly distributed on the surface of MCM-41. Furthermore, with the increase of chromium, peaks in the high angle region (15° to 30°) become smaller and smaller. It means more and more chromium fill the pore and change the pore size of MCM-41 skeleton. These six XRD patterns have similar sharp and peak location, which proved there are no structural change of the MCM-41 shape with chromium loading.

Figure 28 shows the XRD patterns of Mo/MCM-41 catalysts with metal loading from 1% to 50%.

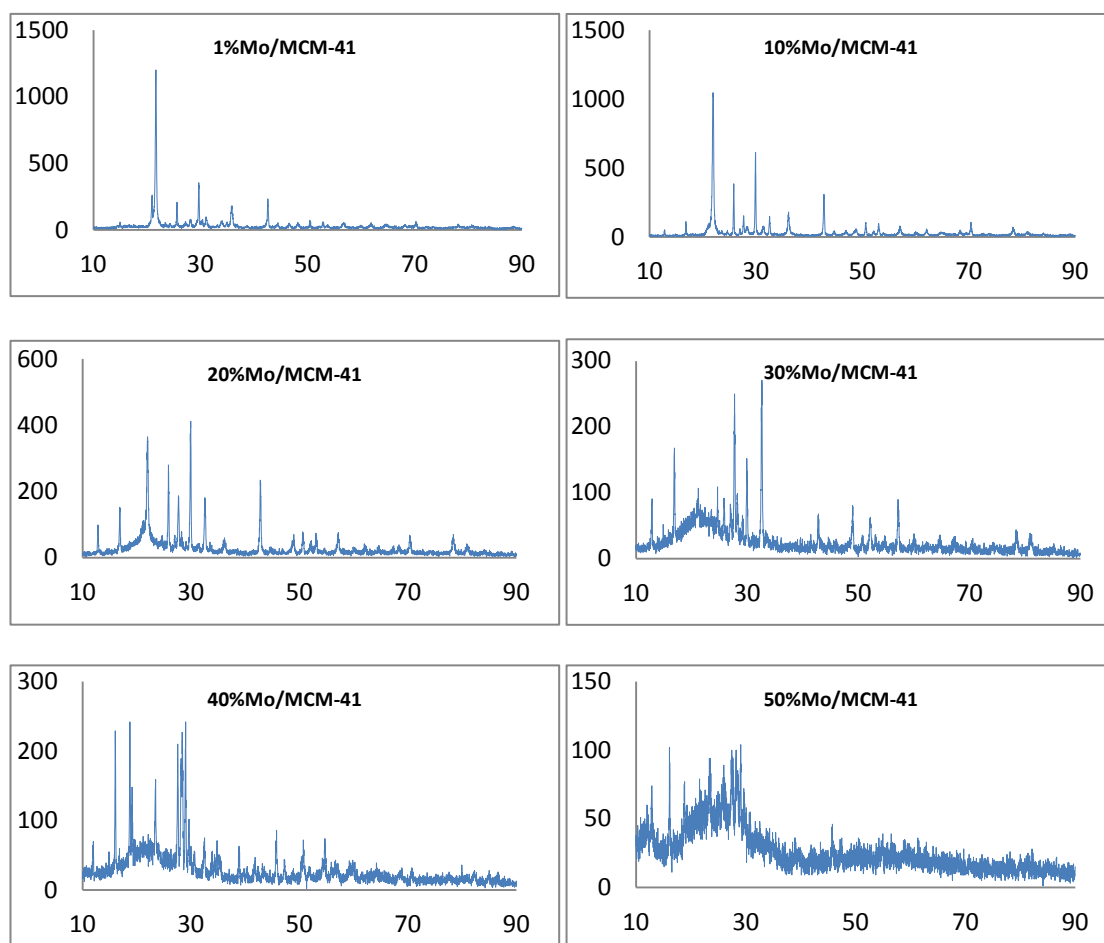


Figure 28 XRD patterns of the Cr/MCM-41 composites with different chromium (1% to 50%, from left to right, top to bottom)

The XRD patterns show there are significant differences between Mo/MCM-41 and Cr/MCM-41. For the catalyst composition with 1% and 10% molybdenum loading, the diffraction peaks' shape and position are similar to which in the XRD patterns of MCM-41. With small amount of metal loading, catalysts surface shows SiO₂ crystal structure. From 20% to 40% metal compounds loading, some new diffraction peaks are found in the pattern. The dragg angle around 23.4°, 25.8°, 27.4°, 33.8° and 39° shows the Mo/SiO₂ structure (Ichikuni, Nakao, Ishizuki, Hara, & Shimazu, 2013). With 50% molybdenum loading, intensive diffraction peaks appeared between 15° and 30°. The structure reprecented by these diffraction peaks need to be explored in further study. In general, as scanning electron microscopy shows, the skeletal structure of Mo/MCM-41 was changed during synthesis.

3.5.3 CATALYSTS SURFACE AREA AND POROSITY DETERMINATION

The nitrogen adsorption-desorption isotherm method was selected to measure catalysts specific surface area and porosity. Adsorption is the process of atoms, ions, or molecules transferred from a gas or liquid to a solid surface. The components aggregate on the solid surface is called adsorbate, and the solid is called the adsorbent. Adsorption can be roughly divided into two categories (Ferrari, Kaufmann, Winnefeld, & Plank, 2010), chemisorption (characteristic of covalent bonding) and physisorption (characteristic of weak van der Waals forces). In this study, nitrogen adsorption is a kind of physisorption that can cover the whole surface and enter the pore interiors (Lowell, Shields, Thomas, & Thommes, 2004). The specific surface area, pore volume and pore size can be calculated based on B.E.T. theory and B.J.H. theory.

B.E.T. theory: B.E.T. theory (Brunauer–Emmett–Teller theory) is the most widely used theory in the multilayer adsorption isotherm. In 1938, Stephen Brunauer, Paul Hugh, Emmett, and Edward Teller established a model assumes that the adsorbent surface is uniform, there are no interaction between adsorbate molecules, the adsorption is multilayer adsorption and the adsorption heat is equal to the heat of liquefaction. The theory is an extension of the Langmuir theory (a theory for monolayer molecular adsorption) which explained the physical adsorption of gas molecules on a solid surface (Brunauer, Emmett, & Teller, 1938; Y. Yang, Wang, & Kou, 2004).

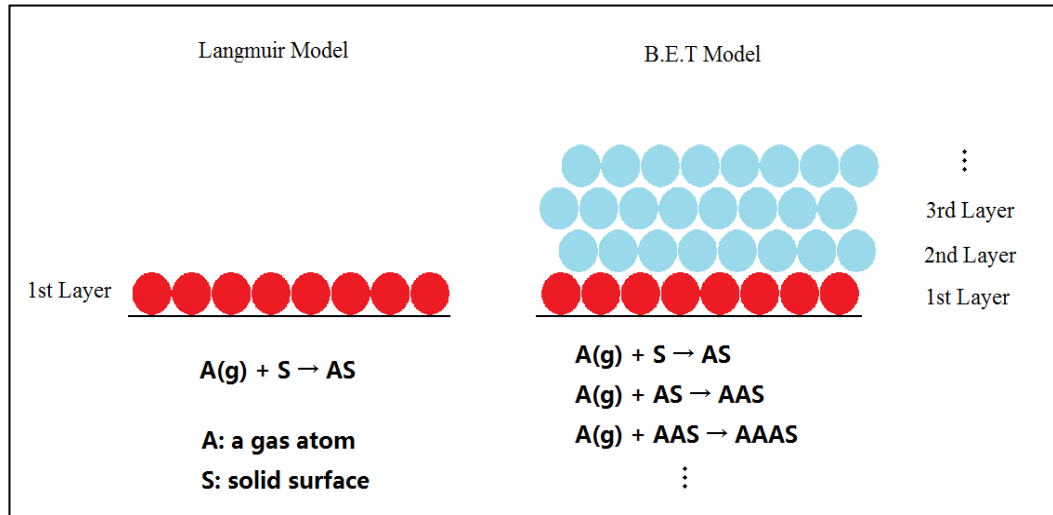


Figure 29 Comparison of Langmuir and BET models for gas adsorption

B.E.T. equation is written as:

$$\frac{P}{v(P_0 - P)} = \frac{1}{v_m c} + \frac{c-1}{v_m c} \left(\frac{P}{P_0} \right)$$

In this equation, P is the equilibrium pressure and P_0 is the saturation pressure at adsorbent temperature, v is the adsorbed volume and v_m is the monolayer adsorbed volume, c is the B.E.T. constant (see below).

$$c = \exp\left(\frac{E_1 - E_L}{RT}\right)$$

Where E_1 is the heat of adsorption for the first layer, and E_L is that for the second and higher layers and is equal to the heat of liquefaction (Li, 2011; R. T. Yang, 1987). The suitable relative pressure (P/P_0) range for B.E.T. equation is between 0.05 and 0.35. During this range, the adsorption isotherm can be plotted. With the $P/v(P_0 - P)$ on the y-axis and P/P_0 on the x-axis, a straight line can be plotted. Then the slope (K) and y-intercept (I) can be used for the calculation:

$$v_m = \frac{1}{K + I} \quad \text{and} \quad c = 1 + \frac{K}{I}$$

Finally, the total surface area (S_{total}) and the specific surface area (S_{BET}) can be written as:

$$S_{\text{total}} = \frac{(v_m N s)}{V} \quad \text{and} \quad S_{\text{BET}} = \frac{S_{\text{total}}}{a}$$

Which N is Avogadro's number, s is the adsorption cross section, V is the molar volume of the adsorbate gas and a is the mass of the absorbent.

According to the definition of IUPAC, there are 6 types of adsorption-desorption isotherms:

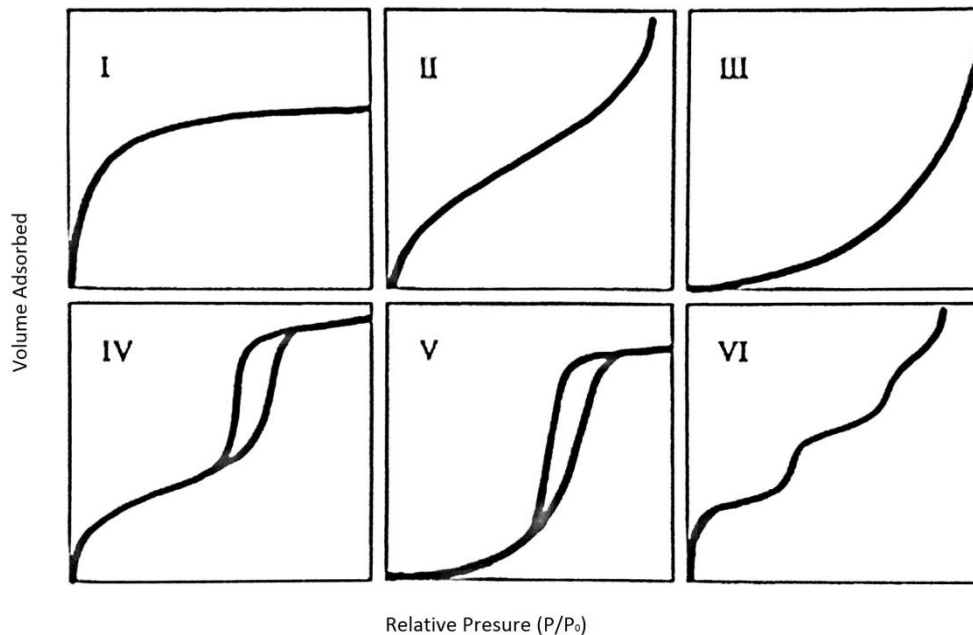


Figure 30 The IUPAC Classification of Adsorption Isotherms for Gas–Solid Equilibria (Donohue & Aranovich, 1998)

Type I – Microporous solids Langmuir isotherm.

Type II – Multilayer adsorption on non-porous / macroporous solids.

Type III – Adsorption on non-porous /macro-porous solids with weak adsorption.

Type IV – Adsorption on meso porous solids with an hysteresis loop.

Type V – Same as IV type with weak adsorbate-adsorbent interaction.

Type VI – Stepped adsorption isotherm, on different faces of solid.

The following figure shows the adsorption isotherm for Cr/MCM-41.

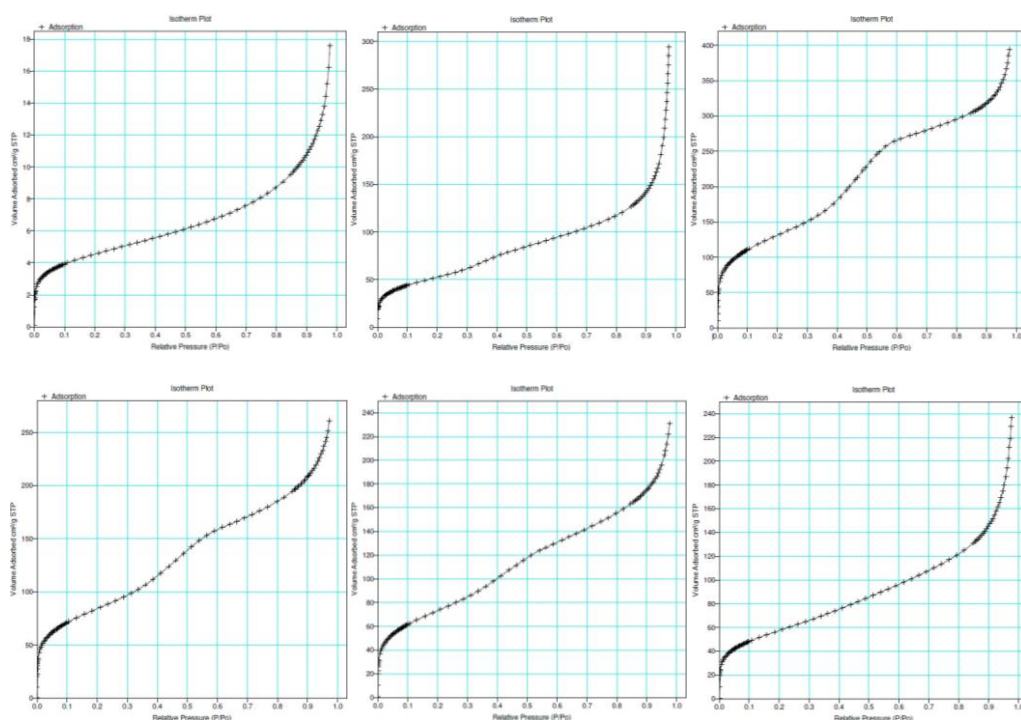


Figure 31 Adsorption isotherm for Cr/MCM-41 (1% to 50%, from left to right, up to down)

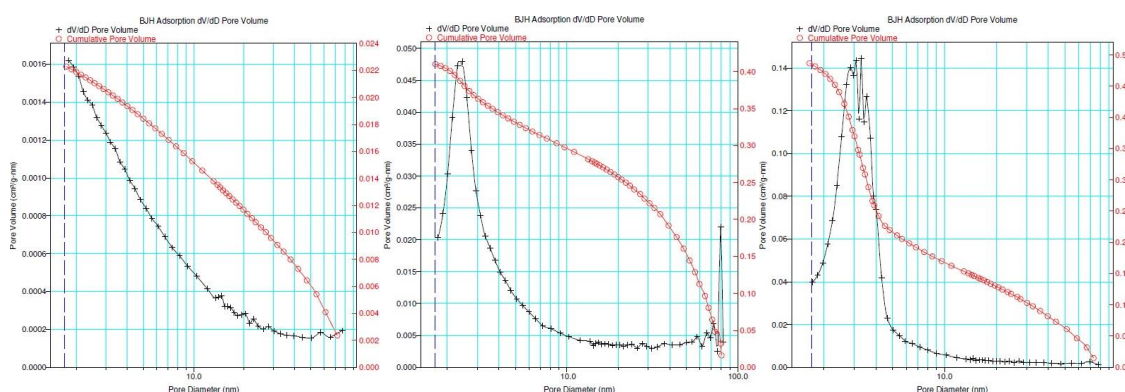
From **Figure 31**, in the adsorption isotherm for 10%, 20%, 30% and 40% Cr/MCM-41, obvious plateaus can be found at the P/P_0 between 0.5 and 0.8. They are similar to the type IV adsorption isotherm above. This shows that these samples still maintain the mesoporous structure with chromium loading. The other two samples shows multilayer adsorption on non-porous / macroporous solids.

The BET specific surface area, BJH pore volume and average BJH pore diameter of Cr/MCM-41 are shown in **Table 16**.

Table 16 Surface area and porosity properties of Cr/MCM-41 catalysts

	BET specific surface area (m ² g ⁻¹)	BJH pore volume (cm ³ g ⁻¹)	BJH pore diameter (nm)
1% Cr/MCM-41	16.2885	0.022286	9.6163
10% Cr/MCM-41	191.8008	0.410111	9.8073
20% Cr/MCM-41	476.5395	0.486688	4.6962
30% Cr/MCM-41	305.9367	0.33088	5.2202
40% Cr/MCM-41	266.9557	0.285102	5.54
50% Cr/MCM-41	208.8943	0.305924	8.2022

With higher presentage (From 20% to 50%) of chromium loading, the specific surface area and pore volume have a declining trend. Because the MCM - 41 molecular sieve hole wall is thin, chromium cannot completely replace silicon into the molecular sieve skeleton, part of the chromium exposed on the surface or filled in the pore of MCM-41 molecular sieve. In this way, chromium blocked the channel in order to changed the specific surface area and pore volume of the molecular sieves. But the pore diameter increases as the metal content increases. This is consistent with some previous work (Amama et al., 2005; Morey, Davidson, Eckert, & Stucky, 1996; Parvulescu, Anastasescu, & Su, 2004). This result might be due to Cr-O bond being longer than Si-O bond, so chromium loading increases the molecular sieve's diameter (Morey et al., 1996). The tendency of pore size change can also be seen from the following figure.



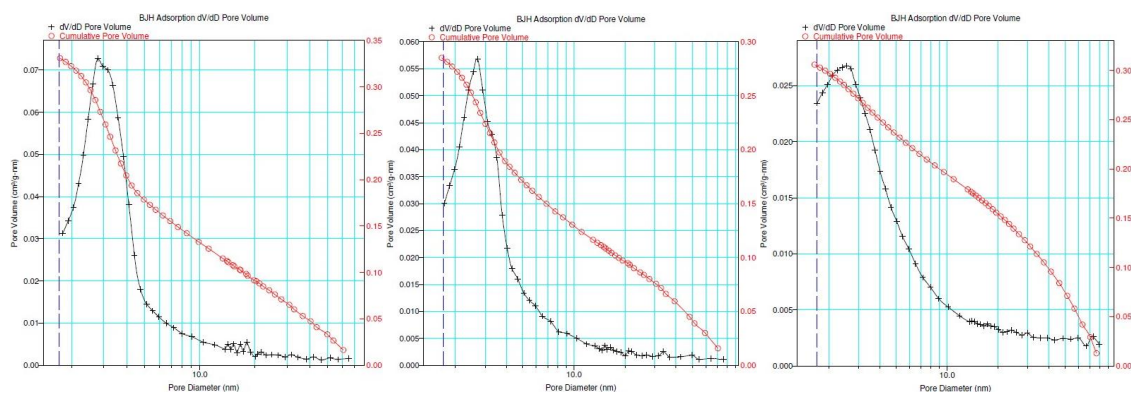


Figure 32 The pore size distribution curves of Cr/MCM-41 (1% to 50%, from left to right, up to down)

Mo/MCM-41 catalysts have completely different pore structure. As shown in **Figure 33**, the adsorption isotherm belongs to type II adsorption isotherm above. The characteristic of Mo/MCM-41 is macroporous materials. Pore volume and pore size of this kind of catalyst need to be further discussed.

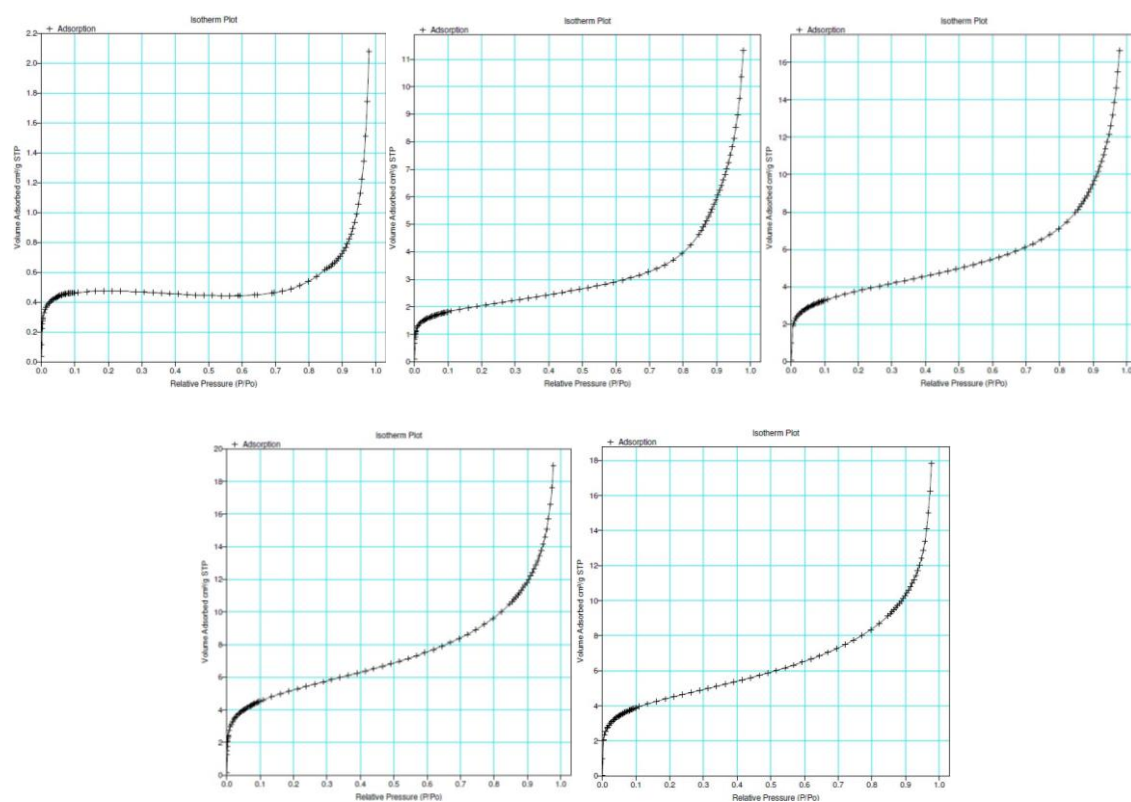


Figure 33 Adsorption isotherm for Mo/MCM-41 (10% to 50%, from left to right, up to down)

The BET specific surface area, BJH pore volume and average BJH pore diameter of Cr/MCM-41 are shown in **Table 17**.

Table 17 Surface area and porosity properties of Mo/MCM-41 catalysts

	BET specific surface area (m ² g ⁻¹)	BJH pore volume (cm ³ g ⁻¹)	BJH pore diameter (nm)
10% Mo/MCM-41	1.5857	0.002547	32.2643
20% Mo/MCM-41	7.1961	0.015346	14.5589
30% Mo/MCM-41	13.4965	0.021355	11.5421
40% Mo/MCM-41	15.8707	0.022512	10.4728
50% Mo/MCM-41	18.673	0.023524	9.6403

With an increase in molybdenum content, the specific surface area and pore volume increased while pore diameter decreased at the same time. Perhaps because the Mo-O bond is much longer than the Si-O bond, so molybdenum loading increases the diameter and change the skeleton structure of the molecular sieve. These reasons formed the macroporous structure of Mo/MCM-41.

These two groups of transition metal modified MCM-41 catalysts have different specific surface area, pore volume and average pore diameter, but both of them have a good catalytic ability. So the catalytic activities may also depend on their active sites and acid strength.

3.6 TYPE OF ACTIVE SITES AND ACID STRENGTH

3.6.1 ACTIVE SITES

Active sites were analyzed using Infrared (IR) spectroscopy as discussed in section 3.4.1. The following figure shows the IR spectrum for MCM-41 structure.

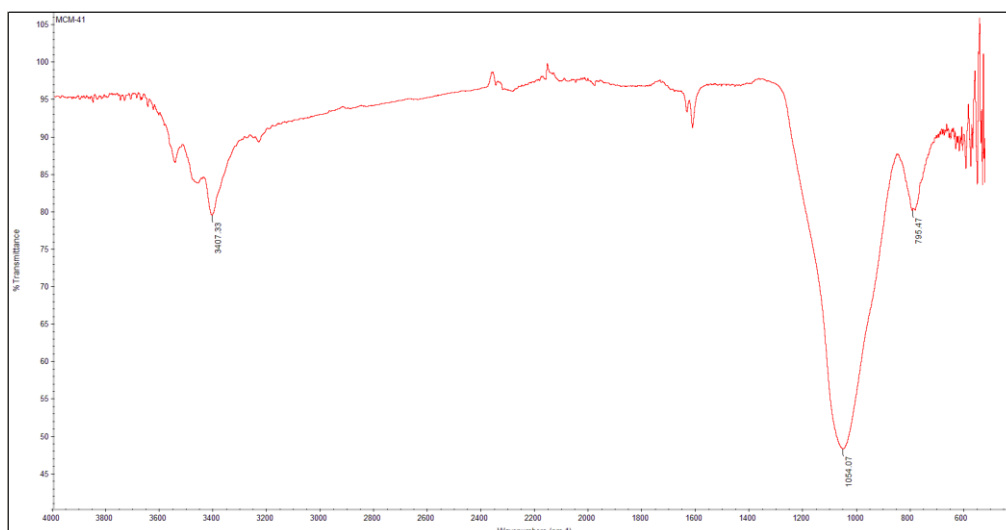


Figure 34 IR spectrum for MCM-41 without metal loading

As shown in this spectrum, four characteristic peak can be seen. The peak around 3400 cm^{-1} shows the O-H bond stretching (water and inorganic hydroxyls). And the small peak near 1630 cm^{-1} represents the O-H bond twisting of water. The band around 1050 cm^{-1} is the Si-O antisymmetric stretch and the Si-O bond symmetric stretching gives a peak around 795 cm^{-1} . Because the IR spectroscopy with diamond window has a minimum wavelength which is 525 cm^{-1} . So the peak caused by Si-O bond twisting at about 460 cm^{-1} cannot be measured.

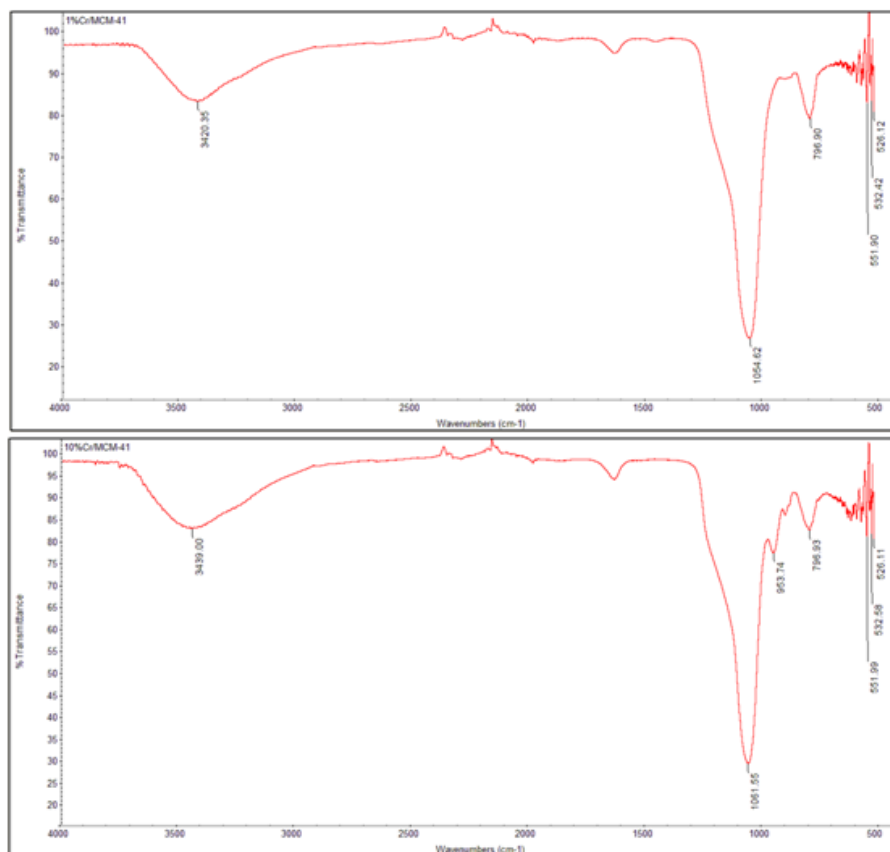


Figure 35 IR spectra for 1%Cr/MCM-41(above) and 10%Cr/MCM-41(below)

For Cr/MCM-41 catalysts, a new peak appeared around 950 cm^{-1} , it represent that Si-O-Cr bond stretching. In the IR spectrum for 1% Cr/MCM-41 catalyst, only a few chromium was load on the molecular sieve. This might be the reason these is no peak appeared around 950 cm^{-1} in the spectrum. A lot of researchers (Guzman-Castillo et al., 2003; Li, 2011; Noda, de Almeida, Probst, & Goncalves, 2005; Ropero-Vega et al., 2010; Wang et al., 2009) have shown that the two peaks around 980 and 1075 cm^{-1} are characteristic of bidentate sulfate ions. Further study is necessary to prove if bidentate sulphate ions are formed in Cr/MCM-41 catalysts.

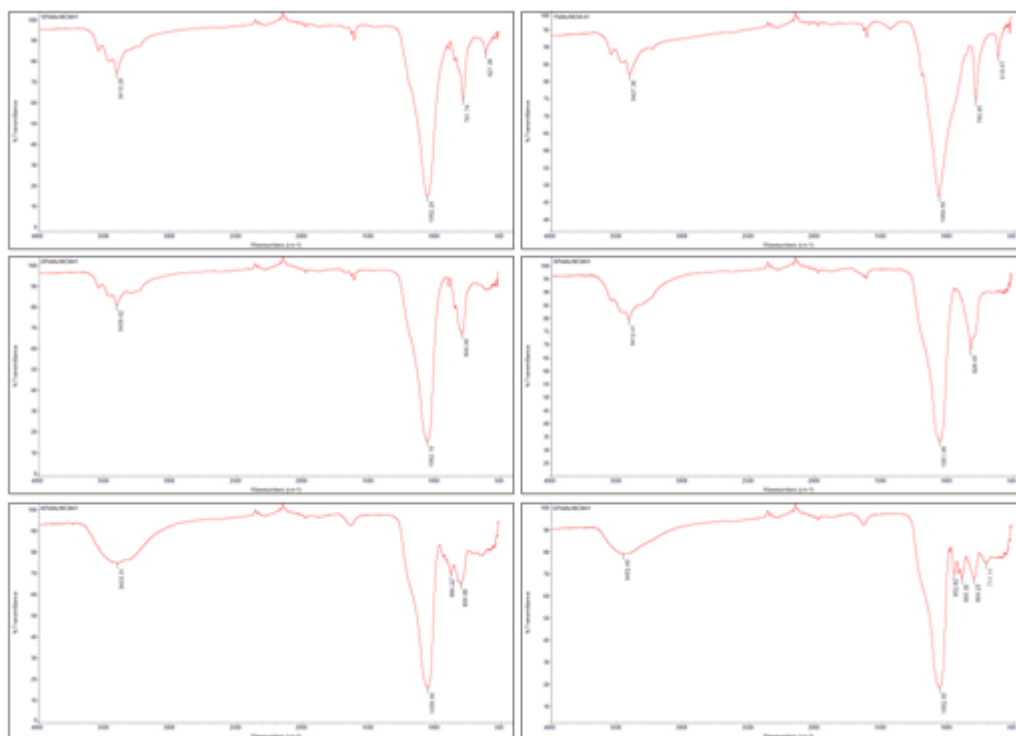


Figure 36 IR spectra for Mo/MCM-41 catalysts(from left to right, up to down:1% to 50%)

The IR spectra for Mo/MCM-41 catalysts show different characteristics with different presentages of metal loading. Compared with the pure MCM-41 molecular sieve, 1% to 30% molybdenum loading catalysts show little . In the IR spectra for high presentage (40% and 50%) Mo loading catalysts, some small peaks appears between 880cm^{-1} to 950cm^{-1} . These peaks are caused by Si-O-Mo bond vibration (Li, 2011; Wang et al., 2009).

Compared with MCM-41, the active sites for metal loading MCM-41 catalysts is Si-O-M group (M = Cr or Mo). The type of these active sites were detected using pyridine adsorption method and hammett indicator method.

Pyridine adsorption: Because of the strong basicity ($\text{pK}_a < 9$), pyridine can react with different types of acids and produce pyridinium cation. By observing the absorption

band between 1700cm^{-1} and 1400cm^{-1} for pyridine one can determine the acid type and acid strength (Parry, 1963; Y. Yang et al., 2004).

This has been used for determination of the acidity of solid acids. There are two common vibrations for pyridine. One is reacting with Brønsted acid, and the products PyH^+ (BPy) cases adsorption peaks around 1540cm^{-1} and 1630cm^{-1} . The other is reacting with Lewis acid. LPy coordinated complexes have adsorption bands around 1450cm^{-1} and 1600cm^{-1} (Y. Yang et al., 2004). By comparing the location of peaks in IR spectra, the type of acid in the catalysts can be determined.

By studying the spectrum changes with increasing the sample temperature. The pyridine adsorption recorded by IR spectroscopy can also be a useful method to identify catalyst deactivation (Voskoboinikov et al., 1998).

Type of active sites: *Figure 37* shows the IR spectra of MCM-41 with pyridine adsorption

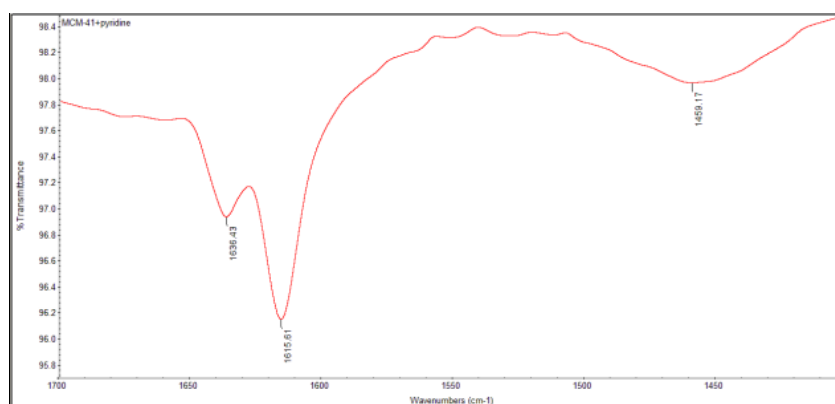


Figure 37 IR spectrum of MCM-41 with pyridine adsorption

From this spectrum, three peaks (around: 1630cm^{-1} , 1615cm^{-1} and 1460cm^{-1}) were found. The following are a series of IR spectra of MCM-41 with different ratio metal loading.

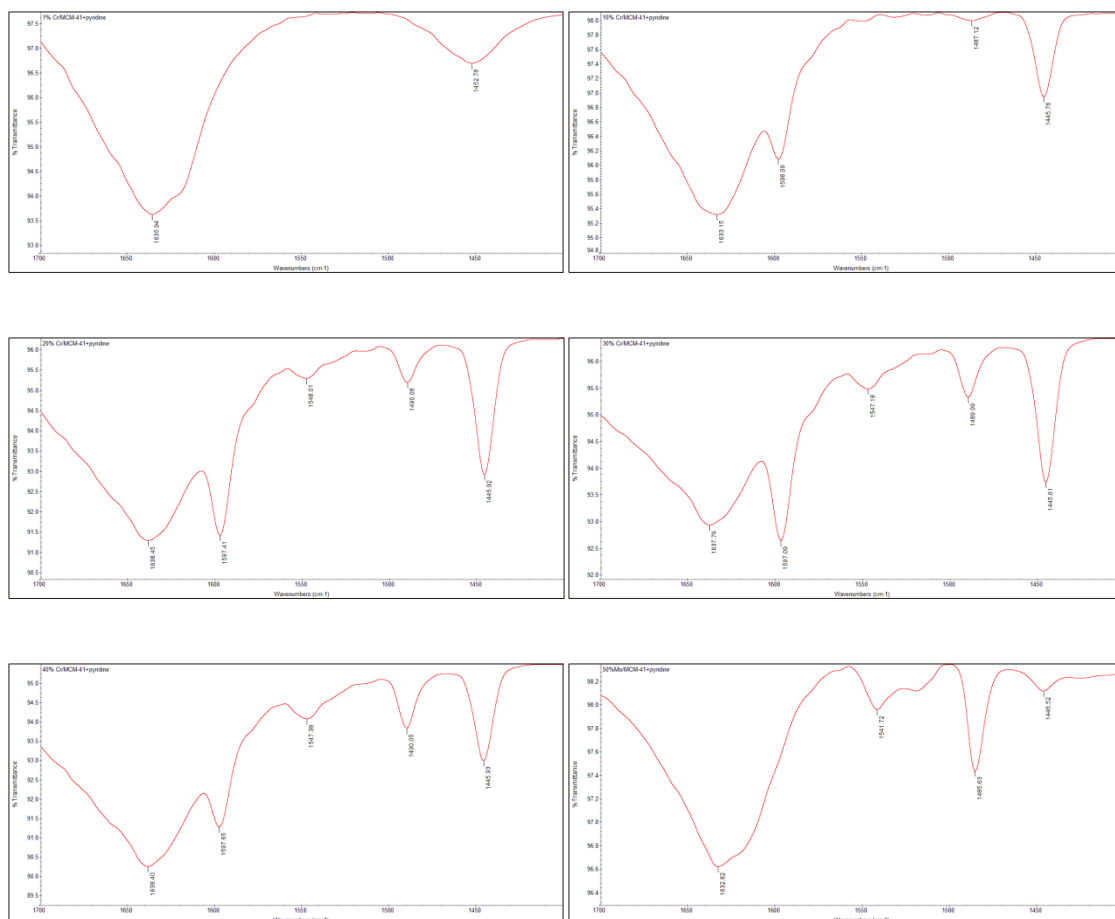


Figure 38 IR spectra of Cr/MCM-41 catalysts with pyridine adsorption (from left to right, up to down: 1% to 50%)

From the IR spectra of Cr/MCM-41 samples (see **Figure 38**), different ratio of chromium loading gave different characteristic peak. For 1% Cr/MCM-41 catalysts, there are two peaks which located around 1635 cm^{-1} and 1450 cm^{-1} . Compared with the spectrum of pure MCM-41, the peak around 1450 cm^{-1} become larger. It means even a little chromium loading can create a Lewis acid sites. When the metal ratio increased to 10%, two new absorption bands appeared around 1600 cm^{-1} and 1485 cm^{-1} . The absorption bands around 1600 cm^{-1} can be assigned to the presence of Lewis acid sites in the solids and another one can represent either Lewis or Brønsted acid sites. Along with the increase in metal loading, the characteristic peak for Brønsted acid sites was found around 1550 cm^{-1} . And at the same time, the peak around 1450 cm^{-1} become larger and

larger. It means both Lewis and Brønsted acid sites grow in number or quantity with increasing the chromium loading. Furthermore, the wide bands between 1610 cm^{-1} and 1640 cm^{-1} represent that in this sample strong Lewis acid sites formed instead of Brønsted acid sites (Corma, 1995; Dalai, Sethuraman, Katikaneni, & Idem, 1998; Gui et al., 2005; Li, 2011; Noda et al., 2005; Parry, 1963).

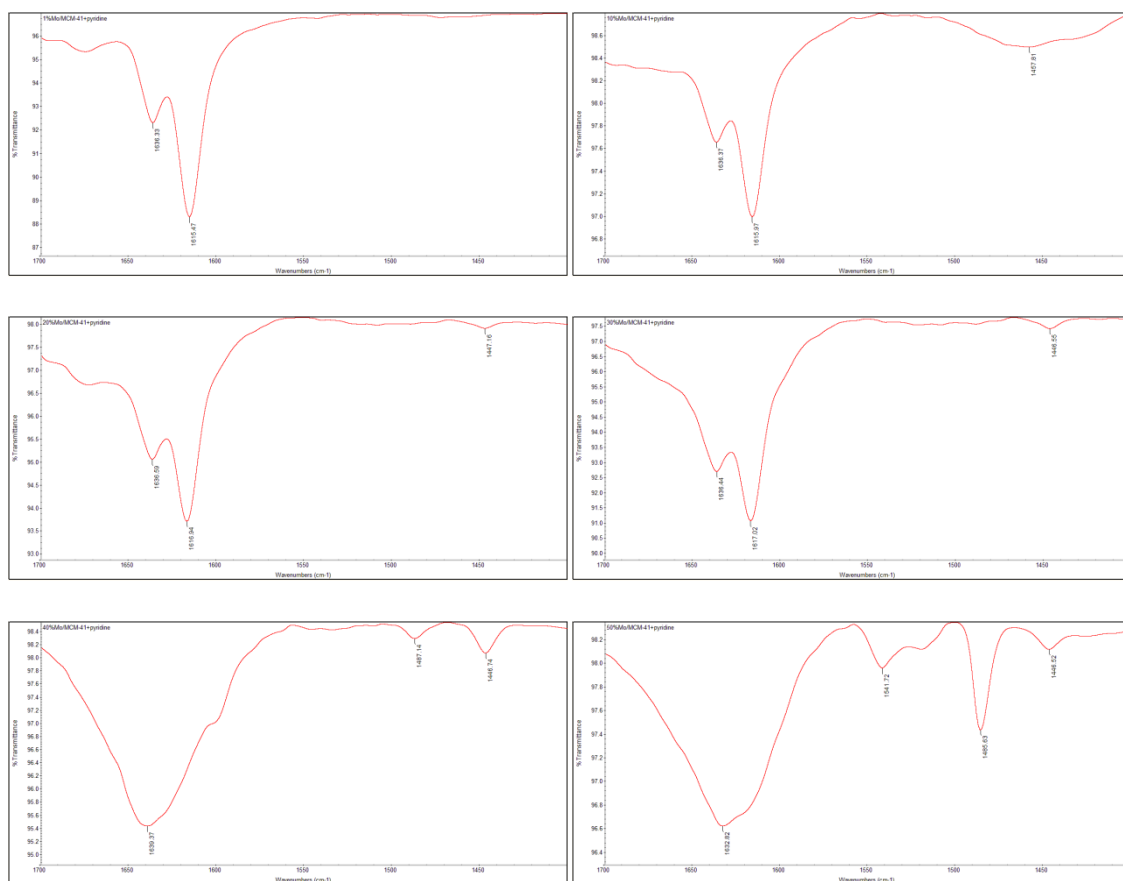


Figure 39 IR spectra of Mo/MCM-41 catalysts with pyridine adsorption (from left to right, up to down: 1% to 50%)

The IR spectra for Mo/MCM-41 reflect dissimilar results. As shown in **Figure 39**, with low presentage (1% to 30%) of molybdenum loading, there are no obvious peaks can represent the pyridine chemisorbed on Brønsted acid sites. Only a small peak around 1450 cm^{-1} shows there are some weak Lewis acid sites in these samples. For 40% Mo/MCM-41 catalysts, obvious Lewis acid sites absorbtion band can be found around 1445 cm^{-1} . In this group, 50% Mo/MCM-41 catalysts show the strongest acidity, similar

with 50% Cr/MCM-41, strong Lewis acid sites formed and gave a wide peak between 1610 cm^{-1} and 1640 cm^{-1} .

3.6.2 THE DEACTIVATION OF ACTIVE SITES

The deactivation of these catalysts were analysed by IR spectroscopy from 0°C to 400°C . With the disappearance of characteristic peaks, the decomposition temperature of active sites can be found.

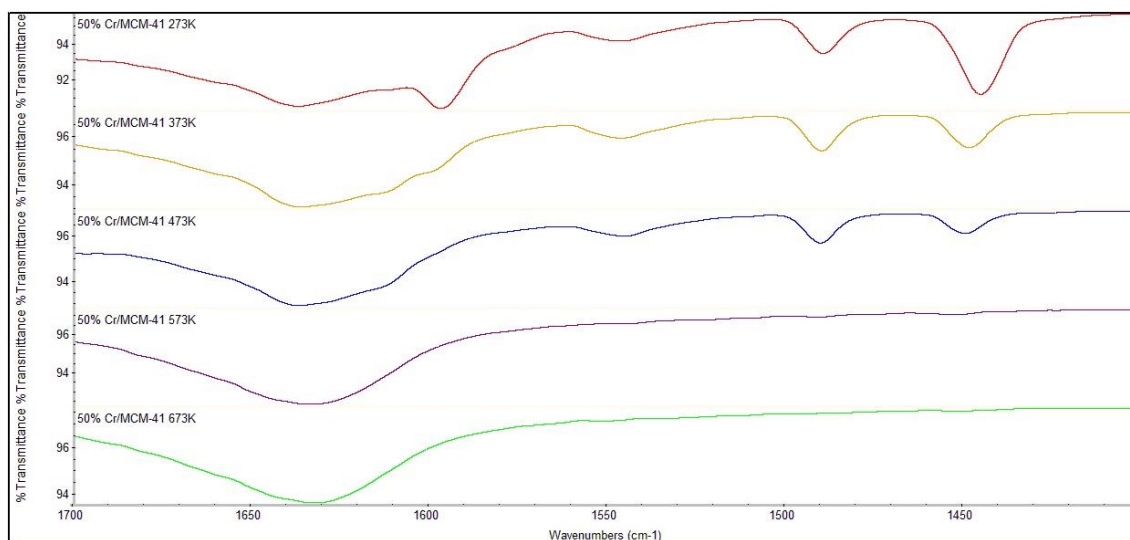


Figure 40 IR spectra of 50 %Cr/MCM-41 catalysts with pyridine adsorption from 0°C to 400°C

As shown in **Figure 40**, at 0°C , the characteristic peaks for both Brønsted and Lewis acid sites can be seen clearly. From 0°C to 200°C , characteristic peaks slightly decreases with the temperature increase. When the temperature reached 300°C , both of the Brønsted and Lewis acid peaks disappearing. It means both Brønsted and Lewis acid sites decomposed above this temperature. From this result, the temperature range of application Cr/MCM-41 catalysts is between 0°C and 200°C .

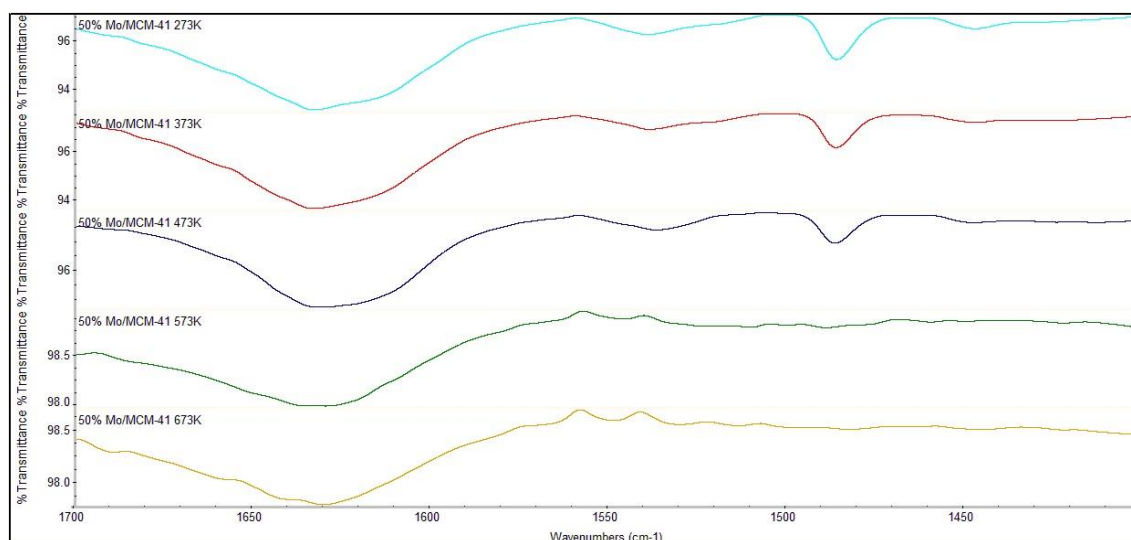


Figure 41 IR spectra of 50 %Mo/MCM-41 catalysts with pyridine adsorption from 0 °C to 400 °C

Similar with the results from 50 % Cr/MCM-41 catalysts, both Brønsted and Lewis acid sites in 50 % Mo/MCM-41 decomposed above 300 °C.

In general, this kind of MCM-41 molecular sieve catalysts with metal loading are not thermally stable enough for a reaction which happened in a high temperature.

3.6.3 ACID STRENGTH

Hammett indicator method: In 1930s, the most famous acidity function was proposed by American physical chemist Louis Plack Hammett (Hammett, 1940). He defines the Hammett acidity function (H_0), which uses a series of bases to measure the acidity of an acid. The calculation process is shown below:

When a neutral basic indicator (B) receives a proton in the solution, a corresponding conjugated acid (BH^+) and base (A^-) were formed (see equation below).



So the acid strength in the solution can be expressed as:

$$H_0 = pK_a + \log \frac{[B]}{[BH^+]} \quad (2)$$

[B] means the concentration of the neutral basic indicator and [BH⁺] means the concentration of conjugated acid.

According to the theory described above, the acid strength can be measured using different indicators. If the indicator shows a acid colour, it means the pK_a of sample is less than or equal to the pK_a of the conjugated acid of the indicator. By using different indicators, the pK_a rang of sample can be measured roughly.

Cr/MCM-41 acid strength: The acid strength of different presentage of Cr loading catalysts are shown in **Table 18**. In **Table 18** and **19**, ‘+’ means a acid colour, ‘-’ means a base colour and ‘0’ means catalysts background colour.

Table 18 Acidity strength of Cr/MCM-41 catalysts measuring with Hammett indicators

Cr/MCM-41	H_0 value				
	$\leq + 7.2$	$\leq + 4.8$	$\leq + 3.8$	$\leq + 1.2$	≤ -0.2
Cr ₁	+	+	-	-	0
Cr ₁₀	+	+	+	+	+
Cr ₂₀	+	+	+	+	0
Cr ₃₀	+	+	+	+	0
Cr ₄₀	0	+	0	+	0
Cr ₅₀	0	+	0	+	0

The colour change of indicators on the surface of catalysts was observed. In this table, most of catalysts shown a acid colour using different Hammett indicators. Because of the Cr/MCM - 41 is a green catalyst, with the chromium concentrantion increased, some acid colour change are not sensitive enough based on the deep green colour. The results shows, all the Cr/MCM-41 catalysts have a acid strength $H_0 \leq 1.2$ except 1% Cr/MCM-41 ($3.8 \leq H_0 \leq 4.8$). It means all these catalysts are solid acids.

Mo/MCM-41 acid strength: The acid strength of different presentage of Mo loading catalysts are shown in **Table 19**.

Table 19 Acidity strength of Mo/MCM-41 catalysts measuring with Hammett indicators

Mo/MCM-41	H_0 value				
	$\leq +7.2$	$\leq +4.8$	$\leq +3.8$	$\leq +1.2$	≤ -0.2
Mo1	+	+	-	-	-
Mo10	+	+	-	-	-
Mo20	+	+	+	-	-
Mo30	+	+	+	-	-
Mo40	+	+	+	+	+
Mo50	+	+	+	+	+

All Hammett indicators gave a acid colour results for high presentage Mo loading (40% and 50%). The other four kinds of catalysts in this group shows the weak acidity. The result for Hammett indicators test is consistent with the IR result (Brønsted and Lewis acid sites formed with high presentage Mo loading).

The Hammett indicator method has a lot of limitations. This method is only applicable to a colorless or white sample. As the colour deepens, the colour change is harder to identify. And each hammett indicator only corresponds to a pKa which cause an inaccurate measurement result. In this study, because of the limitation of Hammett indicator species. The acidity range of most catalysts are unable to detect. In further, some new indicator with a lower pKa can be used to get a more accurate result.

CHAPTER 4 CONCLUSIONS AND FUTURE WORK

4.1 CONCLUSIONS

Two different transition metal modified mesoporous silica catalysts were successfully prepared using a direct impregnation method.

For Cr/MCM-41 catalysts, up to 50 ratio percentage of chromium was loaded onto the molecular sieve. The template (CTAB) was decomposed between 200 °C and 300 °C, and the chromium sulfate was decomposed from about 600 °C. During the calcination, the highly stable hexagonal close packed structure of chromic oxide formed under high temperature. The crystal structure of the mesoporous silica was maintained with chromium evenly distributed both on the surface and in the pore. Specific surface area, pore volume and pore size changed regularly with the increase of chromium. Both Brønsted and Lewis acid sites are found on the surface of the new synthesis catalysts and have good stability under 200 °C. With the increase of chromium content, the catalytic activity for the esterification of acetic acid and *n*-butanol increased significantly.

For Mo/MCM-41 catalysts, up to 50 ratio percentage of molybdenum was loaded on the molecular sieve. The template (CTAB) was decomposed between 200 °C and 300 °C, and molybdenum sulfate was decomposed from about 600 °C. During the synthesis, ammonium molybdate decomposed and changed the pH value. The structure of MCM-41 was changed and mesoporous silica with a larger pore was formed. Specific surface area, pore volume and pore size changed regularly with the increase of molybdenum. Both Brønsted and Lewis acid sites are found on the surface of the new catalysts and have good stability under 200 °C. With the increase of molybdenum content, especially from 30% to 40%, the catalytic activity for esterification of acetic acid and *n*-butanol had a significant increase.

Both of these catalysts can be reused after calcining, this gives them an industrial value.

4.2 LIMITATIONS AND FUTURE WORK

Because of the limitation of instruments, the characterization of some properties of catalysts was not possible. For example, the structure of Mo/MCM-41 was not determined and Hammett indicator test are not accurate. For further work, more methods like transmission electron microscope for pore structure and Raman spectrum for chemical bonds can be used.

For these two kinds of catalysts, the thermal stabilities for their active sites are not good enough. In further studies, other synthesis methods and metals could be used to improve the performance of this molecular sieve to get a wider range of applications.

REFERENCES

- Amama, P. B., Lim, S., Ciuparu, D., Yang, Y., Pfefferle, L., & Haller, G. L. (2005). Synthesis, characterization, and stability of Fe-MCM-41 for production of carbon nanotubes by acetylene pyrolysis. *The Journal of Physical Chemistry B*, 109(7), 2645-2656.
- Anandan, S., & Okazaki, M. (2005). Dynamics, flow motion and nanopore effect of molecules present in the MCM-41 nanopores—An overview. *Microporous and Mesoporous Materials*, 87(2), 77-92.
doi:<http://dx.doi.org/10.1016/j.micromeso.2005.07.036>
- Bates, R. G. (1964). Determination of pH: theory and practice.
- Beck, J. S., Vartuli, J. C., Roth, W. J., Leonowicz, M. E., Kresge, C. T., Schmitt, K. D., ... Schlenker, J. L. (1992). A new family of mesoporous molecular sieves prepared with liquid crystal templates. *Journal of the American Chemical Society*, 114(27), 10834-10843.
- Bentor, Y. (2012). *Periodic Table: Transition Metals*. Retrieved from <http://www.chemicalelements.com/groups/transition.html>
- Blin, J., Otjacques, C., Herrier, G., & Su, B.-L. (2000). Pore size engineering of mesoporous silicas using decane as expander. *Langmuir*, 16(9), 4229-4236.
- Brønsted, J. N. (1923). Some remarks on the concept of acids and bases. *Recueil des Travaux Chimiques des Pays-Bas* 42, 718-728.
- Brown, W. H. (1995). *Organic chemistry*. Orlando: Saunders College Publishing (1995).
- Brunauer, S., Emmett, P. H., & Teller, E. (1938). Adsorption of gases in multimolecular layers. *Journal of the American Chemical Society*, 60(2), 309-319.
- Carvalho, W. A., Varaldo, P. B., Wallau, M., & Schuchardt, U. (1997). Mesoporous redox molecular sieves analogous to MCM-41. *Zeolites*, 18(5-6), 408-416.
- Chen, C. L., Cheng, S., Lin, H. P., Wong, S. T., & Mou, C. Y. (2001). Sulfated zirconia catalyst supported on MCM-41 mesoporous molecular sieve. *Applied Catalysis A: General*, 215(1-2), 21-30.
- Chen, C. L., Li, T., Cheng, S., Lin, H. P., Bhongale, C. J., & Mou, C. Y. (2001). Direct impregnation method for preparing sulfated zirconia supported on mesoporous silica. *Microporous and Mesoporous Materials*, 50(2-3), 201-208.
- Chen, J., Sun, R. H., Tang, J., Guo, M., & Wang, W. (2006). Solid Superacid S₂O₈²⁻/TiO₂ Supported on MCM-41: Preparation and Catalytic Performance for Esterification [J]. *Chinese Journal of Inorganic Chemistry*, 3, 006.

- Chiola, V. (1971). PROCESS FOR PRODUCING LOW-BULK DENSITY SILICA.
- Choudhary, V. R., Jana, S. K., & Kiran, B. (2000). Highly active Si-MCM-41-supported Ga_2O_3 and In_2O_3 catalysts for friedel-crafts-type benzylation and acylation reactions in the presence or absence of moisture. *Journal of Catalysis*, 192(2), 257-261.
- Coats, A., & Redfern, J. (1963). Thermogravimetric analysis. A review. *Analyst*, 88(1053), 906-924.
- Corma, A. (1995). Inorganic solid acids and their use in acid-catalyzed hydrocarbon reactions. *Chemical Reviews*, 95(3), 559-614.
- Dalai, A. K., Sethuraman, R., Katikaneni, S. P. R., & Idem, R. O. (1998). Synthesis and Characterization of Sulfated Titania Solid Acid Catalysts. *Industrial & Engineering Chemistry Research*, 37(10), 3869-3878. doi:10.1021/ie980091x
- Das, D., Tsai, C.-M., & Cheng, S. (1999). Improvement of hydrothermal stability of MCM-41 mesoporous molecular sieve. *Chemical Communications*(5), 473-474.
- Dongsen, M., Guanzhong, L., Qinglin, C., & Wenkui, L. (2001). Advances in the Preparation and Applications of Supported Oxides Solid Superacid Catalysts. *CHEMISTRY-PEKING*-(5), 278-284.
- Donohue, M. D., & Aranovich, G. L. (1998). Classification of Gibbs adsorption isotherms. *Advances in Colloid and Interface Science*, 76–77(0), 137-152. doi:[http://dx.doi.org/10.1016/S0001-8686\(98\)00044-X](http://dx.doi.org/10.1016/S0001-8686(98)00044-X)
- Ecormier, M. A., Wilson, K., & Lee, A. F. (2003). Structure–reactivity correlations in sulphated-zirconia catalysts for the isomerisation of α -pinene. *Journal of Catalysis*, 215(1), 57-65.
- Ferrari, L., Kaufmann, J., Winnefeld, F., & Plank, J. (2010). Interaction of cement model systems with superplasticizers investigated by atomic force microscopy, zeta potential, and adsorption measurements. *Journal of Colloid and Interface Science*, 347(1), 15-24.
- Furuta, S., Matsuhashi, H., & Arata, K. (2004). Catalytic action of sulfated tin oxide for etherification and esterification in comparison with sulfated zirconia. *Applied Catalysis A: General*, 269(1), 187-191.
- Gaydhankar, T. R., Samuel, V., Jha, R. K., Kumar, R., & Joshi, P. N. (2007). Room temperature synthesis of Si-MCM-41 using polymeric version of ethyl silicate as a source of silica. *Materials Research Bulletin*, 42(8), 1473-1484.
- Giraldo, L. F., Lopez, B. L., Perez, L., Urrego, S., Sierra, L., & Mesa, M. (2007). Mesoporous silica applications. *Macromolecular Symposia*, 258(1), 129-141.

- Gui, J., Ban, H., Cong, X., Zhang, X., Hu, Z., & Sun, Z. (2005). Selective alkylation of phenol with tert-butyl alcohol catalyzed by Bronsted acidic imidazolium salts. *Journal of Molecular Catalysis A: Chemical*, 225(1), 27-31.
- Guo, X., Lin, Q., Fu, L., & Deng, X. (2002). Influence of Calcining Temperature on Structure and Catalytic Activity of Zirconium Cross-linking Clay Solid Acid Modified by SO_4^{2-} . *Journal of Molecular Catalysis (China)*, 4. doi:10.3969/j.issn.1001-3555.2002.04.005
- Guzman-Castillo, M. L., Lopez-Salinas, E., Fripiat, J. J., Sanchez-Valente, J., Hernandez-Beltran, F., Rodriguez-Hernandez, A., & Navarrete-Bolanos, J. (2003). Active sulfated alumina catalysts obtained by hydrothermal treatment. *Journal of Catalysis*, 220(2), 317-325.
- Hall, N. F., & Conant, J. B. (1927). A study of superacid solutions. I. The use of the chloranil electrode in glacial acetic acid and the strength of certain weak bases. *Journal of the American Chemical Society*, 49(12), 3047-3061.
- Hammett, L. P. (1940). *Physical Organic Chemistry*
- Himmel, D., Goll, S. K., Leito, I., & Krossing, I. (2010). A unified pH scale for all phases. *Angewandte Chemie International Edition*, 49(38), 6885-6888.
- Housecroft, C., & Sharpe, A., &. (2001). *Inorganic Chemistry*: Prentice Hall, Pearson Education Limited, Harlow, UK.
- Huo, Q., Margolese, D. I., Feng, P., Gier, T., & Sieger, P. (1994). *Generalized syntheses of periodic surfactant/inorganic composite materials*: DTIC Document.
- Ichikuni, N., Nakao, Y., Ishizuki, K., Hara, T., & Shimazu, S. (2013). Effect of Local Structure of Mo Oxide on Selective Photo-Oxidation of Propane to Acetone. *Catalysis Letters*, 143(2), 154-158.
- Jenkins, R., & Snyder, R. L. (1996). *Introduction to X-ray powder diffractometry* (Vol. 138). New York: John Wiley & Sons, Inc.
- Kim, J. M., Jun, S., & Ryoo, R. (1999). Improvement of hydrothermal stability of mesoporous silica using salts: reinvestigation for time-dependent effects. *The Journal of Physical Chemistry B*, 103(30), 6200-6205.
- Kim, S. S., Zhang, W., & Pinnavaia, T. J. (1998). Ultrastable mesostructured silica vesicles. *science*, 282(5392), 1302-1305.
- Kleitz, F. (2009). *Ordered Nanoporous Materials: Synthesis, Characterization and Functionalization Methods*.

- Kresge, C., Leonowicz, M., Roth, W., Vartuli, J., & Beck, J. (1992). Ordered mesoporous molecular sieves synthesized by a liquid-crystal template mechanism. *nature*, 359(6397), 710-712.
- Kulkarni, R., Chaudhari, M., & Mishra, S., &. (2013). *UV cure acrylate monomers: synthesis, analysis and storage* [Pigment & Resin Technology].
- Lekhal, A., Glasser, B. J., & Khinast, J. G. (2001). Impact of drying on the catalyst profile in supported impregnation catalysts. *Chemical Engineering Science*, 56(15), 4473-4487.
- Lekhal, A., Glasser, B. J., & Khinast, J. G. (2004). Influence of pH and ionic strength on the metal profile of impregnation catalysts. *Chemical Engineering Science*, 59(5), 1063-1077.
- Lekhal, A., Khinast, J. G., & Glasser, B. J. (2001). Predicting the effect of drying on supported coimpregnation catalysts. *Industrial & Engineering Chemistry Research*, 40(18), 3989-3999. doi:10.1021/ie010126k
- Lewis, G. N. (1923). *Valence and the structure of atoms and molecules*. New York: The Chemical Catalog Co., Ltd.
- Li, S. (2011). *Synthesis of sulphated transition metal oxides supported on mesoporous silica using direct impregnation method and their catalytic activities*. AUT University.
- Lin, D.-J., She, S.-F., Pan, H.-B., Chen, N.-S., & Huang, J.-L. (2000). Preparation and Characterization of Nano Solid Superacid $\text{SO}_4^{2-}/\text{CoFe}_2\text{O}_4$. *Chinese Journal of Inorganic Chemistry*, 16(5), 757-762.
- Lowell, S., Shields, J. E., Thomas, M. A., & Thommes, M. (2004). *Characterization of porous solids and powders* (4 ed.). Biston: Kluwer Academic Publisher.
- Matsushashi, H., Sato, D., & Arata, K. (2004). Influence of calcination temperature on surface acidity of the solid superacid of sulfated alumina. *Reaction Kinetics and Catalysis Letters*, 81(1), 183-188.
- Matsumoto, P. S. (2005). Trends in ionization energy of transition-metal elements. *Journal of chemical education*, 82(11), 1660.
- Miessler, G. L., & Tarr, D. A. (Eds.). (1991). *Inorganic Chemistry*: Pearson Prentice-Hall.
- Mokaya, R. (2001). Hydrothermally stable restructured mesoporous silica. *Chemical Communications*(10), 933-934.
- Morey, M., Davidson, A., Eckert, H., & Stucky, G. (1996). Pseudotetrahedral O₃/2V O Centers Immobilized on the Walls of a Mesoporous, Cubic MCM-48 Support:

- Preparation, Characterization, and Reactivity toward Water As Investigated by 51V NMR and UV-Vis Spectroscopies. *Chemistry of materials*, 8(2), 486-492.
- Nagaraju, N. (1997). Synthesis of isoamyl acetate using NaX and NaY zeolites as catalysts. *Reaction Kinetics and Catalysis Letters*, 61(1), 155-160.
- Naught, M., Wilkinson, A., Nic, M., Jirat, J., Kosata, B., & Jenkins, A. (2006). IUPAC, compendium of chemical terminology. *XML on-line corrected version: <http://goldbook.iupac.org>. ISBN 0-9678550-9-8. doi, 10.*
- Noda, L. K., de Almeida, R. M., Probst, L. F. D., & Goncalves, N. S. (2005). Characterization of sulfated TiO₂ prepared by the sol-gel method and its catalytic activity in the n-hexane isomerization reaction. *Journal of Molecular Catalysis A: Chemical*, 225(1), 39-46.
- Olah, G. A. (2005). Crossing conventional boundaries in half a century of research. *The Journal of organic chemistry*, 70(7), 2413-2429.
- Olah, G. A., Prakash, G. K. S., & Sommer, J. (1985). *Superacids*. Wiley, New York.
- Olah, G. A., Prakash, G. S., & Sommer, J. (1979). Superacids. *science*, 206(4414), 13-20.
- Osborne, M. (2004). Adsorption isotherms.
- Parry, E. P. (1963). An infrared study of pyridine adsorbed on acidic solids. Characterization of surface acidity. *Journal of Catalysis*, 2(5), 371-379.
- Parvulescu, V., Anastasescu, C., & Su, B. (2004). Bimetallic Ru-(Cr, Ni, or Cu) and La-(Co or Mn) incorporated MCM-41 molecular sieves as catalysts for oxidation of aromatic hydrocarbons. *Journal of Molecular Catalysis A: Chemical*, 211(1), 143-148.
- Rao, C. N. R., & Raveau, B. (1995). *Transition metal oxides*. New York: VCH Publishers
- Reddy, B. M., Sreekanth, P. M., Lakshmanan, P., & Khan, A. (2006). Synthesis, characterization and activity study of SO₄²⁻/Ce_xZr_{1-x}O₂ solid superacid catalyst. *Journal of Molecular Catalysis A: Chemical*, 244(1), 1-7.
- Regalbuto, J. (2007). *Handbook of catalyst preparation* Boca Raton Taylor & Francis.
- Ropero-Vega, J. L., Aldana-Perez, A., Gomez, R., & Nino-Gomez, M. E. (2010). Sulfated titania [TiO₂/SO₄²⁻]: A very active solid acid catalyst for the esterification of free fatty acids with ethanol. *Applied Catalysis A: General*, 379(1-2), 24-29.
- Rouquerol, J., Avnir, D., Everett, D. H., Fairbridge, C., Haynes, M., Pernicone, N., ... Unger, K. K. (Eds.). (1994). Guidelines for the Characterization of Porous Solids. 87, 1-9. Retrieved from

<http://www.scopus.com/inward/record.url?eid=2-s2.0-0002021294&partnerID=40&md5=d3076bb8b6bda0fce98d0fbb5b597abf>

- Ryoo, R., & Jun, S. (1997). Improvement of hydrothermal stability of MCM-41 using salt effects during the crystallization process. *The Journal of Physical Chemistry B*, 101(3), 317-320.
- Sørensen, S. P. L. (1909). Über die Messung und die Bedeutung der Wasserstoffionenkonzentration bei enzymatischen Prozessen. *Biochemische Zeitschrift* 21: 131–304.
- S.Kinugasa, K.Tanabe, & T.Tamura, & AIST. (2013). *IR spectrum of butyl acetate*
- Sayari, A. (1996). Catalysis by Crystalline Mesoporous Molecular Sieves. *Chemistry of Materials*, 8(8), 1840-1852.
- Sayari, A., Yang, Y., Kruk, M., & Jaroniec, M. (1999). Expanding the pore size of MCM-41 silicas: use of amines as expanders in direct synthesis and postsynthesis procedures. *The Journal of Physical Chemistry B*, 103(18), 3651-3658.
- Schüth, F., & Schmidt, W., &. (2002). *Microporous and mesoporous materials* .
- Shi, X., & Wang, Y. (2006). Magnetic nanometer-sized solid superacids for catalytic synthesis of dioctyl adipate [J]. *Chemical Engineering*, 6, 010.
- Sohn, J. R., & Seo, D. H. (2003). Preparation of new solid superacid catalyst, zirconium sulfate supported on γ -alumina and activity for acid catalysis. *Catalysis Today*, 87(1), 219-226.
- Song, W., Venimadhavan, G., Manning, J. M., Malone, M. F., & Doherty, M. F. (1998). Measurement of residue curve maps and heterogeneous kinetics in methyl acetate synthesis. *Industrial & Engineering Chemistry Research*, 37(5), 1917-1928. doi:10.1021/ie9708790
- Stucky, G. D., Huo, Q., Firouzi, A., Chmelka, B. F., Schacht, S., Voigt-Martin, I., & Schüth, F. (1997). Directed synthesis of organic/inorganic composite structures. *Studies in Surface Science and Catalysis*, 105, 3-28.
- Takehira, K., Ohishi, Y., Shishido, T., Kawabata, T., Takaki, K., Zhang, Q., & Wang, Y. (2004). Behavior of active sites on Cr-MCM-41 catalysts during the dehydrogenation of propane with CO₂. *Journal of Catalysis*, 224(2), 404-416.
- Timofeeva, M. N., Matrosova, M. M., Maksimov, G. M., Likholobov, V. A., Golovin, A. V., Maksimovskaya, R. I., & Paukshtis, E. A. (2001). Esterification of n-butanol with acetic acid in the presence of heteropoly acids with different structures and compositions. *Kinetics and Catalysis*, 42(6), 791-795.

- Voskoboinikov, T. V., Coq, B., Fajula, F., Brown, R., McDougall, G., & Luc Couturier, J. (1998). An in situ diffuse reflectance FTIR study of the cyclodimerization of 1,3-butadiene over Cu-exchanged zeolites. *Microporous and Mesoporous Materials*, 24(1-3), 89-99.
- Walcarius, A., & Delacôte, C., & (2003). *Rate of access to the binding sites in organically modified silicates*.
- Wang, Y., Gan, Y., Whiting, R., & Lu, G. (2009). Synthesis of sulfated titania supported on mesoporous silica using direct impregnation and its application in esterification of acetic acid and n-butanol. *Journal of Solid State Chemistry*, 182(9), 2530-2534.
- Wu, C.-G., & Bein, T. (1996). Microwave synthesis of molecular sieve MCM-41. *Chemical Communications*(8), 925-926.
- Xia, Q. H., Hidajat, K., & Kawi, S. (2002). Effect of ZrO₂ loading on the structure, acidity, and catalytic activity of the SO₄²⁻/ZrO₂/MCM-41 acid catalyst. *Journal of Catalysis*, 205(2), 318-331.
- Yadav, G. D., & Nair, J. J. (1999). Sulfated zirconia and its modified versions as promising catalysts for industrial processes. *Microporous and Mesoporous Materials*, 33(1-3), 1-48.
- Yanagisawa, T., Shimizu, T., Kuroda, K., & Kato, C. (1990). The preparation of alkyltrimethylammonium-kanemite complexes and their conversion to microporous materials. *Bulletin of the Chemical Society of Japan*, 63(4), 988-992.
- Yang, R. T. (1987). *Gas separation by adsorption processes*. Boston: Butterworths (1987).
- Yang, Y., Wang, X., & Kou, Y. (2004). Determination of acidity of ionic liquids and alkylation of isobutane with butene by chloroaluminate ionic liquids. *Chinese Journal of Catalysis*, 25(1), 60-64.
- Yao, Y., Zhang, M., & Yang, Y. (2001). Synthesis of MCM-41 nanostructured mesoporous molecular sieve using microwave radiation. *Journal of physical chemistry (China)*, 17(12), 1117-1121.
- Zhang, M., & Chu, J. (1998). MCM-41 synthesis using microwave radiation. *National academy (China)*, 37(2), 128-130.
- Zhao, D., Feng, J., Huo, Q., Melosh, N., Fredrickson, G. H., Chmelka, B. F., & Stucky, G. D. (1998). Triblock copolymer syntheses of mesoporous silica with periodic 50 to 300 angstrom pores *Science*, 279(5350), 548 - 552.
doi:10.1126/science.279.5350.548

- Zhao, D., Feng, J., Huo, Q., Melosh, N., Fredrickson, G. H., Chmelka, B. F., & Stucky, G. D. (1998). Triblock copolymer syntheses of mesoporous silica with periodic 50 to 300 angstrom pores. *science*, 279(5350), 548-552.
- Zhao, Q., Yin, G., Jiang, T., Yin, H., & Tang, Y. (2007). Synthesis and characterization of CuMCM-41 mesoporous molecular sieves under hydrothermal condition. *Journal-Chinese Ceramic Society*, 35(5), 619.
- Zhao, X., & Lu, G. (1998). Modification of MCM-41 by surface silylation with trimethylchlorosilane and adsorption study. *The Journal of Physical Chemistry B*, 102(9), 1556-1561.
- Zhao, X., Lu, G., Whittaker, A., Millar, G., & Zhu, H. (1997). Comprehensive study of surface chemistry of MCM-41 using ²⁹Si CP/MAS NMR, FTIR, Pyridine-TPD, and TGA. *The Journal of Physical Chemistry B*, 101(33), 6525-6531.
- Zhao, X. S., Lu, G. M., & Hu, X. (1999). A novel method for tailoring the pore-opening size of MCM-41 materials. *Chem. Commun.*(15), 1391-1392.
- Zheng, H.-l., Xie, L.-g., Gao, X., Tan, H.-f., Yang, B., & Ji, F.-y. (2009). Preparation of poly-ferric silicate sulfate (PFSS) from tetraethylorthosilicate and its algae removal performance. *Journal of Civil, Architectural & Environmental Engineering*, 6, 016.
- Zhu, L., Hong-yu, G., Chun-hua, G., Ning, L., Yu-chun, J., & Xiang-dong, Z. (2007). The Synthesis and Morphology of Mesoporous MCM- 41. *Journal Of Liaoning University(Natural Sciences Edition*, 34(3).
doi:10.3969/j.issn.1000-5846.2007.03.025